11-1-2001

The Proterozoic ancestry of the Colorado Mineral Belt : ca. 1.4 Ga shear zone system in central Colorado

Annie Marie McCoy

THE PROTEROZOIC ANCESTRY

OF THE COLORADO MINERAL BELT:

ca. 1.4 Ga shear zone system in central Colorado

by

Annie Marie McCoy

B.A., Geology, Hampshire College, 1999

THESIS

Submitted in Partial Fulfillment of the
Requirements for the Degree of

Master's of Science

Earth and Planetary Sciences

The University of New Mexico
Albuquerque, New Mexico

November 15, 2001

Annie Marie McCoy

Candidate

Earth and Planetary Sciences

Department

This thesis is approved, and it is acceptable in quality and form for publication on microfilm:

Approved by the Thesis Committee:

Karl E. Karlstrom, Chairperson

Jane Selverstone

John Wilson

Accepted:

Dean, Graduate School

Date

ACKNOWLEDGEMENTS

I am grateful to my adviser Karl Karlstrom, for always pushing me to do my best work, keeping me on track, providing great advice, and never holding me back. I am grateful to my mom and dad – my best friends – who have always been hugely supportive and encouraging, and were great company on several field excursions. Thank you to Colin, who has been an inspiration. Thanks to my thesis committee members, Jane and John, for giving many helpful comments that made my thesis a better piece of work. Thanks to Jason – I think we have pushed each other to do our best work and I look forward to many more great times together. Thanks to all my good friends, office-mates, and housemates, who helped me through many days.

I am grateful to the organizations that provided funding for this project. These organizations include the National Science Foundation, which provided the Continental Dynamics of the Rocky Mountains grant, the Four Corners Geological Society, the Colorado Scientific Society, the Department of Earth and Planetary Sciences at University of New Mexico, and the Office of Graduate Studies at University of New Mexico.

THE PROTEROZOIC ANCESTRY OF THE COLORADO MINERAL BELT: ca. 1.4 Ga shear zone system in central Colorado

by

Annie Marie McCoy

ABSTRACT OF THESIS

Submitted in Partial Fulfillment of the
Requirements for the Degree of

Master's of Science
Earth and Planetary Sciences

The University of New Mexico
Albuquerque, New Mexico

November 15, 2001

THE PROTEROZOIC ANCESTRY OF THE COLORADO MINERAL BELT:

ca. 1.4 Ga shear zone system in central Colorado

Annie Marie McCoy

B.A., Geology, Hampshire College, 1999

M.S., Geology, University of New Mexico, 2001

ABSTRACT

The Paleocene to Oligocene magmatism and mineralization that are the Phanerozoic expressions of the Colorado Mineral Belt developed along a NE-trending system of subvertical mylonites and ultramylonites that formed in the Mesoproterozoic and that, in turn, overprinted higher-temperature Paleoproterozoic high strain zones of similar orientation. In this thesis, I distinguish the Colorado Mineral Belt itself from a Proterozoic 'Colorado Mineral Belt shear zone system' that includes the Homestake, Gore Range, St. Louis Lake, and Idaho Springs-Ralston shear zone segments. In situ electron microprobe monazite dating of mylonites of the Colorado Mineral Belt shear zone system, coupled with field studies of relative timing of shearing and pluton emplacement, demonstrate a ca. 100 Ma history of recurrent shearing. This history involves movement at 1.45 Ga along Idaho Springs-Ralston shear zones and possibly along Homestake shear zone, synchronous with emplacement of the Mt. Evans pluton. At 1.42 Ga, movement took place along St. Louis Lake and again along Idaho Springs-Ralston shear zones, synchronous with emplacement of the Silver Plume pluton. At 1.38 Ga, movement took place along Homestake

and Idaho Springs-Ralston shear zones, synchronous with emplacement of the St. Kevin pluton, and post-1.38 Ga movements reactivated Homestake, St. Louis Lake, and Idaho Springs-Ralston shear zones. In each shear zone segment, kilometer-wide Mesoproterozoic mylonite zones consist of multiple, parallel, one to ten meter-wide mylonite strands, which overprint higher-temperature Paleoproterozoic high-strain domains that are several kilometers wide. Monazite dating of the higher temperature high-strain domains indicates pulses of Paleoproterozoic deformation that occurred at 1.71-1.69 Ga, 1.67 Ga, 1.65, and 1.62 Ga. Thus, the tectonic fingerprint of the Colorado Mineral Belt shear zone system includes two ~100 Ma long orogenic periods in the Proterozoic, each with important pulses of deformation that occurred every fifteen to twenty million years. This shear zone system may be analogous to modern-day intracontinental zones of weakness like the Tien Shan, which record both original assembly of tectonic blocks and reactivation of intracontinental weaknesses during later plate convergence at a distant margin.

TABLE OF CONTENTS

LIST OF FIGURES

LIST OF TABLES

1.0 PREFACE

For this Master's thesis, I spent about three months over the course of three summers conducting detailed mapping in four areas in the Colorado Mineral Belt, and reconnaissance mapping in several other areas. I analyzed close to twenty thin-sections on the scanning electron microscope, and analyzed 23 monazite grains on the electron microprobe during three sessions at University of Massachusetts and three sessions at New Mexico Tech. I conducted microstructural studies, petrographic studies, and kinematic analyses using optical microscopes at University of New Mexico. I also conducted trace element analyses on seven metasedimentary samples in the x-ray fluorescence laboratory at University of New Mexico.

There are a number of people who have contributed to the research presented in this thesis. Karl Karlstrom, Gerrit Bulman, and Josh Schwartz, all aided me in field mapping and sample collecting during the summers of 1999 and 2000. Mike Spilde trained me to use the scanning electron microscope at University of New Mexico. Mike Williams and Mike Jercinovic guided me through electon microprobe monazite analysis at the University of Massachusetts. Nelia Dunbar guided me through electon microprobe monazite analysis at New Mexico Tech. John Husler and Marcelle Van Reenen did much of the sample preparation and the major element analyses of the metasedimentary samples, and guided me through sample preparation and trace element analyses. As I conducted my field investigations, I used Colin Shaw's work in the Homestake shear zone as a basis for comparing and contrasting each shear zone segment along the Colorado Mineral Belt.

2.0 INTRODUCTION

The Colorado Mineral Belt shear zone system is defined here as a series of NE-trending, mylonitic and ultramylonitic shear zone segments that developed into a coherent shear zone system around 1.4 Ga. Each shear zone segment also overprints similar older Paleoproterozoic structures, and although these structures are present throughout Colorado and do not appear to be unique to the Colorado Mineral Belt region, their presence suggests a common Paleoproterozoic ancestry to the shear zone system. The shear zone system shows evidence for multiple episodes of reactivation throughout the Proterozoic as well as the Phanerozoic.

This study of the structures, kinematics, and timing of movement along each shear zone segment defines a 'tectonic fingerprint,' a unique identity, for the shear zone system as a whole. This study also sheds light on the nature of this long-lived zone of weakness in the lithosphere that has ultimately influenced the geometry of the Phanerozoic Colorado Mineral Belt.

The focus of this thesis is the Proterozoic Colorado Mineral Belt shear zone system, which represents the origins and early evolution of the Phanerozoic

Colorado Mineral Belt. For this reason, I will first describe the Phanerozoic Colorado Mineral Belt, why it is a unique and important geologic feature in central Colorado, and why we want to know about its origins and early evolution in the Proterozoic.

2.1 PHANEROZOIC EXPRESSION OF THE COLORADO MINERAL BELT

The Colorado Mineral Belt is generally defined as a ~200 km long, NE-trending zone in central Colorado that is marked by a concentration of Late Cretaceous to Early Tertiary intrusions and related mineral deposits emplaced during and after the Laramide orogeny (Fig. 1; Tweto and Sims, 1963; Muschler et al., 1987). Tweto and Sims' (1963) boundaries of the Colorado Mineral Belt, defined by the locations of major mining districts of Laramide age in Colorado, are shown in Figure 1. Their 'maximum boundaries' also include intrusions and mineralized areas of Oligocene age in the San Juan volcanic field.

In Figure 1, a gravity map of Colorado shows that the Colorado Mineral Belt is also defined by a negative Bouguer gravity anomaly. As an interesting side project, I have been conducting simple 2 1/2 dimensional forward modeling of this gravity anomaly along profiles that cut across the Colorado Mineral Belt.

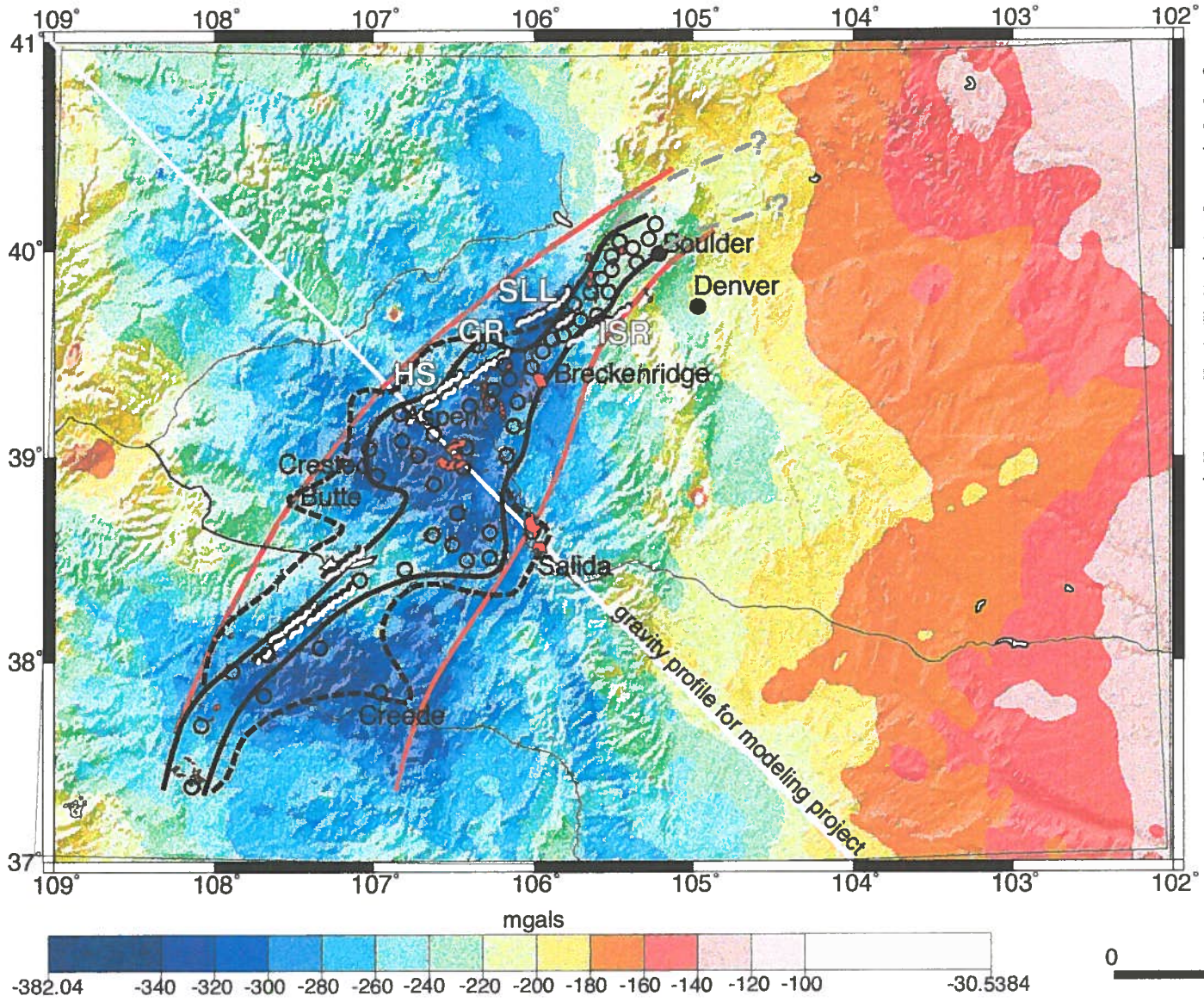

Figure 1: Bouguer gravity data of USGS OFR00-0042 and G. R. Keller draped over 1-km GLOBE DEM topography. White line represents gravity profile of Figure 2. Tweto and Sims' (1963) outline of the Colorado Mineral Belt is a black line (maximum boundaries are dashed). Circles are locations of major mining centers (Tweto and Sims (1963). Red lines are more general boundaries for the Colorado Mineral Belt (this paper).

The results of this modeling project appear to shed light on the subsurface geometry of the Colorado Mineral Belt. A simple model along the profile shown in Figure 1 suggests that the observed gravity anomaly may be approximated by a combination of a very large, relatively low-density body below the Moho (Fig. 2c,e), a sloping Moho (Fig. 2c) or a Moho with subtle topography (Fig. 2e), and a large, relatively low-density body in the crust (Fig. 2c,e). This low-density body in the crust resembles a granitic batholith that is centered beneath the Colorado Mineral Belt.

The San Juan Mountains, located southwest of the Colorado Mineral Belt, contain younger magmatic centers of middle and late Tertiary age and show a negative Bouguer gravity anomaly that is very similar to that of the Colorado Mineral Belt. Like the Colorado Mineral Belt, the San Juans also show evidence for Paleozoic deformation along subvertical structures (Baars et al., 1988), and NE-trending Proterozoic shear zones and faults in the northwestern part of the range (Tweto and Sims, 1963; Baars, 1984). In light of these similarities, we widen the boundaries of the Colorado Mineral Belt to include the San Juan Mountains (Fig. 1).

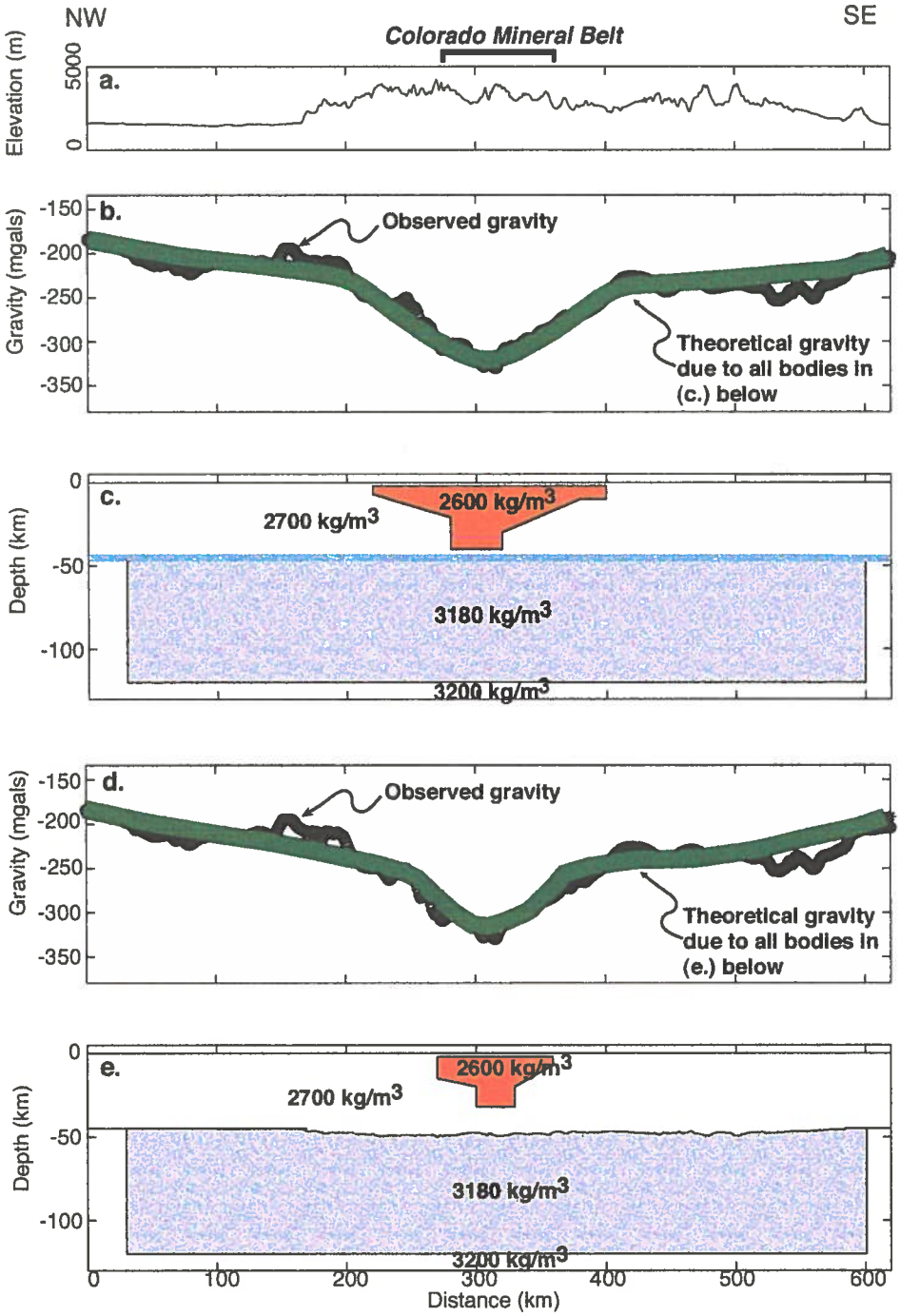

Figure 2: 2 1/2 dimensional models of Bouguer gravity anomaly along the profile shown in Figure 1. a. Topography along profile. b. Observed and theoretical anomaly due to a large body in the crust, a sloping Moho, and a large region of slightly low density in the mantle. c. The bodies that create the theoretical anomaly in b. d. Theoretical anomaly due to a smaller body in the crust, subtle topography on the Moho (1/3 that predicted by topography), and a large region of slightly low density in the mantle. e. The bodies that create the theoretical anomaly in d.

The irregular geometries of Tweto and Sims' Colorado Mineral Belt boundaries (1963) appear to have little structural significance. One exception is the northwesterly jog in the boundary in the southern Gore Range that coincides with the Gore fault. In this paper, we use smoother, more general Colorado Mineral Belt boundaries that include the negative gravity anomalies and major mining districts, and lie parallel to the NE-trending Proterozoic structures.

There are a number of pieces of evidence that suggest that the magmatism and deformation along the Phanerozoic Colorado was influenced by the Proterozoic Colorado Mineral Belt shear zone system, which is parallel to and contained within the Colorado Mineral Belt (Fig. 1). Apatite fission track studies of Kelley et al. (2001) show that the Colorado Mineral Belt shear zone system coincides with a transition in Laramide-age structural style and timing of uplift in the Front Range. To the south of the shear zone system, Laramide structures are dominated by east-vergent thrusts with >100 Ma apatite fission track ages. To the north, Laramide structures are dominated by southwest-vergent back thrusts with 76-45 Ma apatite fission track ages (Kelley et al, 2001).

Stratigraphic studies by Allen (1994) document multiple Paleozoic movements that directly reactivate at least one of the shear zone segments along

the Colorado Mineral Belt shear zone system. The Upper Cambrian Sawatch Quartzite, and specifically its basal conglomerate unit, thins across the mylonite strands of the Homestake shear zone segment in the northern Sawatch Range, suggesting that the zone reactivated during early stages of Sawatch deposition (Allen, 1992). Thinning of the overlying Upper Cambrian Peerless Shale and the absence of the Lower Ordovician Manitou Dolomite suggest S-side up reactivation of Homestake shear zone and erosion prior to deposition of Middle Ordovician Harding Sandstone (Allen, 1993). Subtle thickness and facies variations in the Upper Devonian Chaffee Group and Lower Mississippian Leadville Formation suggest further reactivations (Allen, 1993). In all, variations in facies and thickness of Paleozoic strata indicate that Homestake shear zone has reactivated at least four times between Cambrian and late Devonian time, and at least one time after Early Mississippian time (Allen, 1994).

Teleseismic studies by Dueker et al. (in preparation, 2001) show an anomaly of slow lithosphere that is contained within the Colorado Mineral Belt. When viewed in a N-S cross-section across Colorado (Fig. 3), this anomaly has a linear geometry that projects up into the Colorado Mineral Belt, suggesting that this geologic feature is lithospheric in scale.

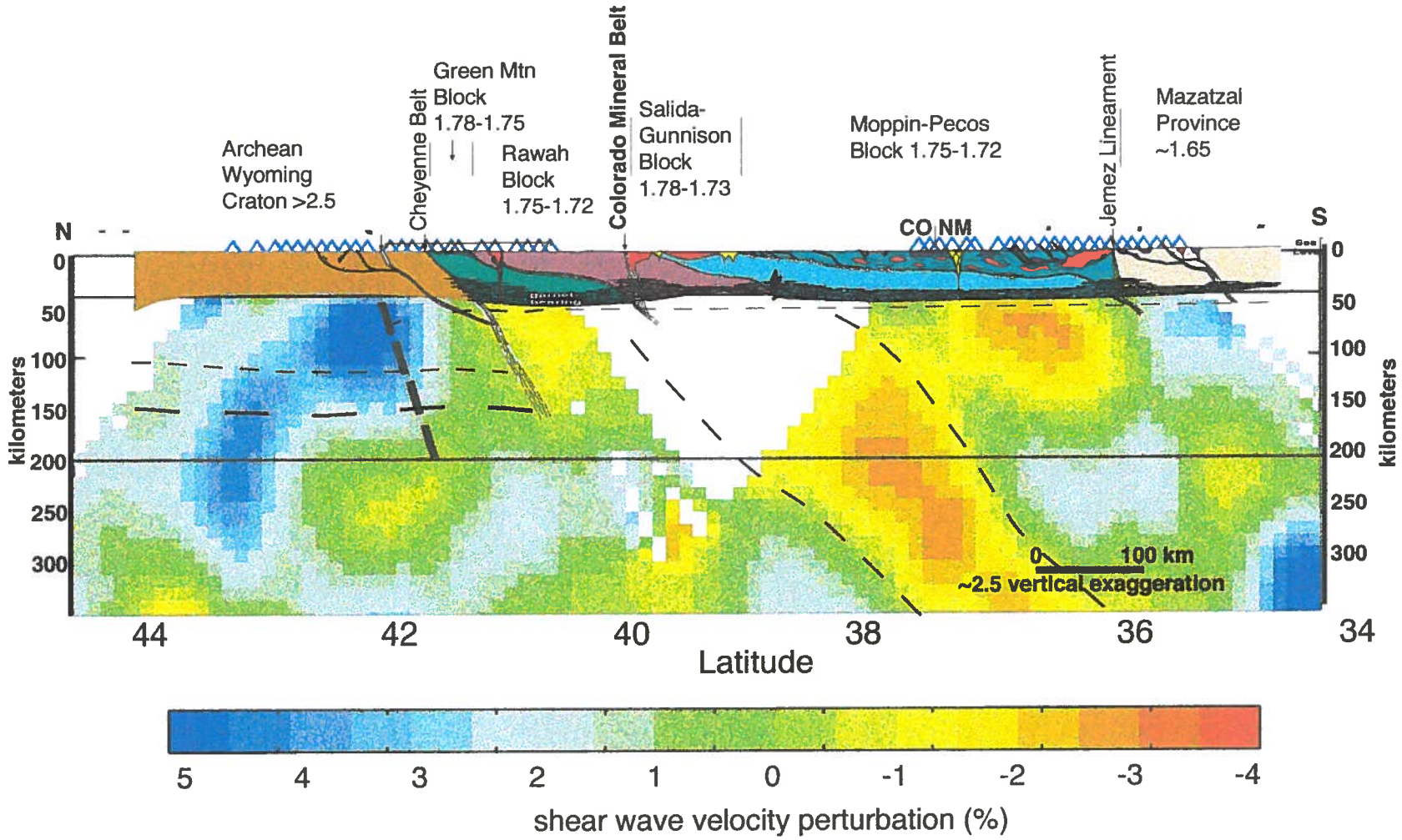

Figure 3: Schematic N-S cross-section of Colorado lithosphere with mantle tomography profile of Dueker et al. (in preparation). Anomaly of slow mantle and lithosphere projects up into Colorado Mineral Belt, suggesting the presence of a lithosphere scale structural/magmatic feature.

In the next section, I will begin to describe the Colorado Mineral Belt shear zone system, which represents the Proterozoic origins and early evolution of this lithospheric-scale feature.

2.2 COLORADO MINERAL BELT SHEAR ZONE SYSTEM: 'TYPE EXAMPLE' OF A PROTEROZOIC INTRACONTINENTAL ZONE OF DEFORMATION

It has long been argued that the magmatism and mineralization of the Colorado Mineral Belt were influenced by pre-existing weaknesses in the lithosphere, as indicated by the presence of Proterozoic shear zones and plutons (Fig. 4; Tweto and Sims, 1963; Warner, 1978). We now know that this Precambrian ancestry involves focused deformation and magmatism at ~1.4 Ga and ~1.7 Ga (Reed et al., 1987; Nyman et al., 1994; Shaw et al., 2001), and molybdenite mineralization at ~1.4 Ga (Sims and Stein, 1999). Although Tweto and Sims (1963) recognized Proterozoic shear zones in the Colorado Mineral Belt, they did not describe the variety of different fault rocks, or 'tectonites,' present in the shear zones, nor did they recognize evidence for multiple Proterozoic movements in the shear zones. Tectonites such as cataclasite,

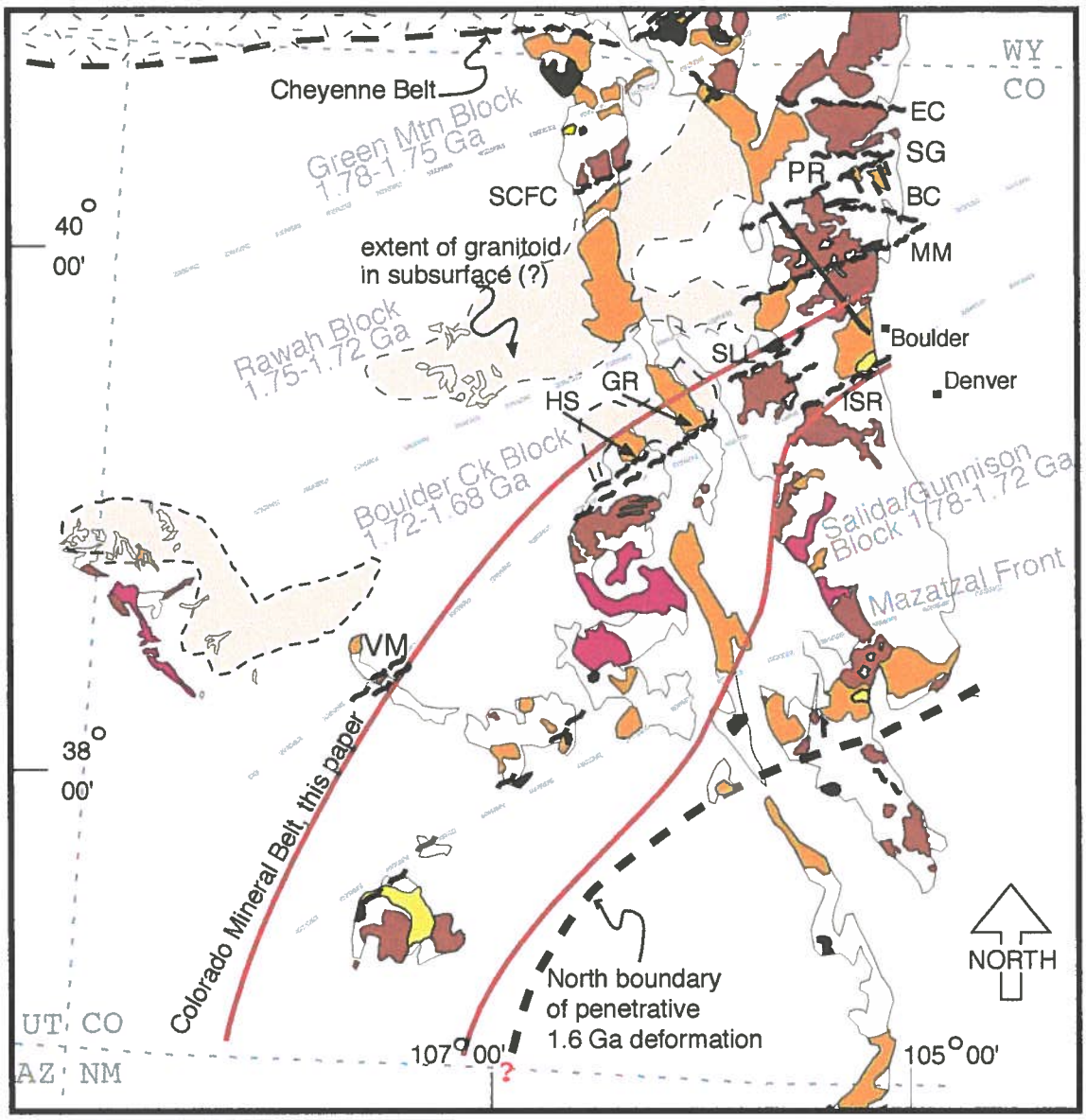

Explanation 0 50 km

- ~1.4 Ga granite
- ~1.4 Ga mafic dikes
- ~1.7 Ga granite
- XY granite (unknown age)
- quartzite (meta-quartz arenites)
- mafics and ultramafics
- undivided
- Archean Wyoming craton
- shear zone

Figure 4: Colorado Mineral Belt and the Proterozoic tectonic and magmatic features of Colorado. Shear zones show evidence for high strain at ~1.7 Ga and reactivation at ~1.4 Ga. The coincidence of Homestake, Gore Range, St. Louis Lake, and Idaho Springs-Ralston shear zones with the Colorado Mineral Belt suggests that the Mineral Belt may have a Proterozoic ancestry.

Shear zones

EC Elkhorn Creek	HS Homestake
SG Skin Gulch	GR Gore Range
PR Poudre River	SLL St. Louis Lake
BC Buckhorn Creek	ISR Idaho Springs-Ralston
MM Moose Mountain	
SCFC Soda Ck-Fish Creek	
VM Vernal Mesa	

ultramylonite, mylonite, and high-temperature striped gneisses, were grouped under the term 'cataclastic rock.' Moench (1964) began to distinguish different tectonites along Idaho Springs-Ralston shear zone, distinguishing high-temperature striped gneiss from a younger tectonite that he described as "granulation of the previously foliated and deformed rocks.....confined largely to a narrow zone." The efforts of Tweto and Sims (1963) and Moench (1964) came before geologists widely recognized and used asymmetric fabrics and microstructures in tectonites to determine kinematic shear sense, multiple periods of movement, and strain rate and temperature conditions associated with crustal deformation. Therefore, re-examination and re-mapping of these shear zones, according to a new understanding of microstructures and kinematic indicators, is presented in this thesis.

In this study, I suggest that the Colorado Mineral Belt shear zone system, a discrete, branching system of mylonites and ultramylonites that formed in the Mesoproterozoic, is a 'type example' of a Proterozoic intracontinental zone of deformation exposed at middle crustal levels. Studying this shear zone system sheds light on fundamental questions about the origins and nature of intracontinental deformation, and the processes of reactivation.

Intracontinental zones of deformation, located thousands of kilometers from plate margins, may be the loci of shortening, extension, or strike-slip tectonics that accommodate an important part of the observed plate convergence at the distant margin (Tien Shan of central Asia, Atlas Mountains of northern Africa), and may also record lithosphere/asthenosphere interactions. For example, intracontinental shortening in the Tien Shan has accounted for a considerable fraction of the overall crustal shortening associated with India's indentation into Asia (Yin et al., 1998; Burov and Molnar, 1998). Intracontinental shortening in the Atlas Mountains has accommodated 17% to 45% of the total African-Eurasian plate convergence since the early Miocene (Gomez et al., 2000; Brede et al., 1992).

Processes controlling intracontinental zones of deformation, and the behavior of these zones at depth and over significant time intervals, remain poorly understood. If intracontinental zones of deformation are controlled by far-field stresses associated with plate behavior at convergent margins, what makes discrete zones susceptible to deformation within the continents? Intracontinental zones of deformation may have become weak due to heat, due to a pre-history that imparted chemical or mineralogical differences between the weak zone and

the surrounding lithosphere, due to unusually thick crust, and/or due to the presence of major pre-existing structures or domains of grain size reduction and strain-softening (Burov and Molnar, 1998). Karlstrom and Humphreys (1998) propose that inheritance of Proterozoic structural grains throughout the southwest U.S. involves 'volumetric' and 'interface' inheritance. 'Volumetric' inheritance means that the density and fertility of compositionally different lithospheric blocks influences isostatic and magmatic responses to tectonism. 'Interface inheritance' means that mechanical boundaries are zones of weakness and mass transport.

The middle crustal view exposed in Proterozoic rocks along the Colorado Mineral Belt shear zone system reveals a pattern of progressive overprinting of increasingly narrower, higher strain rate/lower temperature tectonites that suggests that discrete structures at shallower crustal levels grade into wider, more diffuse zones at deeper crustal levels. The shear zone system appears to have experienced strain-softening through increasingly more ductile deformation processes with increasing depth. Greenschist grade ultramylonites overprint wider zones of mylonites, which overprint even wider, amphibolite grade, high-strain domains. Each generation of tectonite appears to have caused grain size

reduction and weakening along the shear zone system, leaving it prone to further reactivations.

In this thesis, detailed mapping, petrographic, and microstructural study define the structures along the Colorado Mineral Belt shear zone system. Kinematic studies of deformational fabrics along the shear zones, studied in outcrop and under the microscope, define the shear sense associated with the formation of each deformational fabric. Dating of metamorphic monazite from shear zone rocks, using an in situ electron microprobe technique, defines the timing of movement associated with the formation of each deformational fabric. Together, these data define the Colorado Mineral Belt shear zone system 'tectonic fingerprint' and describe the initiation and early evolution of a long-lived zone of weakness in the lithosphere.

3.0 THE COLORADO MINERAL BELT SHEAR ZONE SYSTEM

Here, I define the characteristics common to the Mesoproterozoic mylonitic/ultramylonitic shear zone segments of the Colorado Mineral Belt shear zone system. I describe map patterns, structures, microstructures, kinematics, and timing of movement in each shear zone segment.

The shear zone segments studied in this thesis lie between Leadville and Golden, Colorado, and include the Homestake shear zone (Fig. 5, Fig. 6a; Shaw et al., 2001; Allen, 1994; Tweto and Sims, 1963), the Gore Range shear zone (Fig. 5, Fig. 6b; Bergendahl, 1969; Tweto and Sims, 1963), the St. Louis Lake shear zone (Fig. 5, Fig. 7a; Taylor, 1980; Bryant et al., 1981; Tweto and Sims, 1963), and the Idaho Springs-Ralston shear zone (Fig. 5, Fig. 7b; Graubard et al., 1990; Sheridan et al., 1969; Wells et al., 1967; Tweto and Sims, 1963; Moench et al. 1964). These segments comprise a shear zone system that extends at least 100 kilometers in length.

A recent detailed study of tectonites, kinematics, and timing of movement in Homestake shear zone, conducted by Shaw et al. (2001), sets the stage for this thesis, which correlates the Homestake shear zone and the other shear zone segments along the Colorado Mineral Belt. Adjacent to the Homestake

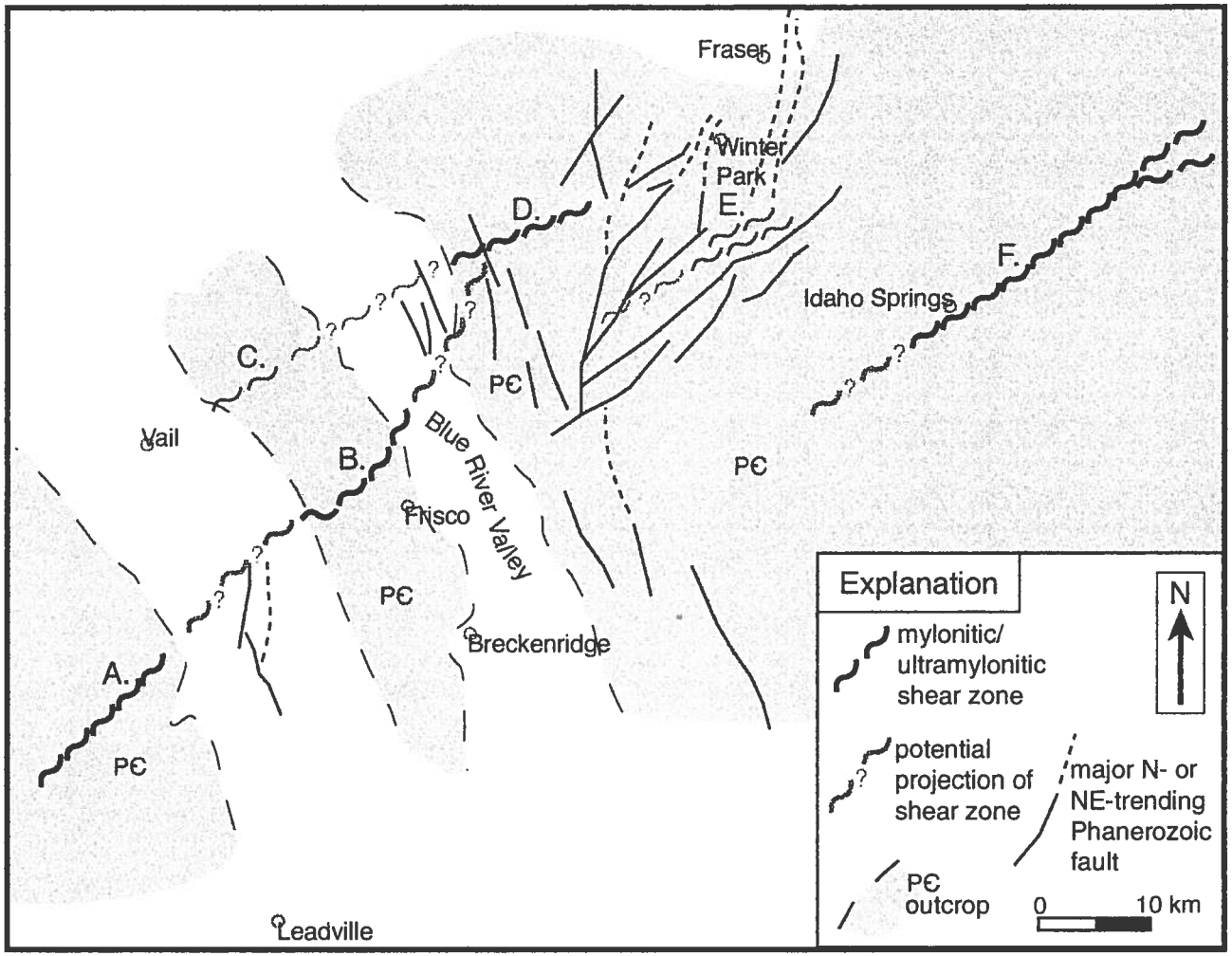

Figure 5: Colorado Mineral Belt shear zone system and potential relationship between segments. A. Homestake shear zone, B. Gore Range shear zone, C. Booth Lake mylonite strand, D. St. Louis Lake shear zone, E. Berthoud Pass mylonite strand, and F. Idaho Springs-Ralston shear zone.

Figure 6a: Map of part of Homestake shear zone near the confluence of Homestake Ck and Eagle Rv showing initially low-angle S1 folded by open to isoclinal F2 and transposed into NE-trending S2 high-strain domains. S2 is reactivated by narrower SE-side down mylonites that are overprinted by even narrower SE-side up ultramylonites.

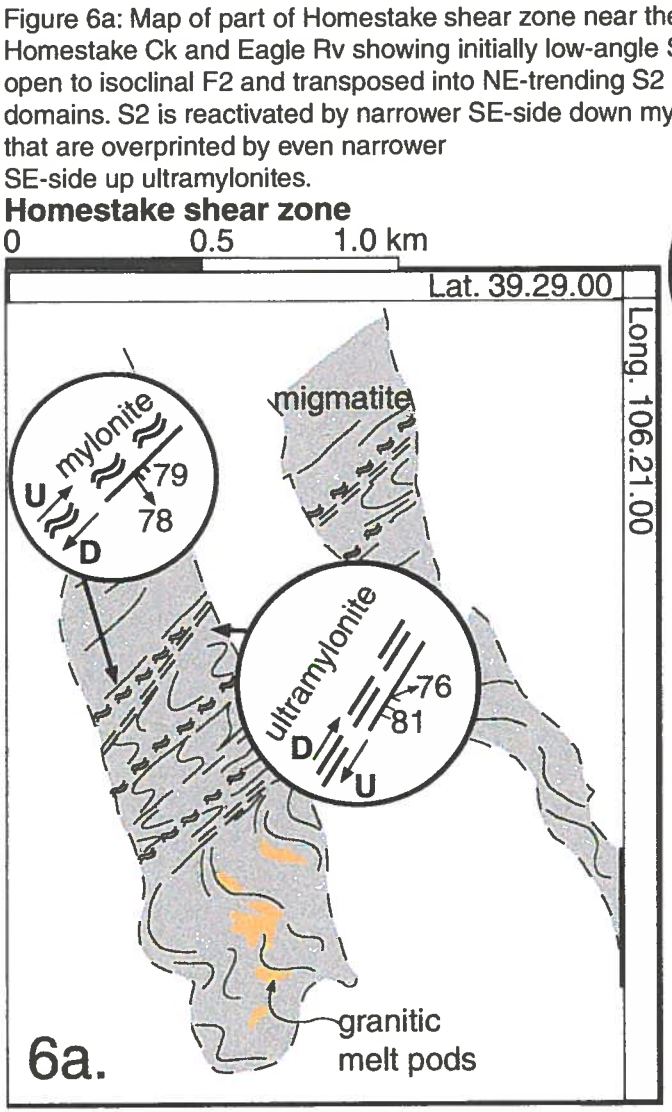

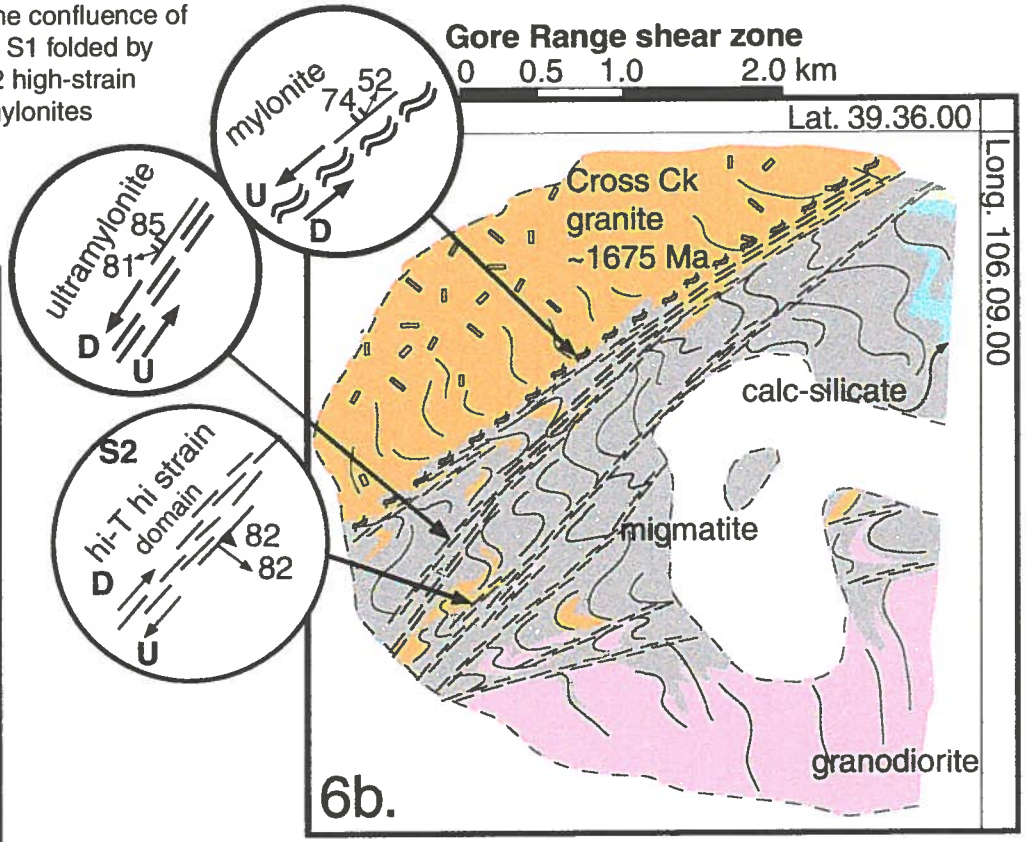

Figure 6b: Map of central part of Gore Range shear zone south of Buffalo Mtn. Initially low-angle S1 is folded by open to isoclinal F2 and transposed into NE-trending S2 high strain domains. S2 is reactivated by narrower SE-side down mylonites that are overprinted and drag-folded by narrower SE-side up ultramylonites. See Appendix 8 (1:24,000 map in back pocket) for more detailed mapping.

Figure 7a: Map of part of St. Louis Lake shear zone near St. Louis Lake. S1 is transposed into S2 along NE-trending high strain domains. Silver Plume age SE-side up mylonites reactivate S2 at the N margin of Silver Plume pluton, and are overprinted by narrower SE-side down mylonites. See Appendix 8 for more detailed mapping.

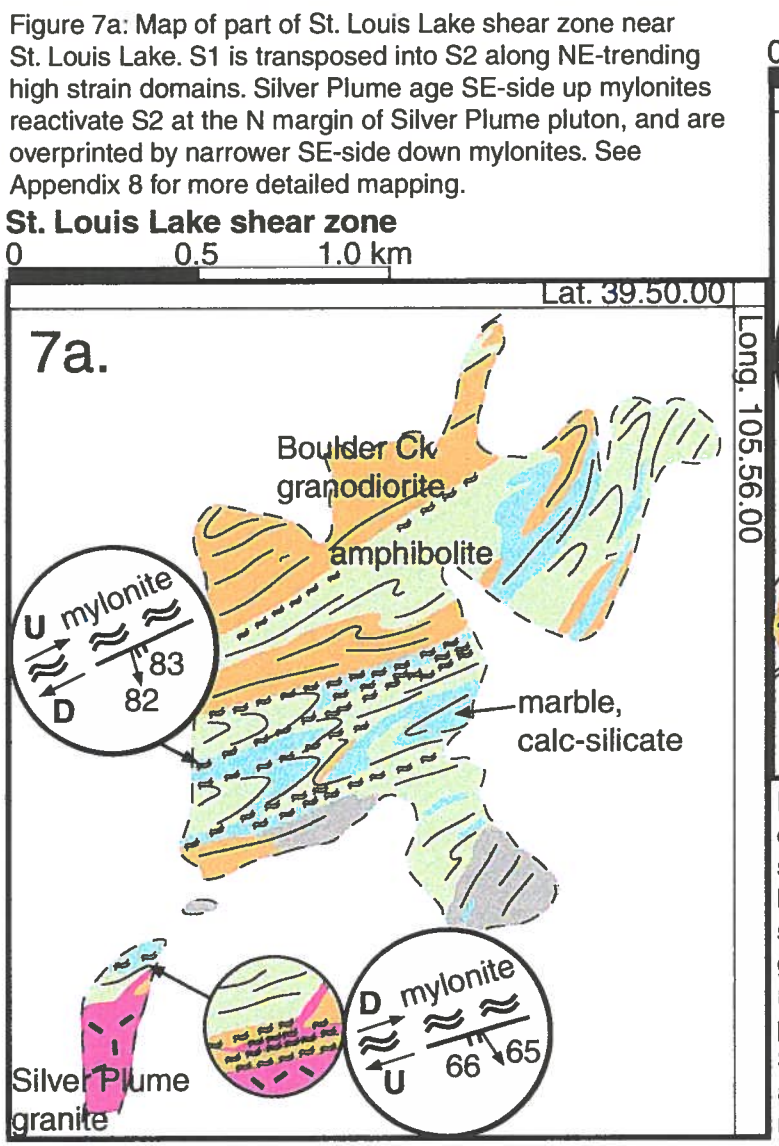

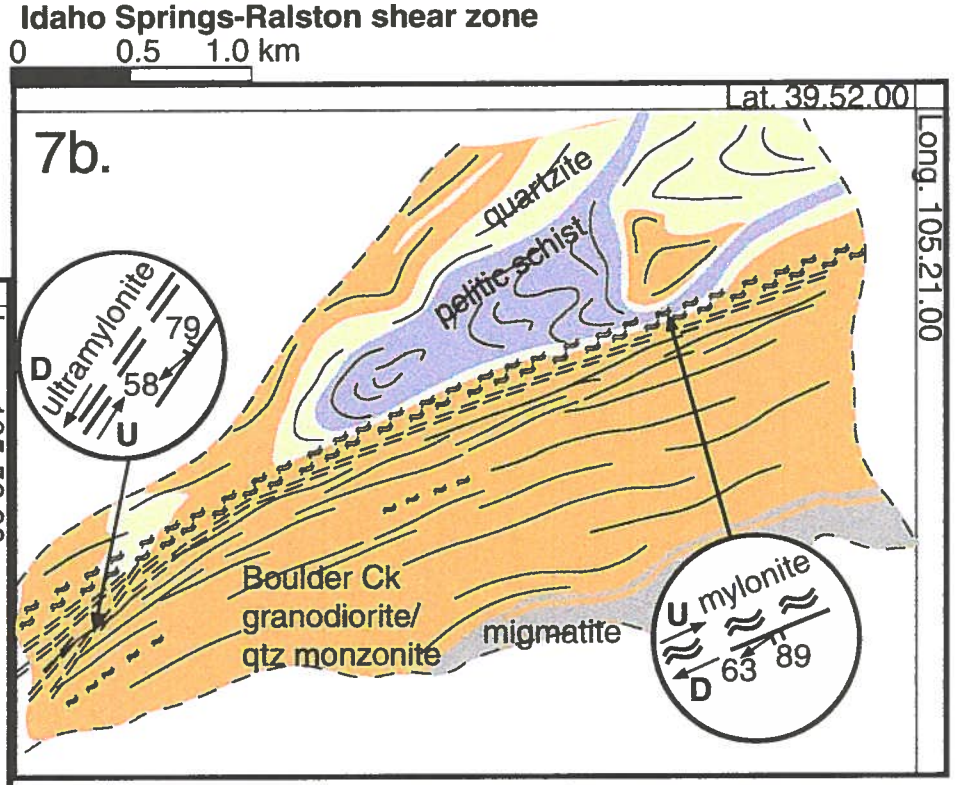

Figure 7b: Map of the central part of Idaho Springs-Ralston shear zone north of Ralston Creek in Golden Gate State Park. The shear zone follows the south contact of Coal Creek quartzite/schist and granites of the Boulder Creek batholith. S1 is folded by open to tight S2 folds in the map-scale Coal Ck synform. S1 is transposed into S2 along NE-trending high strain domains in granite along the south contact with quartzite/schist. SE-side down mylonites reactivate S2, and are overprinted by SE-side up ultramylonites. The south part of Idaho Springs-Ralston shear zone, not included in this map, contains SE-side up phyllonites that moved synchronously with emplacement of the adjacent 1.42 Ga Silver Plume pluton. See Appendix 8 for more detailed mapping.

shear zone segment, Shaw et al. (2001) recognized the development and transposition of an early Paleoproterozoic low-angle S1 fabric synchronous with granite intrusion and migmatization, the steepening of that fabric during the formation of NE-trending, subvertical, S2 high temperature high-strain zones, and the reactivation of those high-strain zones with the formation of ca.1.4 Ga mylonites and ultramylonites. Shaw et al. (2001) used in situ electron microprobe monazite dating to constrain the development or reactivation of S1 at 1700 +/- 7 Ma, movement along S2 at 1658 +/- 5 Ma and 1637 +/- 13 Ma, SE-side down mylonitization at 1376 +/- 11 Ma, and SE-side up ultramylonitization after 1376 Ma. Many features of the Homestake shear zone of Shaw et al. (2001) are common to each shear zone segment of the Colorado Mineral Belt shear zone system. Therefore, we use the Homestake study of Shaw et al. (2001) as a benchmark – a basis for comparison of the major shear zone segments of the Colorado Mineral Belt shear zone system.

In the following sections, I describe the general map patterns along the Colorado Mineral Belt shear zone system, including the geometry and possible relationships between each shear zone segment, and rock types observed along each segment. Then, I present the details of the Paleoproterozoic ancestry of

each segment, including the earliest preserved structures and the steepening of that early fabric into subvertical high temperature high-strain domains, and the timing of deformation associated with the development of these structures. Finally, I present the details of the Mesoproterozoic mylonites/ultramylonites that overprint the Paleoproterozoic subvertical high temperature high-strain domains and that define the discrete geometry of the Colorado Mineral Belt shear zone system. I then document the timing of movement of these Mesoproterozoic mylonites/ultramylonites.

As I describe each common shear zone feature in this paper, I first describe the feature as it is expressed in the Homestake shear zone, then in the Gore Range shear zone, the St. Louis Lake shear zone, and the Idaho Springs-Ralston shear zone. In this way, each description begins with the southernmost and most well-studied shear zone segment (the Homestake), and progresses northeastward along the length of Colorado Mineral Belt shear zone system.

3.1 MAP PATTERNS

The mylonite and ultramylonite shear zone segments of the Colorado Mineral Belt shear zone system lie along the northern edge of the Colorado Mineral Belt (Fig. 1). The segments appear to represent en echelon shears and branches of a shear zone system, or even one continuous shear zone, if Laramide dextral motion has offset it (Fig. 5). The Homestake shear zone disappears under Phanerozoic cover east of the Eagle River in the northern Sawatch Range. Where Proterozoic rocks surface again, just east of Vail Pass, the Gore Range shear zone segment is directly along strike of the 044, 79S Homestake shear zone. About 10 kilometers north, and parallel to the Gore Range shear zone, several NE-trending ultramylonite strands are present at Booth Lake. These strands are considered part of the Colorado Mineral Belt shear zone system, but are not discussed in detail in this paper.

The northeast extent of the Gore Range shear zone segment bends northward to an orientation of 210, 76W just before it disappears beneath the Phanerozoic cover of the Blue River Valley (Fig. 5). If projected across the Blue River Valley and Williams Fork Range at this orientation, the Gore Range shear zone connects with the St. Louis Lake shear zone. About ten kilometers west of

the St. Louis Lake shear zone, several mylonite strands deform Silver Plume granite at Berthoud Pass. In this paper, these few strands are considered to be part of the St. Louis Lake shear zone because of similar orientations, shear sense, and timing of movement.

The Idaho Springs-Ralston shear zone segment is not along strike with the St. Louis Lake shear zone, but is roughly aligned with the trend of the Homestake shear zone (Fig. 5). Ancestral Rockies and/or Laramide movements along the Loveland Pass-Berthoud Pass fault system may have caused dextral strike-slip offset of tens of kilometers between the St. Louis Lake and the Idaho Springs-Ralston shear zones.

In each mylonitic shear zone segment of the Colorado Mineral Belt shear zone system, kilometer-wide mylonite zones contain multiple parallel mylonite strands that are one to tens of meters wide. The shear zones also contain ultramylonite strands that are typically narrower than mylonite strands.

Each mylonitic shear zone segment is E- to NE-trending, with trends ranging from 090° to 028° (Fig. 8a; Table 1), although the northeast trends dominate. The shear zone segments are subvertical and dip steeply to the

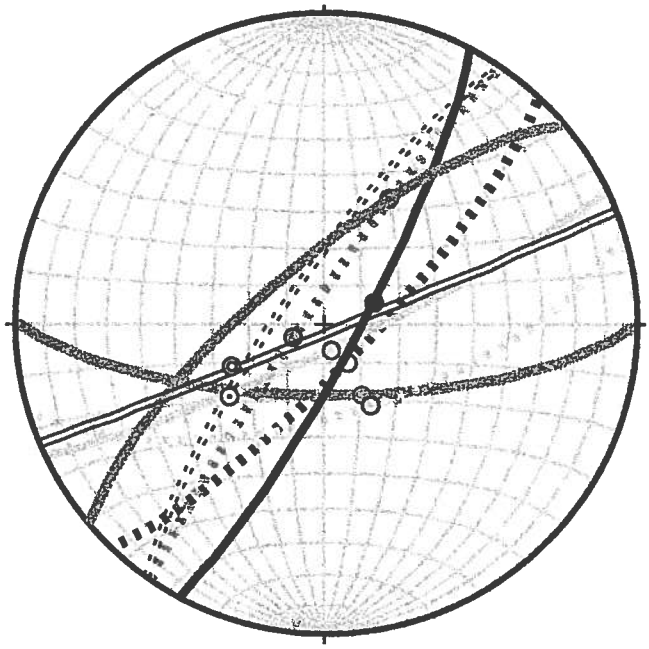

Figure 8a: Equal area projection of mylonite and ultramylonite orientations, and associated mineral stretching lineations. All zones are subvertical and have steeply-plunging mineral stretching lineations. Plotted data are listed in Table 1.

- SE-side down mylonite Homestake
- SE-side up ultramylonite Homestake
- SE-side down mylonite Gore Range
- SE-side up ultramylonite Gore Range
- SE-side down mylonite St. Louis Lake
- SE-side up mylonite St. Louis Lake
- SE-side down mylonite Idaho Springs-Ralston
- SE-side up ultramylonite Idaho Springs-Ralston

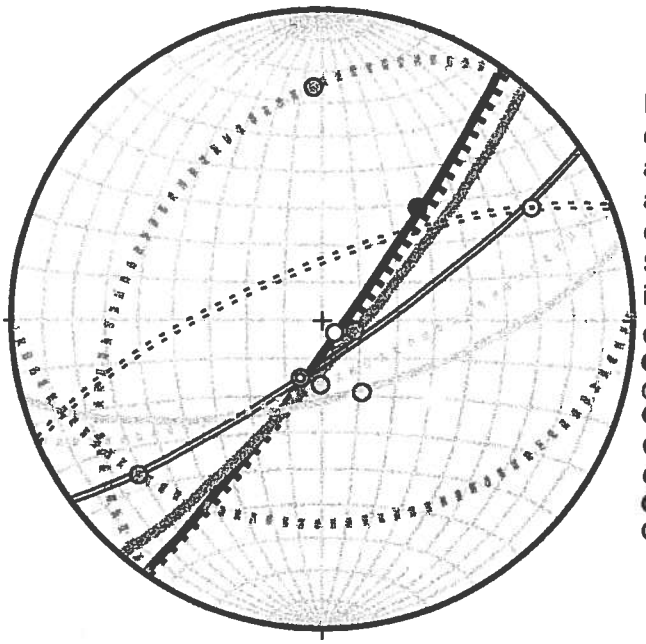

Figure 8b: Equal area projection of S2 high-strain domain orientations and associated mineral stretching lineations, and axial planes and fold axes of F2 folds contained in macrolithons spaced between S2 domains. Plotted data are listed in Table 2.

- S2 Homestake
- F2 Homestake
- S2 Gore Range
- F2 Gore Range
- S2 St. Louis Lake
- F2 St. Louis Lake
- S2 Idaho Springs-Ralston
- F2 Idaho Springs-Ralston

*Figures 8a and 8b show average orientations. For more detailed structural data and equal area projections, see Appendices 4 and 5.

northwest or southeast, with dips ranging from 74° to the northwest to 66° to the southeast. They contain steeply-plunging mineral stretching lineations.

Table 1: Average orientations of mylonite fabrics. Field measurements of Proterozoic structures and fabrics reported in this text have not been restored to their Proterozoic orientations. However, Table 3 (Appendix 2) presents the values of important Proterozoic shear zone orientations as restored according to regional field and paleomagnetism studies. Table 3 includes the restored values of the field measurements presented in Table 1 and Table 2 in this text. Appendix 2 also includes a brief discussion of studies used to restore each shear zone.

	Shear zone	Homestake	Gore Range	St. Louis Lake	Idaho Spgs-Ralston
SE-side up mylonite/phyllonite	strike and dip			073, 66S	085, 72N
	trend and plunge			65 to 150	32 to 062
SE-side down mylonite (overprints SE-side up mylonite at Idaho Spgs-Ralston)	strike and dip	044, 79S	090, 71S/ 230, 74N		068, 89S
	trend and plunge	78 to 147	68 to 152/ 52 to 028		63 to 246
S5 SE-side up ultramylonite (overprints SE-side down mylonite at Homestake)	strike and dip	028, 81E	214, 85W		214, 79W
	trend and plunge	76 to 067	81 to 248		58 to 232
S6 SE-side down mylonite (overprints SE-side up mylonite at St. Louis Lake)	strike and dip			065, 83S	
	trend and plunge			82 to 165	

In all of the shear zone segments, mylonites and ultramylonites overprint NE-trending domains of Paleoproterozoic, high-strain, upper amphibolite grade tectonites. In the Homestake and Gore Range shear zones, mylonites and ultramylonites overprint high-temperature tectonites in biotite gneiss and migmatite (Fig. 6a,b). At St. Louis Lake, mylonites and ultramylonites overprint high-temperature tectonites in a tectonic melange primarily composed of amphibolite and granodiorite (Fig. 7a). Along the Idaho Springs-Ralston shear zone, mylonites and ultramylonites overprint high-temperature tectonites in quartz monzonite along the southern limb of the Coal Creek synform (Fig. 7b).

Although most of the shear zone segments do not appear to separate regions with distinctly different structures or metamorphic histories, they all show juxtaposition of different rock types that hint at the long tectonic evolution of the zone. The St. Louis Lake shear zone segment overprints a tectonic melange containing boudinaged rocks of oceanic affinity. This tectonic melange contains marble, calc-silicates, quartzite, biotite schist, and amphibolite, with boudins of gabbro and ultramafic rocks, all interlayered on the mesoscopic to map scales (Fig. 7a). The rock types within this melange are similar to the rock types in melanges identified within continent-arc collision zones (Chang et al., 2000; Polat

and Kerrich, 1999). The presence of this isolated fragment of oceanic melange, surrounded by granites and mica schists, suggests that the shear zone has an ancestry as a lithospheric scale structure that facilitated transport and tectonic juxtaposition of far-travelled rocks. The significance of this melange is discussed in greater detail in the discussion section of this thesis.

The Coal Creek quartzite/pelitic schist sequence along the Idaho Springs-Ralston shear zone is one of several isolated Proterozoic meta-quartz arenites in central and northern Colorado (Fig. 7b; Finiol, 1994). These quartzites are characterized as 'mature' from a petrographic standpoint, containing few oxide minerals or micas, and often appear to have been deposited on rhyolites or granites. The relationship between the Coal Creek quartzite and the surrounding granite is unclear, and is addressed in detail later. The Coal Creek synform, along the Idaho Springs-Ralston shear zone, preserves a remnant of what may have once been a more continuous quartzite 'cover' sequence.

The shear zones typically follow Paleoproterozoic pluton margins (Fig. 4), and show evidence for deformation synchronous with Paleoproterozoic pluton emplacement. In the Homestake and Gore Range shear zones, mylonites follow the southern margin of the Cross Creek batholith (~1675 [Rb-Sr], Tweto and

Lovering, 1968). In the St. Louis Lake and Idaho-Springs Ralston shear zones, mylonites follow the southern margin of the Boulder Creek batholith (1721 +/- 15 Ma [U-Pb SHRIMP], Premo and Fanning, 2000). Along each shear zone segment, biotite schist is interlayered and transposed with granite stringers and dikes, with late granite and pegmatite dikes cutting across the foliation, suggesting that granite intrusion outlasted deformation. Along the Homestake and Gore Range shear zones, there is evidence for widespread migmatization (Fig. 6a,b).

The shear zones also typically follow Mesoproterozoic pluton margins (Fig. 4), and show evidence for deformation synchronous with Mesoproterozoic pluton emplacement, yet these shear zone segments also extend tens of kilometers beyond the pluton margins. This relationship indicates that shear zone movement was not isolated along the margins of individual plutons, but part of a more regional system. In the Homestake shear zone, mylonites also follow the northern margin of the Mesoproterozoic St. Kevin batholith (1396 +/- 40 Ma [U-Pb], Doe and Pearson, 1969) and show evidence for syn-plutonic mylonitization (Shaw et al., 2001). SE-side down mylonites deform granite of the St. Kevin batholith, but are also cut by undeformed granite dikes of the St. Kevin (Shaw et

al., 1999). SE-side up mylonites in the St. Louis Lake shear zone, and SE-side up phyllonites in the Idaho Springs-Ralston shear zone, follow the margins of the Mesoproterozoic Silver Plume pluton (1422 +/- 3 Ma [U-Pb], Hedge, 1969). At St. Louis Lake, within a few meters of the Silver Plume pluton margin, the granite is undeformed, yet the gabbroic country rock has narrow mylonite strands giving SE-side up shear sense. This field relationship suggests that mylonitization took place before the emplacement of the granite, because the highly competent gabbro is mylonitized while the less competent granite is not. However, some Silver Plume granite dikes are mylonitized with SE-side up shear sense, while other dikes are undeformed and cross-cut these mylonites, indicating pre- to syn-plutonic mylonitization (Fig. 7a). The Idaho Springs-Ralston shear zone also follows the margin of the Mt. Evans pluton (1442 +/- 2 Ma [U-Pb], Aleinikoff et al., 1993), and there is field evidence for mylonitization synchronous with pluton emplacement. One strand of the Idaho Springs-Ralston shear zone ends in a series of synmagmatic to late-magmatic subparallel shears in the Mt. Evans pluton and late pegmatites cut mylonitized Mt. Evans granodiorite (Nyman et al., 1994; Graubard and Mattinson, 1990).

3.2 PALEOPROTEROZOIC STRUCTURES ALONG THE COLORADO MINERAL BELT SHEAR ZONE SYSTEM

Because map patterns show close spatial relationships between Mesoproterozoic mylonite shear zone segments and Paleoproterozoic high strain domains, plutons, and tectonic melanges, the shear zones appear to have a Paleoproterozoic ancestry. Here, I describe a progression of Paleoproterozoic fabrics and structures observed along each shear zone segment, further supporting the idea of a common Paleoproterozoic ancestry.

Within several tens of kilometers of each shear zone segment, shallow foliations in typically migmatitic biotite schist may be observed in kilometer wide domains. Within a few kilometers of each shear zone segment, these early S1 shallow fabrics are folded into open to isoclinal NE-trending F2 folds and steepened into NE-trending, subvertical, S2 high-strain domains of intensified foliation. In contrast to the 'swirling' foliation patterns described in central Colorado by Reed et al. (1987), it appears that fold interference patterns, created by the folding of S1 by F2 and transposition of S1 into S2 high temperature high strain domains, have produced the observed complex map patterns in the Paleoproterozoic rocks along the Colorado Mineral Belt shear zone system.

3.3 D1 LOW ANGLE FOLD AND FOLIATION DEVELOPMENT

The early low angle fabrics are composites of transposed foliations, defined as S1a/S1b/S1c in the Homestake and Gore Range shear zones (Shaw et al., 2001), and S1a/S1b in the St. Louis Lake and Idaho Springs-Ralston shear zones (Fig. 9a,b,c). S1a, defined by aligned sillimanite needles, elongate biotites, and attenuated quartz and granite stringers, has been transposed into isoclinal, recumbent F1b folds. In the Homestake and Gore Range shear zones, S1b has been dragged into asymmetric folds with axial plane S1c. These asymmetric folds are of variable tightness, but are always z-shaped folds in map view, with consistent vergence with respect to S1a/b. Granite stringers are parallel to S1a/b and also follow the axial plane of S1c (Shaw et al., 2001). The terminology S1a/S1b/S1c implies that the development of S1 foliation and the transposition of that foliation occurred during progressive deformation that created an S1 composite foliation.

Adjacent to the Homestake, Gore Range, and St. Louis Lake shear zones, there is evidence that S1 developed during granite and granodiorite intrusion associated with emplacement of the Cross Creek (~1675 [Rb-Sr], Tweto and

Figure 9: Documentation of F1b along Idaho Springs-Ralston shear zone. a. Mesoscopic scale F1b isoclinal folds folded by F2. b. Microscopic scale quartzite layer folded by F1b isoclinal fold in F2 hinge region. F1b crenulation defined by folded micas and sillimanite in close-up view. c. Microscopic scale F1b tight folds in F2 hinge region.

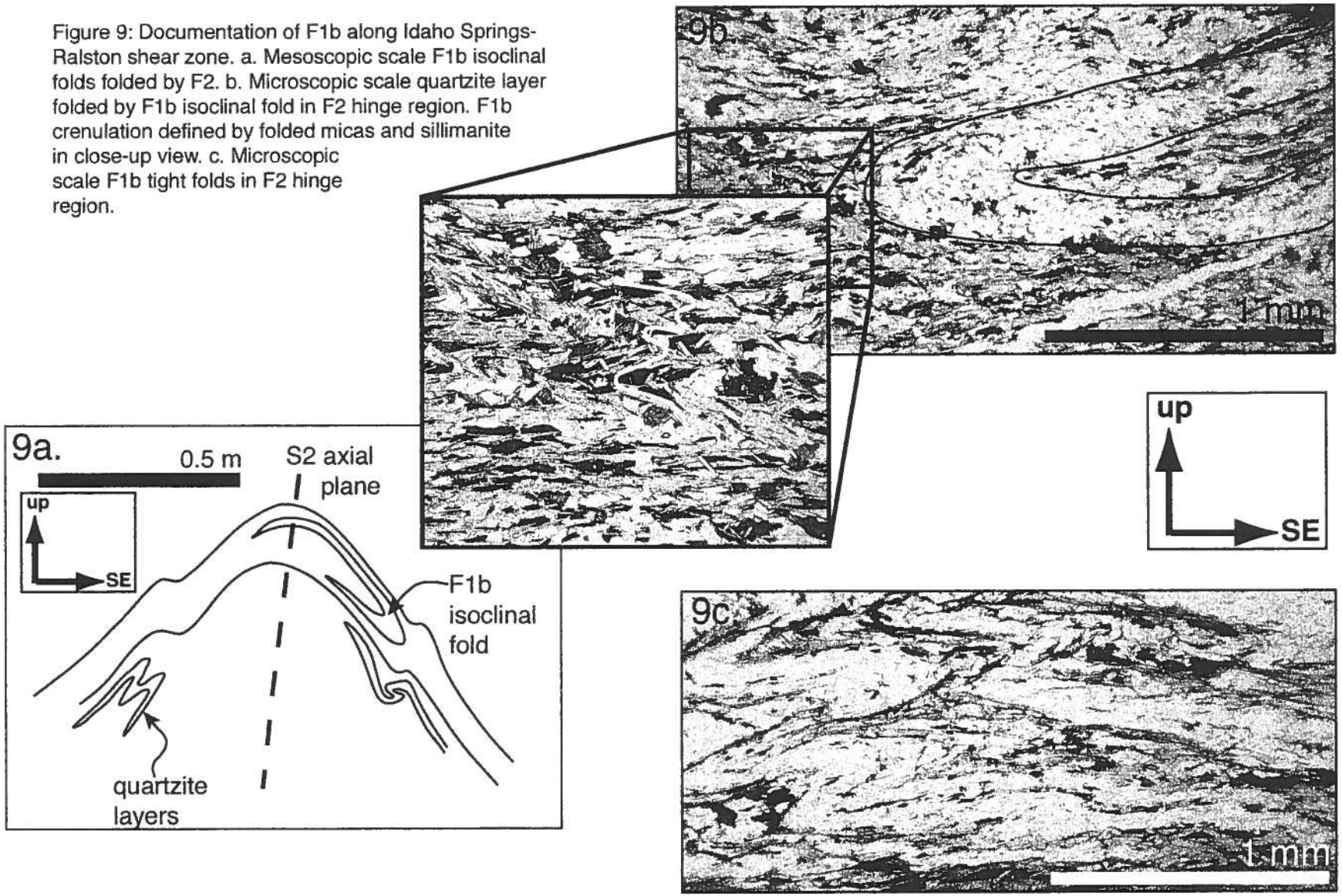

Lovering, 1968) and Boulder Creek (1721 +/- 15 Ma [U-Pb SHRIMP], Premo and Fanning, 2000) batholiths, which are located along the northern boundaries of the shear zone system. In the Homestake and Gore Range shear zones, Cross Creek granite dikes and stringers are interlayered and transposed along S1a/S1b/S1c in biotite schist and migmatite. In the Homestake shear zone, Shaw et al. (2001) suggest that undated granodiorite that intruded during S1a/b foliation development was coeval with Cross Creek batholith intrusion. In the Gore Range, magma mingling and cross-cutting relationships also suggest that granodiorite and diorite intruded during Cross Creek granite emplacement, possibly providing a heat source for the observed widespread migmatization. Unfoliated to weakly foliated post-D1 granite dikes cross-cut S1a/S1b/S1c in variable orientations (Appendix 4), indicating that granite intrusion outlasted D1. Along the St. Louis Lake shear zone, granite and granodiorite are also interlayered and transposed with S1a/S1b in a tectonic melange, with late granite dikes cutting across foliation.

Along the Idaho Springs-Ralston shear zone, the Coal Creek quartzite/schist sequence contains discrete layers of quartzite and pelitic schist that allow mapping of compositional layering, which represents bedding and

cross-bedding, and mapping of foliation surfaces. Thus, the mapping of the Coal Creek quartzite/schist sequence provides a better understanding of the Paleoproterozoic folds and foliation generations along the Colorado Mineral Belt shear zone system (Fig. 7b). This is in contrast to the Homestake, Gore Range, and St. Louis Lake shear zones, where map scale structures in gneisses and migmatites are largely defined based on mapping of foliation trajectories and observations of mesoscopic structures. Unlike the metavolcanic rocks and biotite schists along the other shear zone segments, the Coal Creek quartzite also contains cross bedding that allows determination of younging direction.

Along the Idaho Springs-Ralston shear zone, the Coal Creek quartzite/schist sequence and granitic rocks of the Boulder Creek batholith show S1 fabric that is parallel to the metasediment/granite contact and bedding planes in the quartzite. The metasedimentary rocks show S1a foliation folded into mesoscopic scale F1b isoclinal folds with fold axes that plunge 10 to 35 degrees to the NE (Fig. 9a,b,c). Younging direction in Coal Creek quartzite, defined by cross-beds, alternates from one quartzite layer to the next, suggesting that F1b has folded the package of rocks on map scale (Fig. 10a,b).

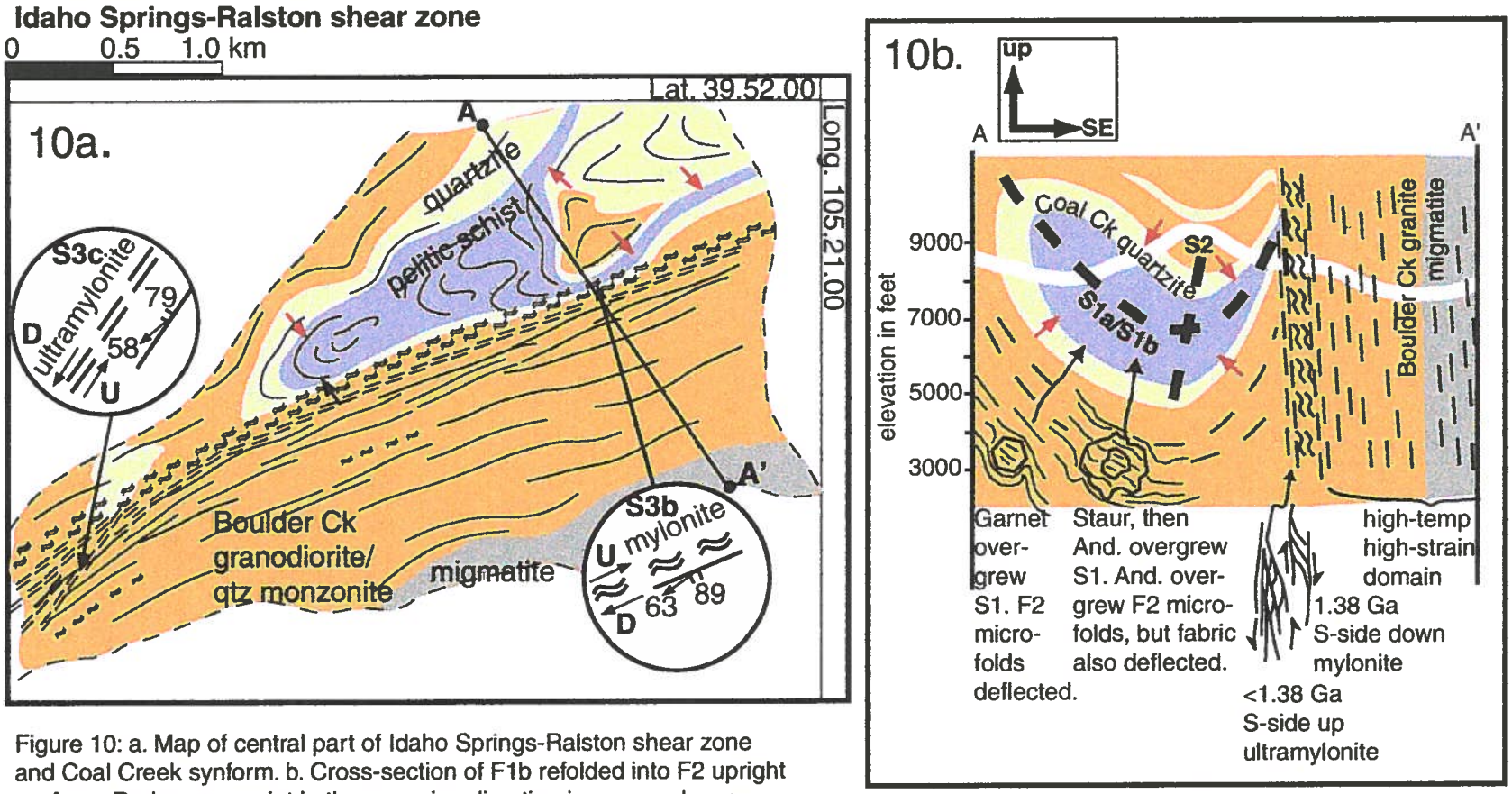

Figure 10: a. Map of central part of Idaho Springs-Ralston shear zone and Coal Creek synform. b. Cross-section of F1b refolded into F2 upright synform. Red arrows point in the younging direction in map and cross-section.

3.4 P-T CONDITIONS OF D1 DEFORMATION

Most of the biotite gneisses, migmatites, amphibolites, and calc-silicate rocks along the Colorado Mineral Belt shear zone system contain metamorphic assemblages that are not particularly useful in determining pressure and temperature conditions associated with deformation stages. The rocks that do contain suitable assemblages, such as biotite-garnet migmatites from the Gore Range shear zone and pelitic schists from the Idaho Springs-Ralston shear zone, provide small fragments of metamorphic histories recorded along these shear zone segments.

Along the Gore Range shear zone, metamorphic assemblages in migmatites with a strong S1 foliation help define metamorphic conditions during D1. Peak temperature conditions are recorded by the assemblage quartz + biotite + garnet + K-feldspar + plagioclase + sillimanite, with prismatic sillimanite oriented within S1. The presence of sillimanite and K-feldspar and absence of prograde muscovite indicates metamorphism on the high-temperature side of the second sillimanite isograd (Fig. 11). The presence of biotite selvages, in which quartz and feldspars are absent and biotite grains have cuspate edges, suggests the melting reaction albite + K-feldspar + quartz + H_2O -> liquid (Spear, 1993).

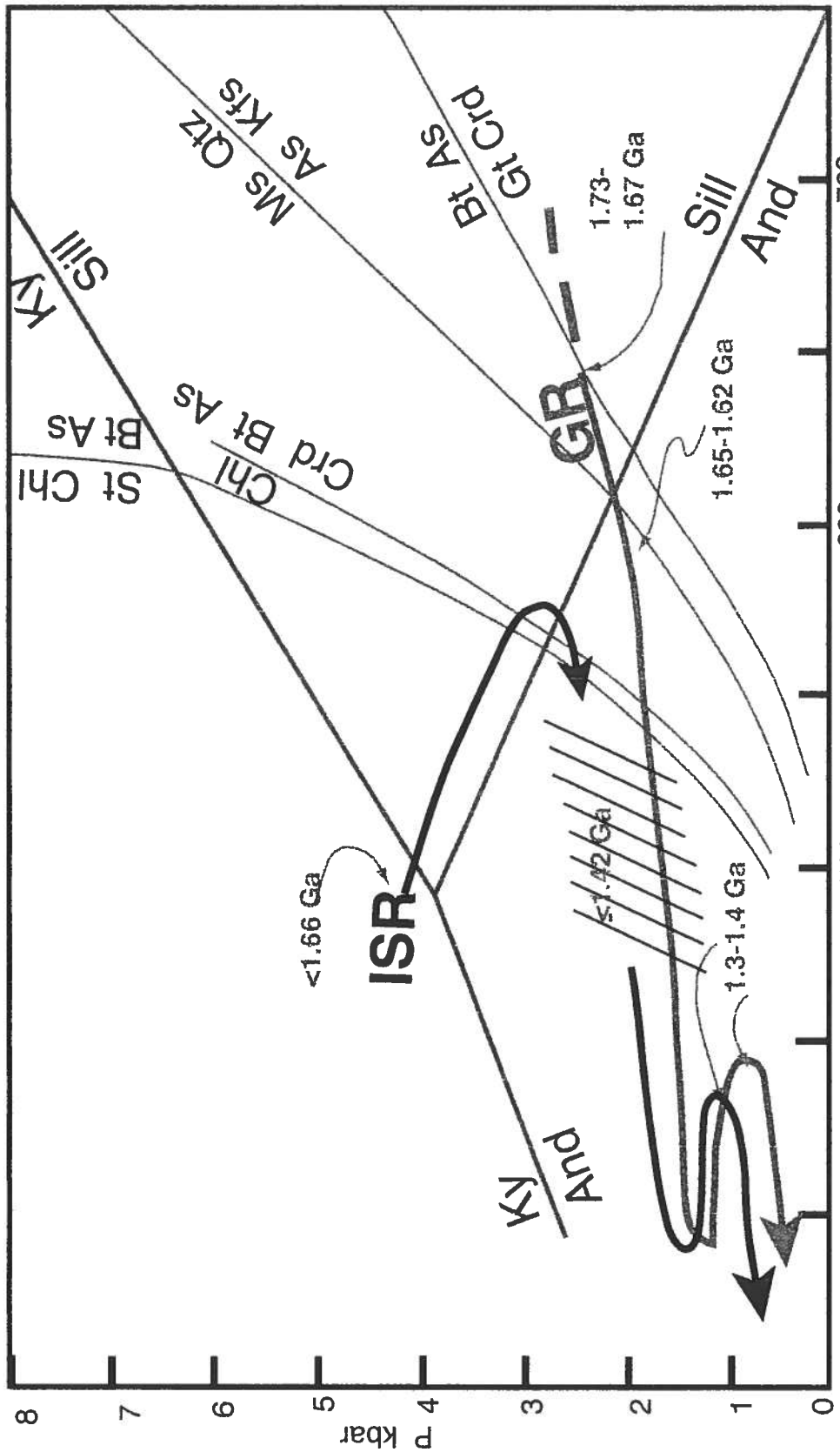

Figure 11: Schematic P-T-t paths for Gore Range (medium gray) and Idaho Springs-Ralston (black) assemblages. Reaction curves are from Spear (1993) and Pattinson et al. (1999).

In some samples, the presence of pinnite and garnet suggests that the high-temperature side of the biotite + aluminosilicate -> garnet + cordierite reaction line may have been crossed at the time of peak metamorphism, with cordierite altering to pinnite during subsequent retrogression (Fig. 11). Textural relationships do not support the reaction garnet +aluminosilicate + quartz -> cordierite because pinnite is not found adjacent to garnet or rimming garnet.

3.5 D2 HIGH ANGLE FOLD AND HIGH STRAIN DOMAIN DEVELOPMENT

Along the Colorado Mineral Belt shear zone system, the S1 composite fabric is folded into F2 folds with NE-trending axial planes (Fig. 8b). The enveloping surfaces of F2 folds are subhorizontal, such that unfolding F2 results in the initial low-angle S1 orientations (Moench, 1964). Open to isoclinal F2 folds with shallowly plunging fold axes occupy 10 to 100 meter wide macrolithons spaced between subvertical high-strain domains oriented subparallel to S2 axial plane cleavage. Near these S2 high-strain domains, F2 folds tighten and F2 axial planes steepen. F2 fold axes become sub-parallel to the steeply-plunging mineral stretching lineations of the high-strain domains. Thus, D2 appears to have resulted in the development of F2 folds as well as S2 high-strain domains.

The following descriptions of subvertical S2 high-strain domains, developed parallel to the axial planes of F2 folds, are in contrast to the model of Moench (1964), who proposed that high-strain zones along the Idaho Springs-Ralston shear zone reactivated the limb regions of F2 folds.

Table 2: Average orientations of S2 high-strain domains and F2 folds.

	Shear zone	Homestake	Gore Range	St. Louis Lake	Idaho Spgs-Ralston
S2 hi-T tectonite	strike and dip	035, 85E	040, 82E	075, 69S	055, 82 S
	trend and plunge	85 to 125	82 to 101	69 to 152	74 to 198
F2	Axial plane strike and dip	035, 85E	215, 37W/ 089, 34S	067, 75S	248, 74 N
	Fold axis trend and plunge	51 to 041	25 to 358/ 22 to 230	73 to 181	25 to 062

Adjacent to the Homestake shear zone, macrolithons that contain F2 folds with subvertical, NE-trending axial planes and moderately plunging fold axes, are spaced between subvertical, NE-trending S2 high-strain domains that have down-dip mineral stretching lineations (Fig. 6a, Fig. 8b, Table 2).

Similarly, in the area surrounding the Gore Range shear zone, macrolithons that contain tight to isoclinal F2 folds are spaced between

subvertical, NE-trending S2 high-strain domains with near down-dip mineral stretching lineations (Fig. 6b, Fig. 8b, Table 2). Along the Gore Range shear zone, some S2 high-strain domains contain asymmetric feldspar augen and melt-filled shear bands that define shear sense. When viewed perpendicular to S2 foliation and parallel to mineral stretching lineations, these asymmetric clasts and fabrics typically indicate SE-side up shear sense. However, most of the S2 high-strain domains along the Colorado Mineral Belt shear zone system do not give unequivocal shear sense and are mainly distinguished from surrounding migmatites and gneisses by intensified foliations, evidence for grain size reduction, and stronger mineral stretching lineations in the domains.

A few hundred meters beyond the S2 domains along the Gore Range shear zone, mesoscopic and map scale F2 folds have average axial planes that dip shallowly to the northwest and southeast, with shallowly plunging fold axes that range between 25 to 358 and 22 to 230. The "porpoising" of F2 fold axes is probably due to a subsequent gentle folding event, with fold axes that trend nearly perpendicular to F2 fold axes. In one outcrop, an open fold with average axial plane of 112, 59S and fold axis 33 to 279 folds F2.

Along the St. Louis Lake shear zone, macrolithons containing isoclinal F2 folds with subvertical, NE-trending axial planes and steeply-plunging fold axes are spaced between subvertical, NE-trending S2 high-strain domains with near down-dip mineral stretching lineations (Fig. 7a, Fig. 8b, Table 2). Away from the S2 high-strain domains, tight F2 folds have axial planes that dip moderately to the southeast, and fold axes that range between 38 to 204 to 24 to 097.

Along the Idaho Springs-Ralston shear zone, the Coal Creek quartzite/schist sequence and granite are refolded into the map scale F2 Coal Creek synform with a NE-trending, subvertical axial plane and fold axis that plunges shallowly to the northeast (Fig. 7b, Fig. 8b, Table 2). At the contact between the Coal Creek quartzite/schist sequence and Boulder Creek granite, the south limb of the F2 synform sweeps into a NE-trending, subvertical S2 high-strain domain with a steeply-plunging mineral stretching lineation.

3.6 P-T CONDITIONS OF D2 DEFORMATION

S2 high-strain domains are composed of high temperature tectonites with deformational textures and mineral assemblages that are distinct from the Mesoproterozoic mylonites and ultramylonites that overprint them. S2 high-strain

domains contain small, recrystallized grains of quartz that are interlocked in polygonal patterns, suggesting that grain boundary area reduction was an important mechanism during the late stages of deformation (Fig. 12a; Passchier and Trouw, 1996). Also present are small, recrystallized grains of feldspar. Mineral stretching lineations are typically defined by hornblende needles or sillimanite needles (Fig. 12b). The observed microstructures and mineral assemblages indicate deformation temperatures that exceed 500°C (Tullis and Yund, 1992; Spear, 1993) and are higher temperature tectonites than the mylonites that overprint them.

Migmatites, pelitic schists, and quartzites found in S2 domains or in hinge regions of tight F2 folds document the P-T conditions of D2. The transition from D1 to D2 appears to have been accompanied by retrogression. Garnets, present in migmatites with a strong S1 foliation folded by F2, show evidence for this retrogression. The garnets have reaction rims that contain andalusite and biotite (Fig. 13a,b). Pinnite is present throughout the sample, suggesting the early coexistence of garnet and cordierite, and later retrogression of cordierite. A possible reaction is garnet + cordierite -> biotite + andalusite (Spear, 1993), with

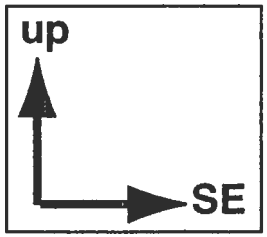

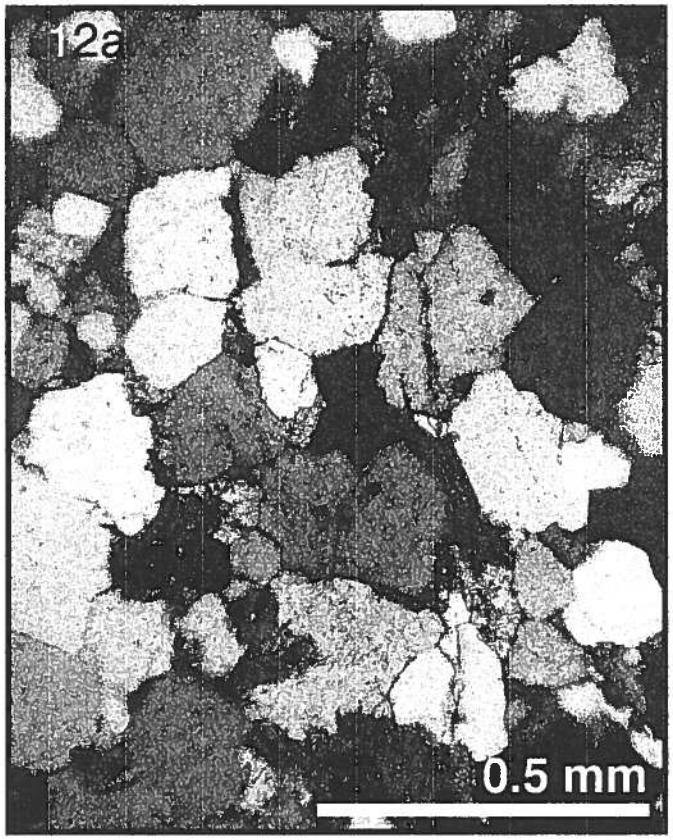

Figure 12: a.In this subvertical S2 high strain domain, along Gore Range shear zone, quartz textures show dominance of recovery processes during late stages of D2 deformation. Polygonal, relatively strain-free grains of quartz are not elongate parallel to subvertical S2 foliation. b. foliation is defined by aligned sillimanite needles, micas, and leucosomes.

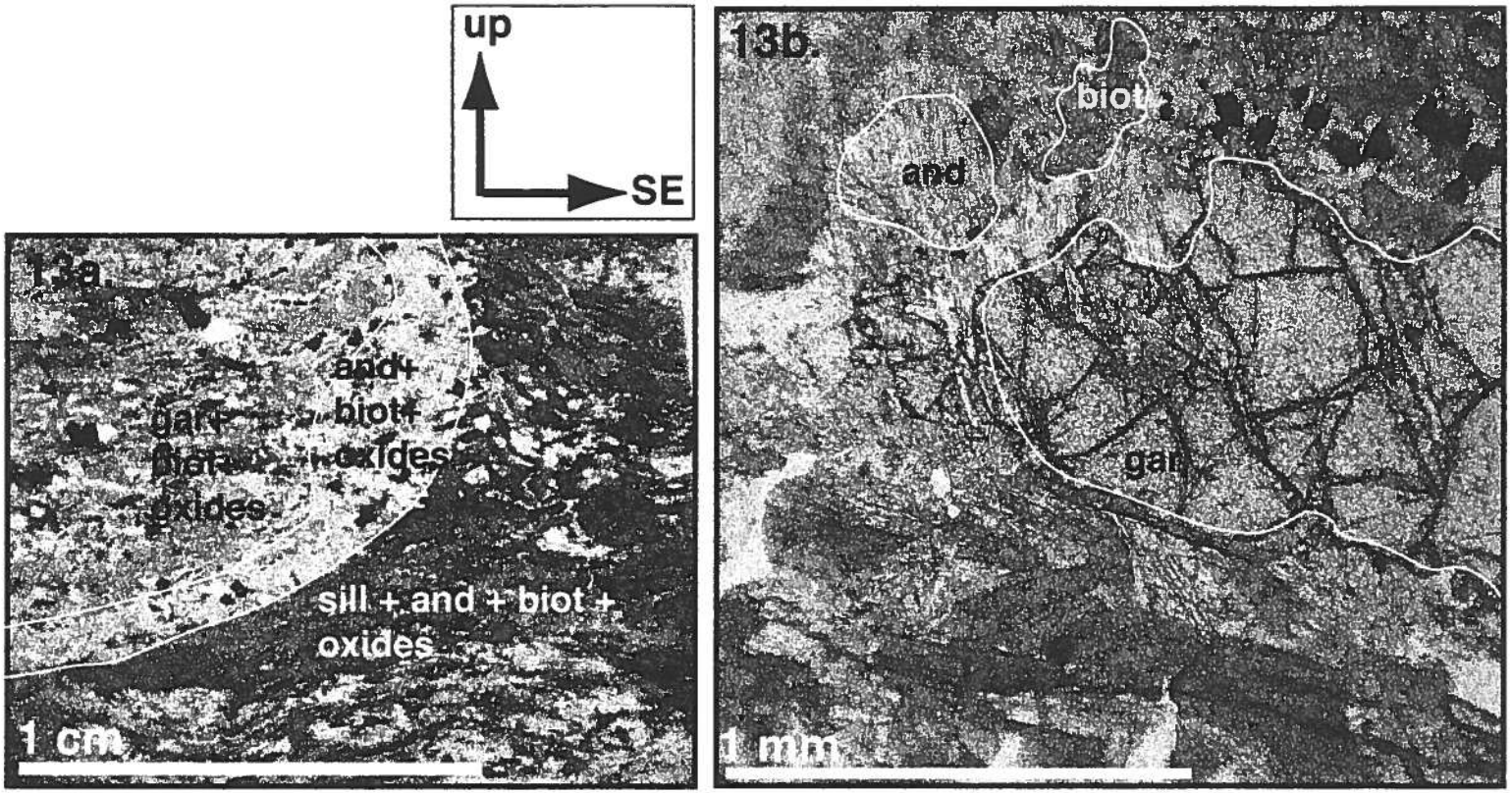

Figure 13: Garnet porphyroblast rimmed and replaced by andalusite and biotite in hinge region of F2 fold, Gore Range shear zone. a. Example of rim domain on garnet. b. Detail of reaction in rim domain shown in 12a.

a transition from the sillimanite stability field to the andalusite field, and retrogression to the low-temperature side of the second sillimanite isograd.

Along the Idaho Springs-Ralston shear zone, the Coal Creek quartzite/ pelitic schist sequence helps constrain the Proterozoic structural evolution of the shear zone segment, as well as the P-T history along the segment. The metamorphic minerals present in the Coal Creek pelitic schists all overgrew S1, and provide information on P-T conditions post-D1 and during or post-D2. In many samples, andalusite forms rims around and replaces staurolite, and both minerals overgrew S1 defined by elongate oxide and quartz inclusions. In several samples, staurolite is intergrown with Fe-rich chlorite and rimmed by andalusite and biotite, suggesting the reaction staurolite + chlorite + muscovite -> andalusite + biotite + H_2O with chlorite as the limiting reactant (Fig. 14). This prograde reaction takes place between 500 and 600°C and records dehydration and an increase in temperature (Spear, 1996).

Andalusite overgrew F2 crenulations, but also appears to have deflected foliation during D2. In several locations, andalusite porphyroblasts are also bent and folded by F2 in outcrop (Finiol, 1992). These observations suggest that andalusite grew post-D1 and syn- or post-D2. Like staurolite and andalusite,

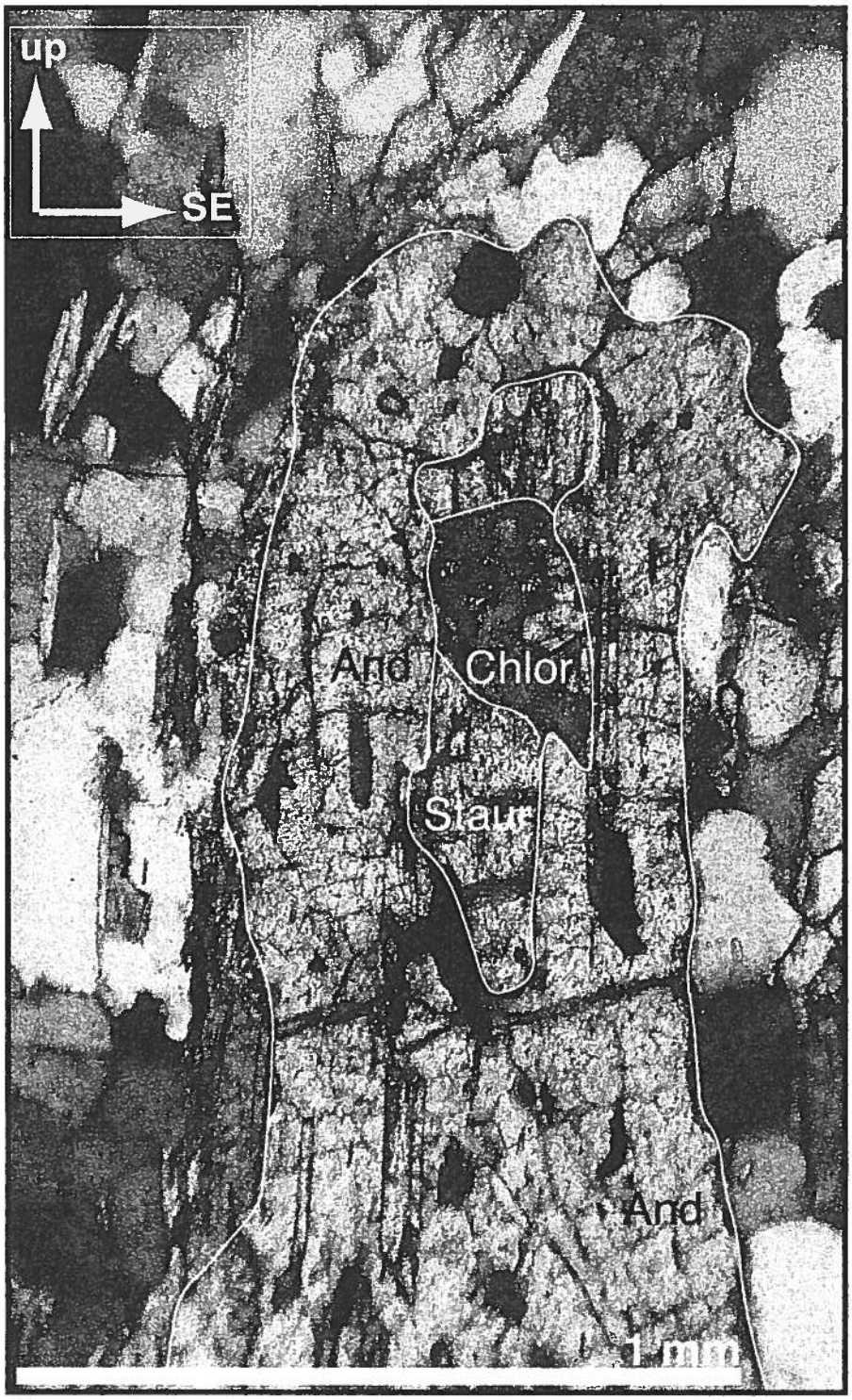

Figure 14: In the subvertical limb region of an F2 microfold, Coal Ck pelitic schist contains staurolite that is intergrown with Fe-rich chlorite and is rimmed by andalusite.

garnet overgrew S1, but also appears to have grown before F2 crenulation development, since fabric is deflected around garnets in the hinges of F2 crenulations (Fig. 15a,b,c).

Cordierite porphyroblasts overgrew S1 and F2 crenulations, and are particularly abundant in the Coal Creek synform hinge region (Fraser, 1938). In Mg-rich schists, Finiol (1992) observed staurolite with cordierite rims. The assemblage of cordierite + staurolite + aluminosilicate + biotite + muscovite is a relatively rare assemblage for pelitic schists, but has been reported for a number of low-pressure (andalusite-sillimanite) regional metamorphic terranes (Pattison et al., 1999).

Kyanite, andalusite, and sillimanite are present together in several thin sections of SE-side down mylonitized Coal Creek quartzite, and the growth of all these aluminosilicates probably occurred prior to 1.38 Ga mylonitization. Andalusite and kyanite appear to have been brittley boudinaged during mylonitization, and muscovite is present in the boudin necks and forms rims on all of the aluminosilicate minerals (Fig. 16a,b; Fig. 17a,b). In some samples, prismatic andalusite and sillimanite cluster together in 'knots' that are wrapped in muscovite. Kyanite is always rimmed by andalusite. These relationships suggest

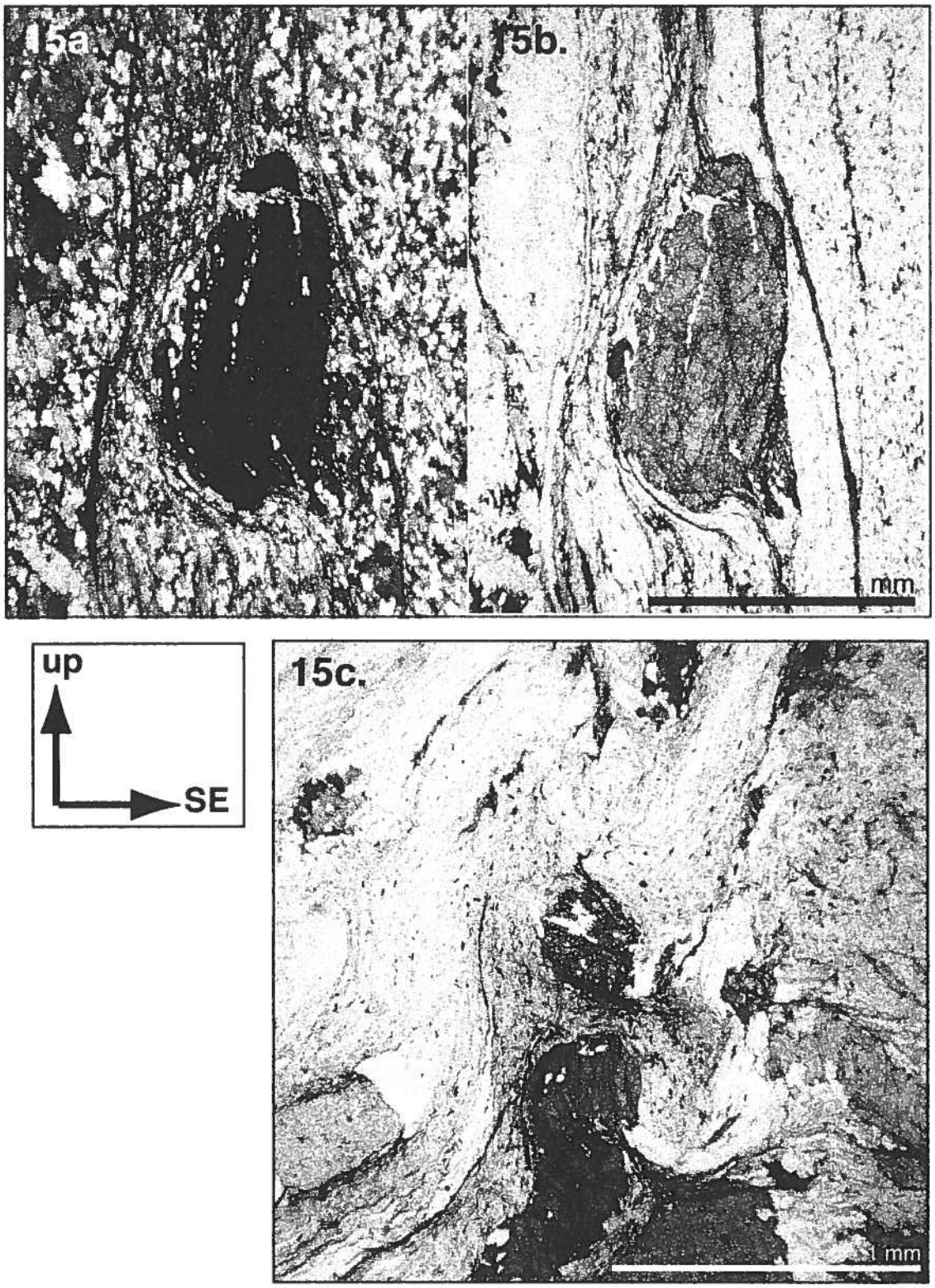

Figure 15: Garnet/matrix relationships. a.(crossed polars) and b. (plane light) Garnet appears to have overgrown S1 while rotating clockwise slightly. b. Garnet overgrew S1 and but deflected foliation during F2 folding and crenulation.

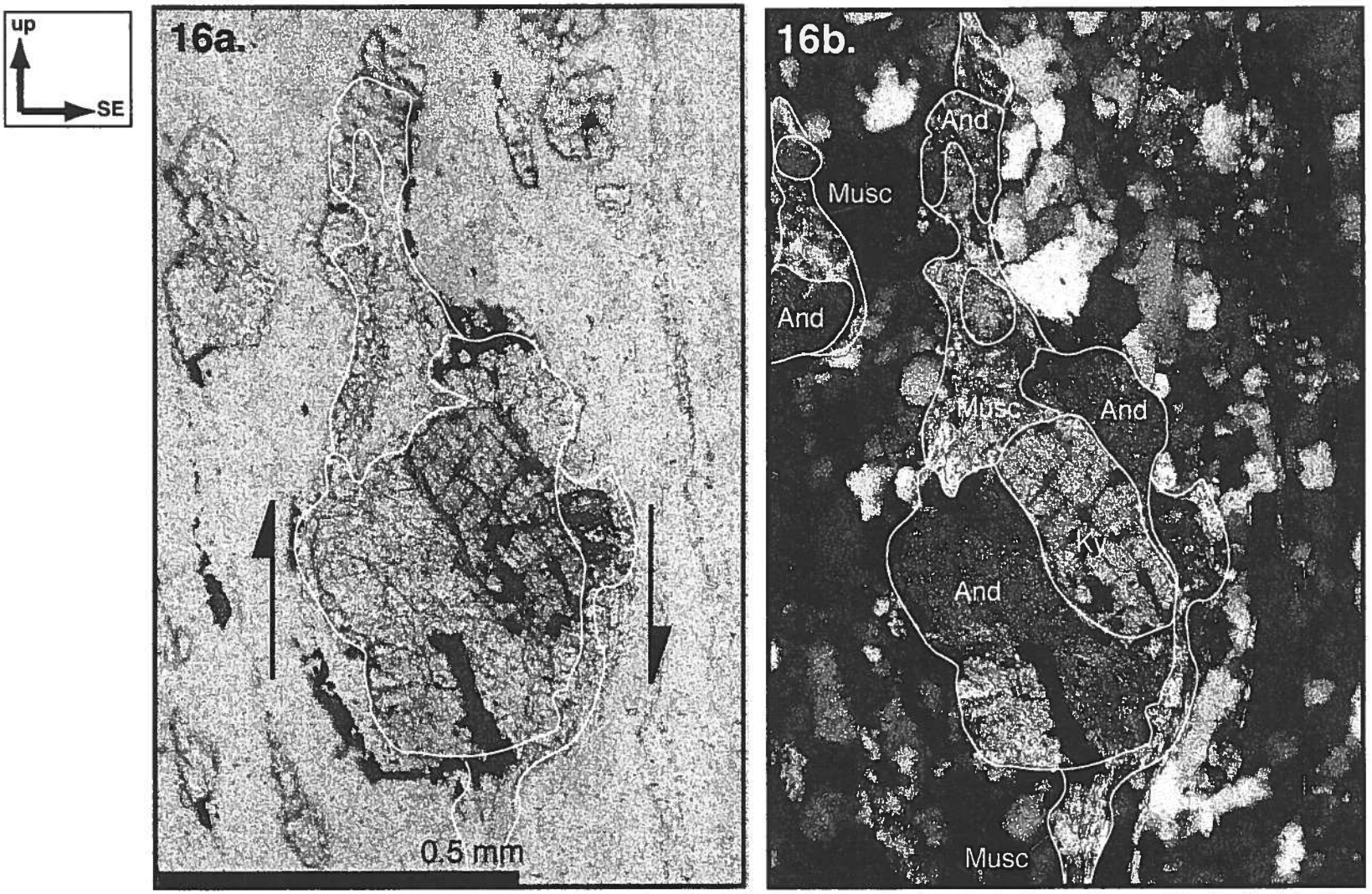

Figure 16: a. (plane light), b. (cross polars), In mylonitized Coal Ck quartzite, kyanite is rimmed by andalusite. Andalusite is boudinaged with muscovite filling the boudin neck. Muscovite also created a thin fringe around andalusite in low strain domains during SE-side down mylonitization.

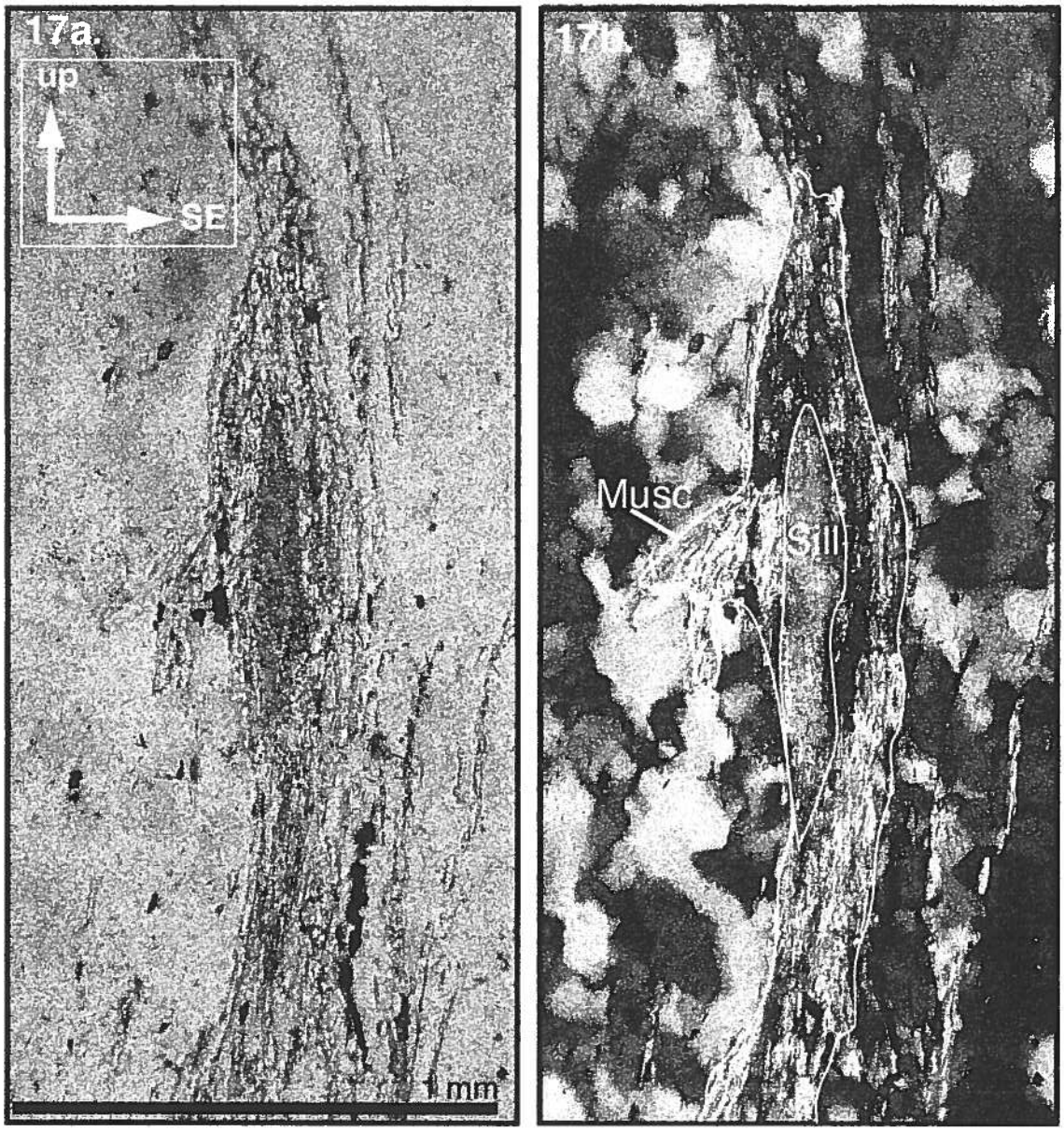

Figure 17: a. (plane light) and b. (crossed polars), In mylonitized Coal Ck quartzite, sillimanite is rimmed by muscovite.

early kyanite growth followed by a transition from the kyanite stability field to the andalusite/sillimanite stability line, prior to 1.38 Ga SE-side down mylonitization in the Idaho Springs-Ralston shear zone.

Along the Idaho Springs-Ralston shear zone, reaction textures indicate that staurolite formed early with respect to andalusite and cordierite. Garnet shows porphyroblast/matrix relationships similar to andalusite. Kyanite grew early with respect to andalusite and sillimanite. A P-T path that incorporates these observations includes prograde metamorphism at moderate depths, followed by decompression with moderate cooling (Fig. 11). The proposed clockwise P-T path appears to loop around the aluminosilicate triple point and record peak temperatures between 500 and 600°C that were achieved after the development of S1 and before or during D2. However, the observed metamorphic reactions may document two P-T paths, one Paleoproterozoic path and one Mesoproterozoic path. Without further evidence, only schematic P-T paths may be drawn (Fig. 11).

3.7 TIMING OF PALEOPROTEROZOIC DEFORMATION

In situ electron microprobe monazite age dating of Paleoproterozoic fabrics, mylonites, and ultramylonites, enabled documentation of timing of deformation along the Colorado Mineral Belt shear zone system. Monazites were located in thin section by conducting full thin section x-ray maps of Ce on the Cameca SX50 electron microprobe at University of Massachusetts, or conducting automated full thin section BSE scans and EDS point analyses on the JEOL scanning electron microscope at University of New Mexico. X-ray maps of U, Th, Pb, and Y, and spot analyses of U, Th, Pb, and Y, were conducted for selected monazite grains on the Cameca SX50 electron microprobe at University of Massachusetts and the Cameca SX100 electron microprobe at New Mexico Institute of Technology. For details on the analytical methods and fundamental assumptions of the monazite technique, see Appendix 1.

Because monazite can grow as a primary mineral from a melt, a hydrothermal mineral during fluid flux, or a metamorphic mineral during deformational/thermal events, we used several parameters to recognize a monazite grain, or an age domain within a monazite grain, as syn-deformational. Syn-deformational monazite grains are inferred to have grown elongate within

foliation. Chemical zoning patterns within an age domain will also commonly be elongate. Though the form of a monazite grain may become elongate through strain influenced dissolution and reprecipitation during a subsequent deformational event, the chemical zoning is interpreted to be growth zoning within the crystal. The geometry of this chemical zoning is interpreted to reflect the strain field at the time of growth. A monazite may rotate during a subsequent deformation, so the elongate grain may come to be aligned within a subsequent foliation. New monazite commonly grows as a rim on an older core (Williams et al., 1999). These rims or caps typically grow in the direction of infinitesimal elongation during strain. In summation, elongate chemical zoning within an age domain in a monazite grain, or an age domain in a rim that grew in the elongation direction during strain, is interpreted to indicate that the age domain is syn-deformational.

Based on in situ electron microprobe dating of syn-deformational monazites, parallel to S1 and S2 high-strain domains along the Homestake shear zone, Shaw et al. (2001) defined a period of Paleoproterozoic orogenesis that spanned 1.71 to 1.63 Ga, with deformation pulses at 1700 +/- 7 Ma, 1658 +/- 5 Ma, and 1637 +/- 13 Ma.

In this study, I find that migmatites with S1 foliation folded by an F2 fold along the Gore Range shear zone also record a Paleoproterozoic period of orogenesis, with deformational pulses that coincide with those documented along the Homestake shear zone by Shaw et al. (2001) (Fig. 18). One monazite grain has an oldest core date of ~1731 Ma, based on several spot analyses, and a rim date of 1619 +/- 24 Ma (Fig. 19a). The ~1731 Ma core is elongate parallel to S1 and appears to have overgrown S1, suggesting that S1 was already developing at about 1.73 Ga. The 1619 Ma rim overgrew oxide and quartz inclusions that are elongate to S1 and the rim has chemical zoning elongate to S1, suggesting that S1 planes were reactivated during deformation (possibly F2 folding) at 1.62 Ga. The cores of several other grains give an average date of 1674 +/- 13 Ma (Fig. 19b,c). The rims on these same grains give an average date of 1647 +/- 15 Ma. The 1.67 Ga cores are elongate parallel to S1, but the relationship of 1.65 Ga rim geometries to external structures is unclear.

In this study, I find that the Idaho Springs-Ralston shear zone also records a Paleoproterozoic orogenic episode that includes at least three deformational pulses. Monazite grains from an S2 domain in biotite schist, adjacent to a mylonite zone along the southwestern section of the Idaho Springs-Ralston shear

Figure 18: Summary of monazite U-Th-Pb age domains, Colorado Mineral Belt shear zone system. Each curve represents frequency distribution for 4-17 spot analyses. Boxes represent 1-3 spot analyses. Multiple peaks on same baseline represent different age domains in single crystal. Peaks of same color represent grains within same sample. Gray bars represent weighted means for age populations that fall within a 95% confidence interval in a pooled t-test, and correspond to pulses of monazite growth.

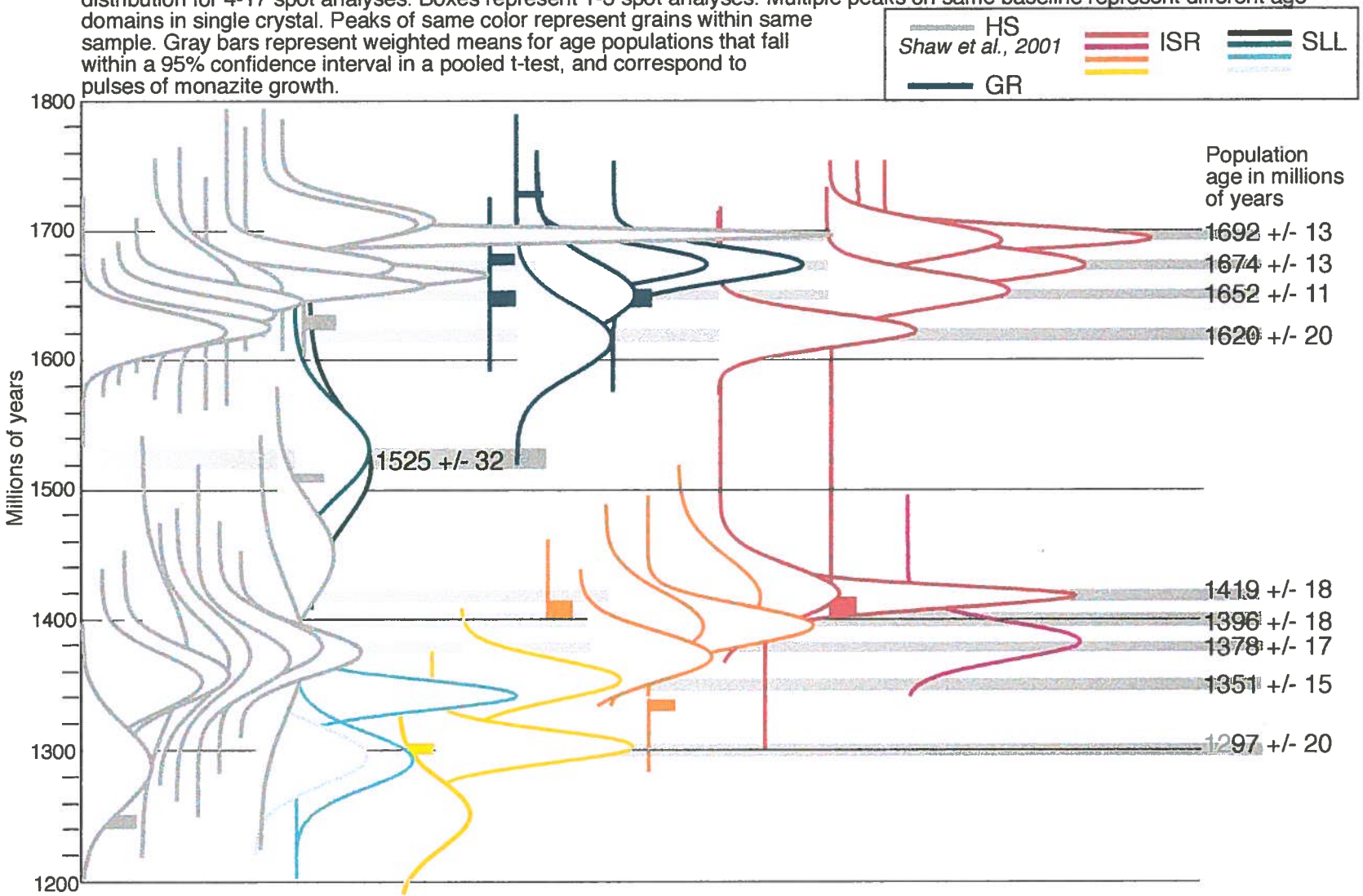

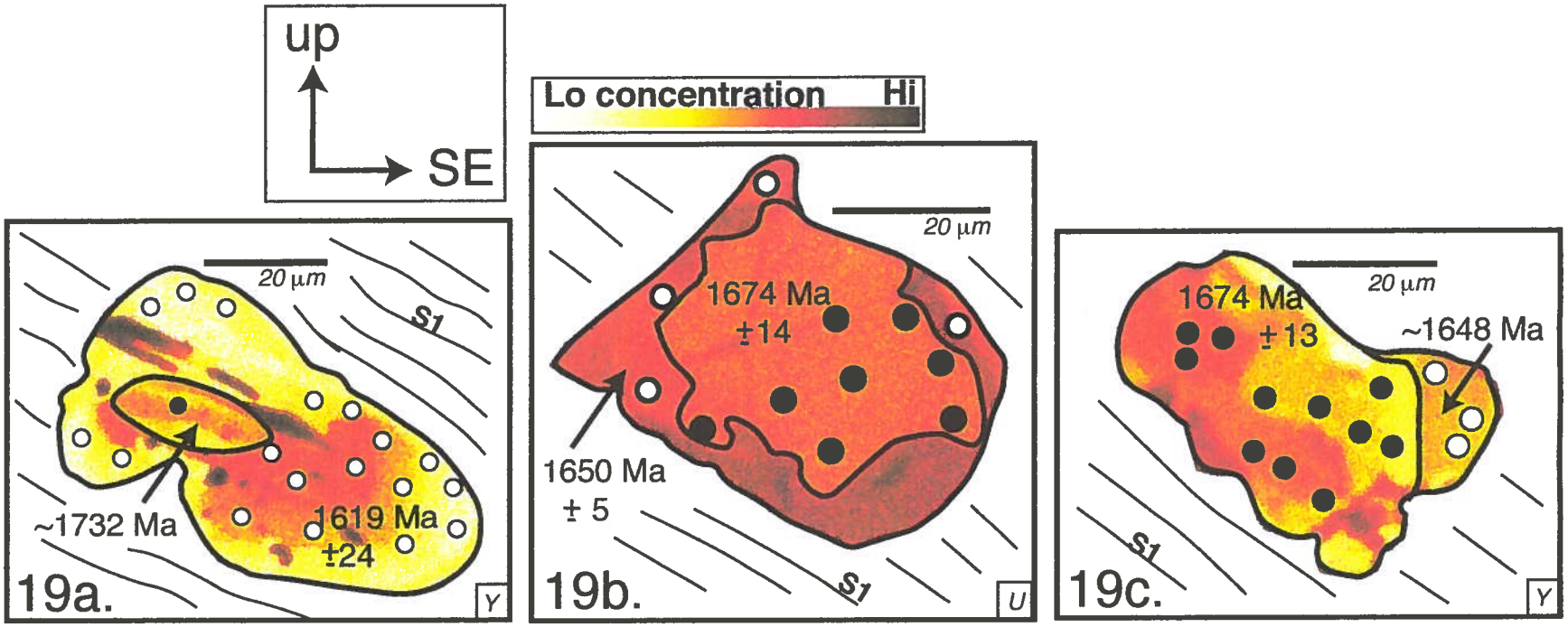

A00TM1 migmatite with S1 foliation, in the hinge region of an F2 fold with subvertical axial plane

Figure 19: Electron microprobe elemental concentration maps showing U and Y zoning in selected monazites from Gore Range shear zone. Black outlines emphasize the date domains that coincide with chemical variations in each grain. a. records a 1.73 Ga date, the oldest date found in monazites along the Colorado Mineral Belt shear zone. This 1.73 date domain has chemical zoning parallel to the external S1 fabric. The 1.62 Ga rim overgrew inclusions that are parallel to S1 and also has chemical zoning parallel to S1, suggesting reactivation of S1 planes during deformation (possibly during F2 folding). b. and c. record the 1.67 Ga date of the adjacent syn-deformational Cross Creek granite. a. and c. also record a 1.65 Ga date. For all monazite data, see Appendix 3.

zone at Chicago Creek, records Paleoproterozoic deformational pulses at 1692 +/- 13 Ma, 1653 +/- 13 Ma, and 1623 +/- 12 Ma (Fig. 18; Fig. 20d,e). The oldest monazite dates documented along the Idaho Springs-Ralston shear zone are spot analyses of ~1739 Ma, ~1735 Ma, and ~1719 Ma from two small, elongate grains.

Further constraints on the timing of D1 and D2 deformation comes from the Coal Creek quartzite/schist sequence along the Idaho Springs-Ralston shear zone. Here, field relationships as well as the identification of a probable regolith surface suggest that Coal Creek quartzite was deposited on top of Boulder Creek granite after the granite was emplaced at about 1.72 Ga. This interpretation is in contrast to the conclusions of Gable (1980) and Wells, et al. (1964), which indicate an intrusive contact with granite intruding the quartzite pre- or syn-D1. Wells et al. (1964) appears to have mapped cross-cutting relationships based on the presence of granite float in areas dominated by outcrops of quartzite. In the current study of the Coal Creek synform, no cross-cutting relationships or xenoliths were observed in outcrop. No interlayering relationships between metasedimentary rocks and granite, as observed along the Homestake, Gore Range, and St. Louis Lake shear zones, were observed. In contrast to the

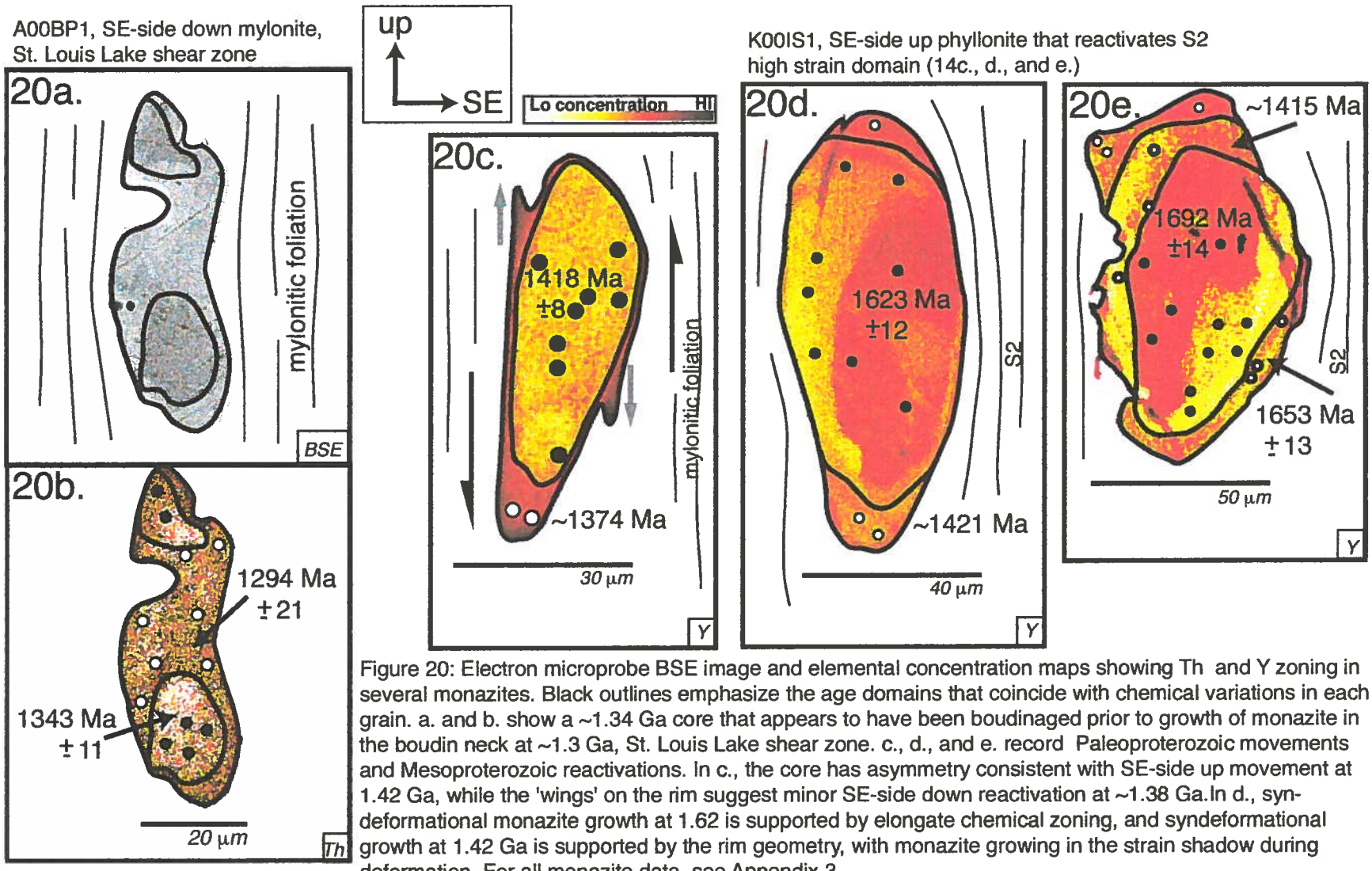

Figure 20: Electron microprobe BSE image and elemental concentration maps showing Th and Y zoning in several monazites. Black outlines emphasize the age domains that coincide with chemical variations in each grain. a. and b. show a ~1.34 Ga core that appears to have been boudinaged prior to growth of monazite in the boudin neck at ~1.3 Ga, St. Louis Lake shear zone. c., d., and e. record Paleoproterozoic movements and Mesoproterozoic reactivations. In c., the core has asymmetry consistent with SE-side up movement at 1.42 Ga, while the 'wings' on the rim suggest minor SE-side down reactivation at ~1.38 Ga.In d., syn-deformational monazite growth at 1.62 is supported by elongate chemical zoning, and syndeformational growth at 1.42 Ga is supported by the rim geometry, with monazite growing in the strain shadow during deformation. For all monazite data, see Appendix 3.

heavily migmatized metasedimentary rocks intruded by the Cross Creek and Boulder Creek batholiths elsewhere along the Colorado Mineral Belt shear zone system, the Coal Creek quartzite/schist sequence does not appear to be migmatized. In several outcrops, the contact between the quartzite and granite is marked by a probable regolith that grades from quartz monzonite to arkosic quartzite over >15 meters.

Preliminary major and trace element analyses of this probable regolith suggest depletion of Na_2O, K_2O, CaO, and Cu, and enrichment in total Cr and Ni, relative to the adjacent quartz monzonite. Two potential regolith samples located several meters into the quartzite from the contact with quartz monzonite have major element patterns that are similar to the quartz monzonite (Fig. 21a), and trace element patterns similar to the quartzite (Fig. 21b). A sample located ~15 meters into the quartzite shows depletion in Na_2O, K_2O, CaO, MgO, and total Fe with respect to the granite (Fig. 21a). Similarly, Holland et al. (1989) observed that almost all CaO and MgO were removed from the upper parts of the Archean Flin Flon paleosol in Canada. The Flin Flon paleosol also showed a slight increase in K_2O from base to top, which has been observed in other Paleozoic and Precambrian paleosols. Preliminary data on the Coal Creek potential regolith

Figure 21: Preliminary major element (a.) and trace element (b.) data for Twin Spruce quartz monzonite at contact with Coal Ck quartzite (Gable, 1980), potential regolith, and Coal Ck quartzite conglomerate. On x axis, '0' is the quartz monzonite, '1' and '2' are the regoliths directly adjacent to the granite, '15' is arkosic quartzite 15 meters from the contact, and '100' is a quartzite conglomerate 100 meters into the main quartzite body. For all geochemical data, see Appendix 6.

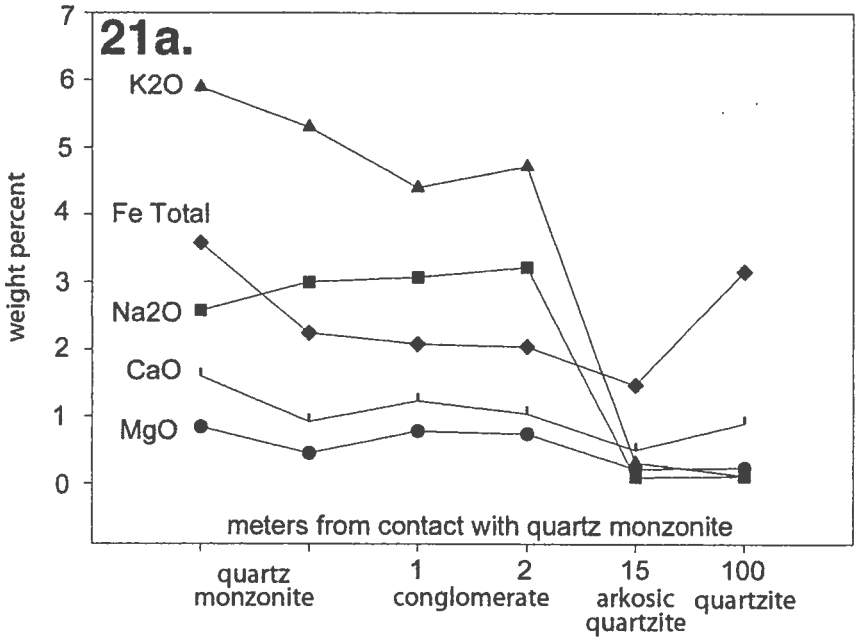

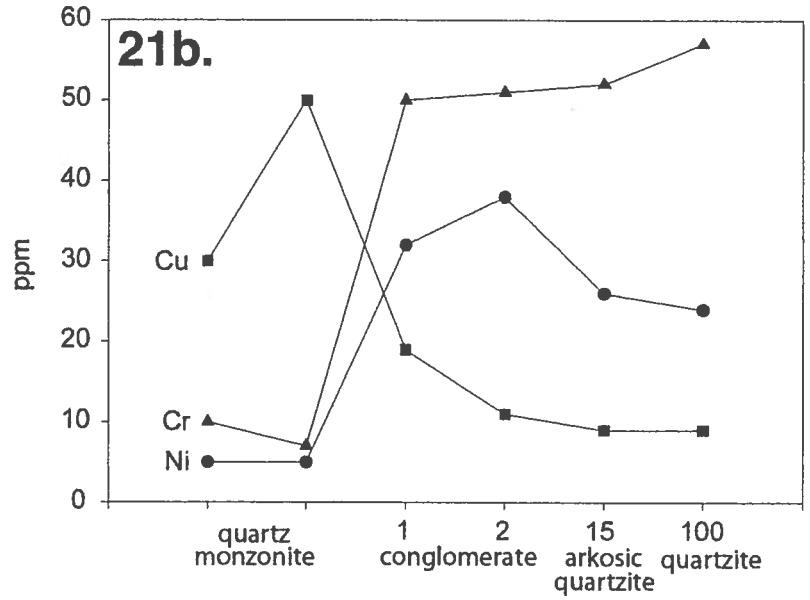

do not show this trend for K_2O. Fe has been found to be mobile (Gall, 1994) as well as immobile (Grandstaff et al., 1986) in paleosols. In order to better understand the behavior of Fe, the FeO and Fe_2O_3 components should be determined (Gall, 1994).

Trace element data for Cr, Ni, and Cu are in contrast to the trends observed in Precambrian paleosols in Ontario, Canada, where a gradual decrease in concentration occurred from base to top (Gay and Grandstaff, 1980). Preliminary results for the Coal Creek potential regolith are intriguing, but further study is needed in order to clearly define the geochemical signature of the horizon along the granite/quartzite contact and, in doing so, identify whether the horizon does indeed represent a deformed nonconformity.

In the Coal Creek quartzite, youngest detrital zircon grains of about 1.66 Ga (Aleinikoff, J.N., written communication, 2001) suggest that the quartzite and underlying granite developed S1 foliation after 1.66 Ga. The youngest reliable (concordant) Coal Creek detrital zircon $^{207}Pb/^{206}Pb$ dates, out of a set of 50 analyses, are 1605 +/- 139 Ma, 1659 +/- 73 Ma, 1663 +/- 58 Ma, 1664 +/- 84 Ma, 1664 +/- 48 Ma, 1688 +/- 81 Ma, 1694 +/- 40 Ma, 1702 +/- 66 Ma, 1705 +/- 53 Ma, 1707 +/- 62 Ma, 1707 +/- 28 Ma, and 1707 +/- 35 Ma (J.N. Aleinikoff, written

communication, 2001). If the Coal Creek quartzite was indeed deposited on 1.72 Ga granite, became buried and lithified sometime after 1.66 Ga, and developed low angle S1 fabric, then deformation along S1 must have lasted from at least 1.73 Ga (based on monazite core dates along the Gore Range shear zone) to 1.66 Ga. The Coal Creek quartzite may correlate temporally with the Ortega quartzite of northern New Mexico and the Blue Ridge quartzite of southern Colorado, both deposited at about 1.70 Ga (Aleinikoff et al., 1993).

3.8 MESOPROTEROZOIC STRUCTURES OF THE COLORADO MINERAL BELT SHEAR ZONE SYSTEM

The mylonites and ultramylonites within the Colorado Mineral Belt shear zone system are distinct from the Paleoproterozoic structures they overprint. They contain microstructures and minerals that record lower temperatures of deformation, they show unequivocal shear sense, and they contain monazites with ~1.4 Ga dates.

3.9 MICROSTRUCTURES AND P-T CONDITIONS OF MESOPROTEROZOIC DEFORMATION

Microstructures are one important way to distinguish temperatures and strain rates associated with different types of tectonites in the Colorado Mineral Belt shear zone system. On the microscopic scale, mylonites are dominated by core and mantle structures in quartz that indicate that subgrain rotation recrystallization was an important recovery mechanism, and that the mylonites deformed at temperatures between 350° and 450°C (Fig. 22a,b; Regime 2-3 for quartz, Hirth and Tullis, 1994). Feldspar grains are brittley deformed and only occasionally show undulose extinction, indicating deformation temperatures below 500°C (Fig. 23a,b). Aluminosilicate minerals, such as sillimanite, are absent or metastable in the mylonites, and retrograde chlorite and muscovite are abundant.

Ultramylonites of each shear zone segment contain large ribbon-like quartz grains that have necklaces of tiny recrystallized quartz grains, indicating that grain boundary migration was an important recovery mechanism in quartz and that the ultramylonites deformed at ballpark temperatures of 250° to 350°C (Fig. 24a,b; Regime 1-2 for quartz, Hirth and Tullis, 1994). Feldspars are broken

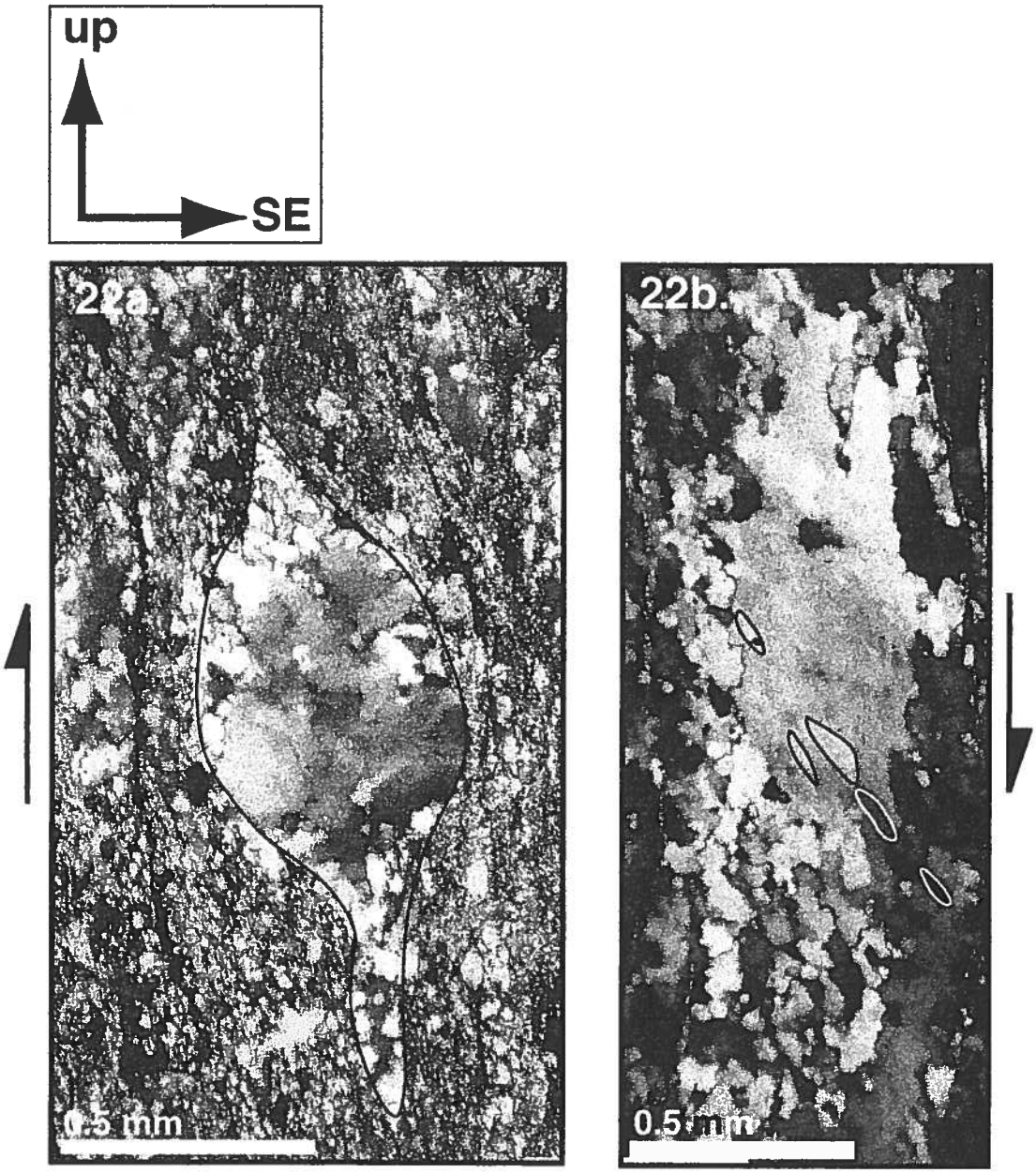

Figure 22: Examples of microstructures in quartz in mylonites. a. Quartz porphyroclast with subgrain rotation recrystallization microstructures has asymmetry consistent with SE-side down shear sense in Gore Range mylonite. b. Subgrain rotation recrystallization in Idaho Springs-Ralston mylonite. Subgrains have asymmetry consistent with SE-side down shear sense.

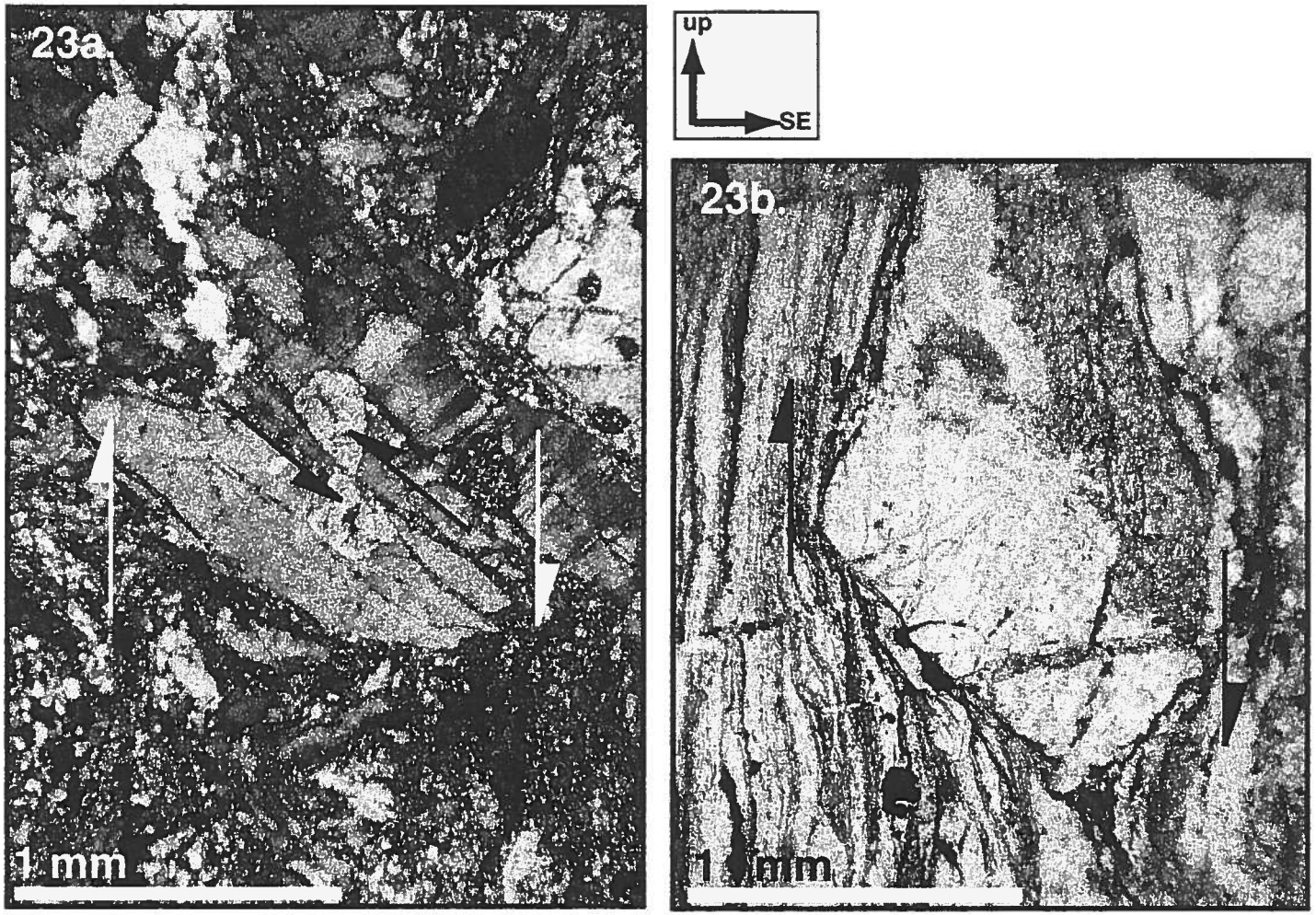

Figure 23: Examples of brittle behavior of feldspar in mylonite. a. Antithetic bookshelf fault in feldspar, SE-side down mylonite. b. Feldspar tilted during SE-side down shearing in mylonite.

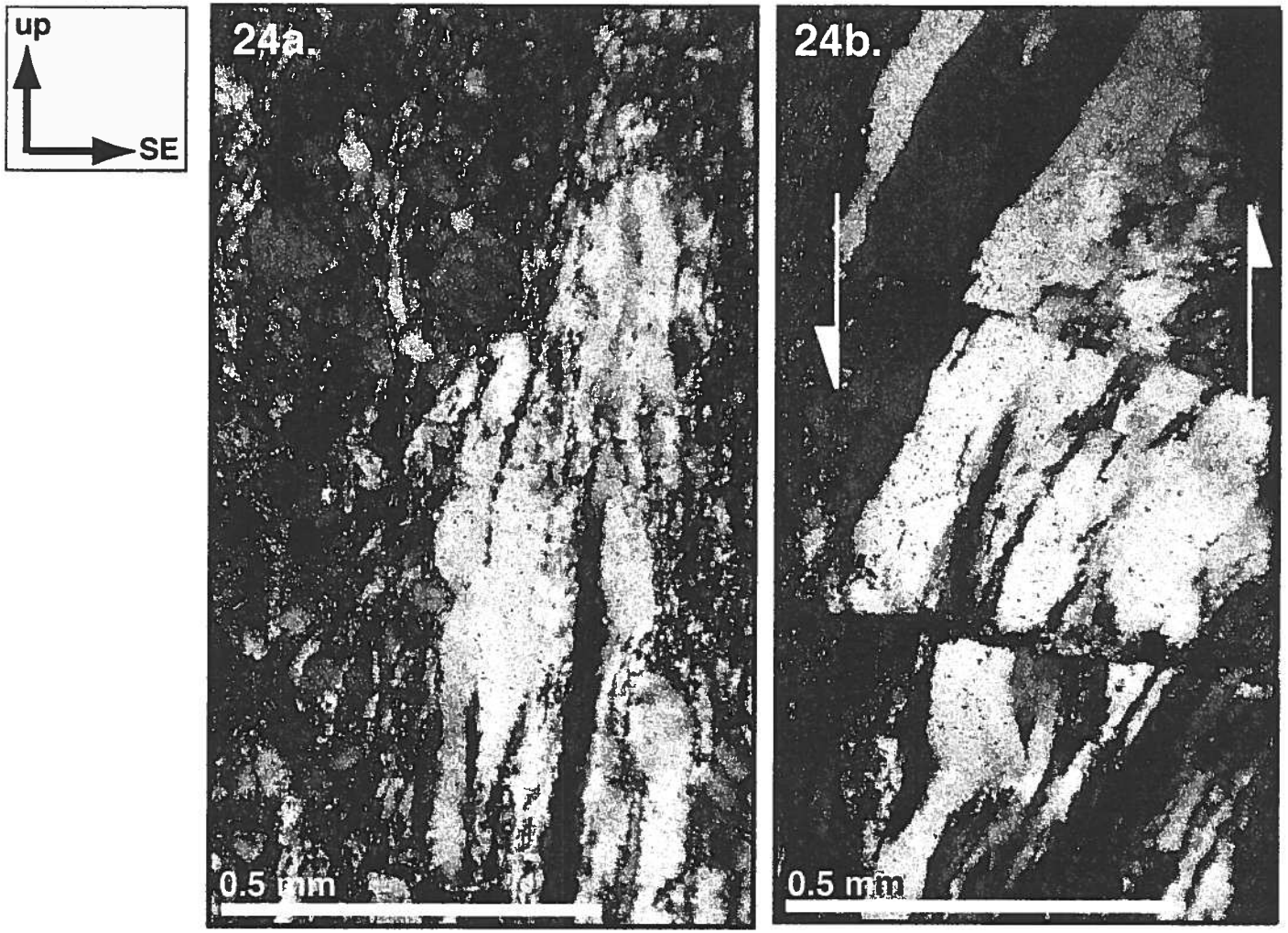

Figure 24: Examples of quartz microstructures in ultramylonite. Attenuated quartz ribbons with necklaces of tiny recrystallized quartz grains indicate that grain boundary migration was the dominant recrystallization mechanism in quartz. In a., feldspars are small and rounded. Quartz ribbons in b. are parallel to schistosity in matrix S-C fabric, indicating SE-side up shear sense in ultramylonite.

into small pieces that have become rounded during shearing. In ultramylonites, as in mylonites, aluminosilicate minerals are absent or metastable, and retrograde chlorite and muscovite are abundant.

3.10 SHEAR SENSE IN MYLONITES AND ULTRAMYLONITES

Mylonites and ultramylonites have strong asymmetric fabrics (S-C and C-C') and quartz porphyroclasts (sigma and delta), indicating that simple shear was important during the deformation of these tectonites (Fig. 25a,b). When observed perpendicular to foliation and parallel to mineral stretching lineations, asymmetric mylonite and ultramylonite fabrics and clasts provide information on shear sense. Because each shear zone segment contains steeply plunging mineral stretching lineations, movements within the zones are interpreted to be primarily dip-slip. The small strike-slip components do not show consistent sense from one shear zone segment to the next, suggesting that there is no regional strike-slip movement pattern. The strike-slip components may be only locally important, because they are consistent within each shear zone, but are not consistent from one shear zone to the next. For example, SE-side down mylonites in the Homestake and Idaho Springs-Ralston shear zones have small dextral

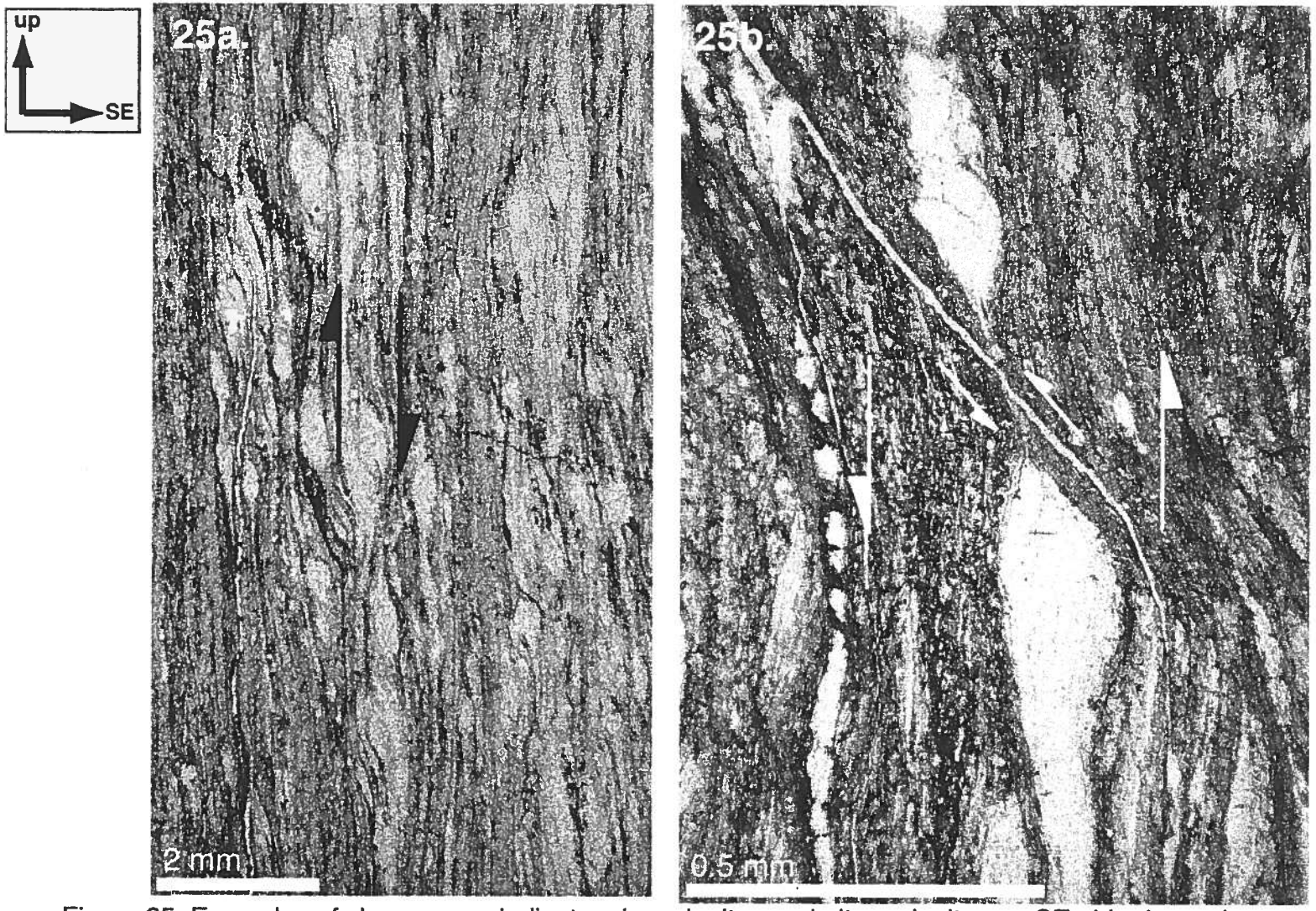

Figure 25: Examples of shear sense indicators in mylonites and ultramylonites. a. SE-side down sigma porphyroclasts in mylonite, Gore Range shear zone. b. SE-side up shear band in ultramylonite, Homestake shear zone.

components to movement, but SE-side down mylonites in the Gore Range shear zone have a small sinistral component.

In each shear zone, ultramylonites appear to overprint mylonites, and show different shear sense than the mylonites they overprint (Fig. 26a,b). In the Homestake and Idaho Springs-Ralston shear zones, SE-side down, subvertical mylonites with strong S-C fabrics and sigma-porphyroclasts are overprinted by SE-side up, sub-vertical ultramylonites with C-C' fabrics, Reidel shears, sigma-porphyroclasts, and pseuodotachylite veins (Shaw et al., 2001). In the Gore Range shear zone, SE-side down mylonites are drag-folded with SE-side up shear sense and overprinted by ultramylonites with quartz ribbons that agree with SE-side up movement (Fig. 26a). At St. Louis Lake, thin SE-side down ultramylonite bands overprint SE-side up mylonites with well-developed S-C fabric (Fig. 26b). Because mylonites and ultramylonites along these shear zone segments have distinctly different mineral stretching lineation orientations, different shear sense, and different deformation microstructures, the two fabrics appear to have formed during separate deformational events. In contrast, some mylonites within the shear zones simply grade into ultramylonites in more mica-rich domains, and the two fabrics have similar mineral stretching lineation

Figure 26: Sketches documenting overprinting of mylonites by ultramylonites in outcrop. a. In Gore Range shear zone, SE-side down mylonites with strong S-C fabric overprinted by SE-side up drag folds and extremely fine-grained, laminated zones with quartz ribbons that show SE-side up shear sense. b. In St. Louis Lake shear zone, 1.42 Ga SE-side up mylonite with strong S-C fabric overprinted by thin strands of SE-side down ultramylonite.

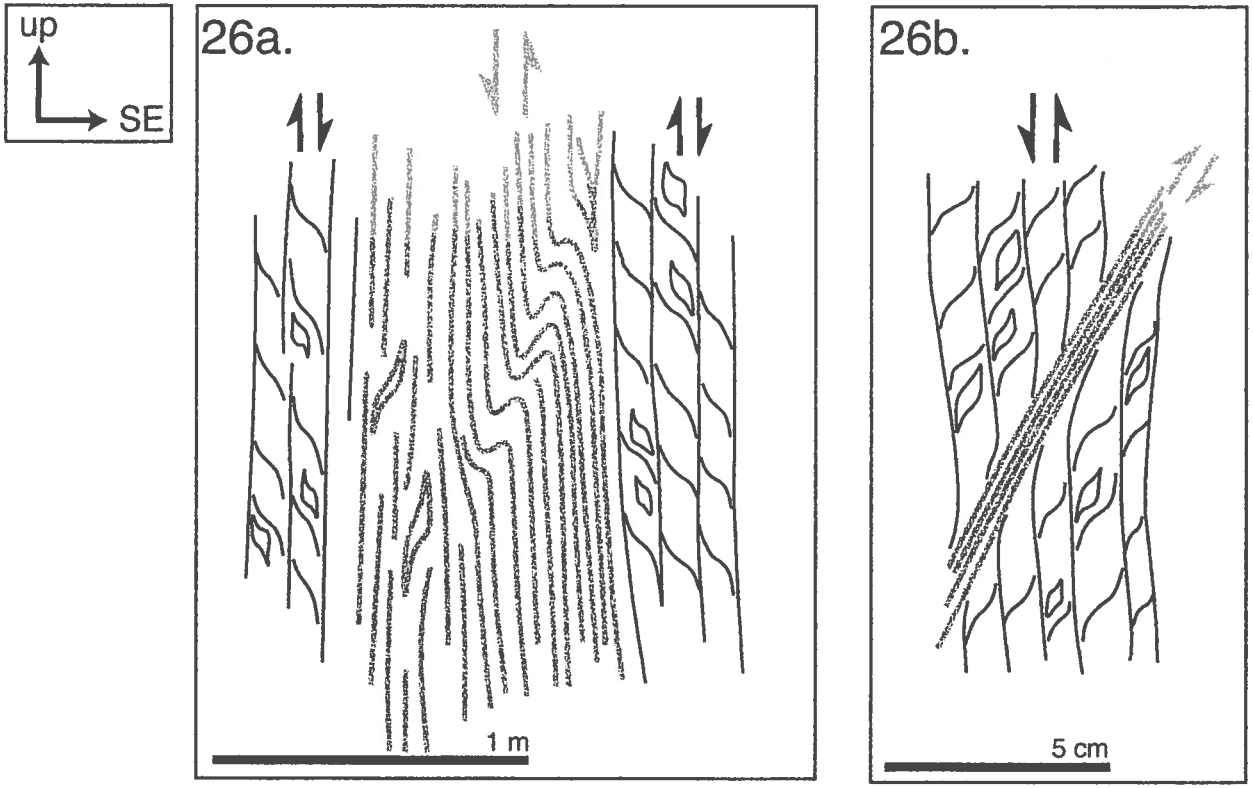

orientations and shear sense. In these cases, mylonites and ultramylonites could have formed in the same event but at different strain rates.

3.11 TIMING OF MESOPROTEROZOIC DEFORMATION

Monazite age dating and field relationships bear on the timing of multiple Mesoproterozoic episodes of mylonitization and ultramylonitization in the Colorado Mineral Belt shear zone system. Here, we present geochronologic data that bears on the timing of movement associated with mylonites and ultramylonites of each shear zone, beginning with the oldest Mesoproterozoic dates documented along the shear zone system.

3.12 THE PRE-1.45 GA MOVEMENTS

Pre-1.45 Ga motion is suggested in the St. Louis Lake shear zone. Monazites from a 100 meter wide SE-side down and slightly dextral strand of mylonitized Boulder Creek granite along the St. Louis Lake shear zone yield dates of 1518 +/- 40 Ma and 1531 +/- 33 Ma (Fig. 18). These monazites are elongate parallel to the subvertical mylonite fabric. The 1518 Ma grain contains elongate quartz and apatite inclusions, which are at a small angle to the mylonite

fabric. These inclusions have orientations that are parallel to the schistosite planes in the matrix S-C fabric, agreeing with SE-side down shear sense. The 1531 Ma grain includes a euhedral apatite crystal. Neither grain shows evidence for internal chemical zoning of U, Th, Y, or Pb. These monazites lie along quartz veins in the mylonite and have coronas of apatite and REE clays, similar to those rimming the post-1.38 Ga monazites in St. Louis Lake shear zone. One observed grain contains only tiny specks of monazite, each several microns in diameter, enclosed in apatite with a corona of REE clay. Deformations between 1.52 and 1.53 Ga are undocumented in Colorado, but the microstructural differences between the ~1.4 Ga mylonites and the ~1.7 Ga higher temperature tectonites they overprint suggest exhumation between ~1.7 Ga and ~1.4 Ga. Exhumation may have involved the dissolution and reprecipitation of monazite along fluid pathways. In this study, St. Louis Lake shear zone is the only segment of the Colorado Mineral Belt shear zone system to record ~1.52 Ga dates and their importance is not yet understood.

3.13 THE 1.45 GA MOVEMENTS

1.45 Ga movements are documented in the Idaho Springs-Ralston shear zone and possibly in the Homestake shear zone. Previous studies have presented field evidence for SE-side down and slightly sinistral movement along the Idaho Springs-Ralston shear zone during emplacement of the Mt. Evans pluton (Nyman et al., 1994; Graubard and Mattinson, 1990) at 1442 +/- 2 Ma ([U-Pb] Aleinikoff et al., 1993). Shaw et al. (2001) also reported several monazite dates of ~1452 Ma from Homestake mylonites (Fig. 18).

3.14 THE 1.42 GA MOVEMENTS

Motion at about 1.42 Ga is recorded in SE-side up mylonites in the St. Louis Lake and Idaho Springs-Ralston shear zones (Fig. 18). Field relations in the St. Louis Lake shear zone indicate SE-side up mylonitization synchronous with emplacement of the Silver Plume pluton (1422 +/- 3 Ma [U-Pb], Hedge, 1969). In the Idaho Springs-Ralston shear zone, monazites in a SE-side up mylonite also indicate movement at 1422 Ma (Fig. 20c). In the S2 domain adjacent to the mylonite, several monazites with Paleoproterozoic core dates have ~1422 Ma rim dates, based on several spot analyses per rim (Fig. 20d,e).

Another monazite has a 1418 +/- 8 Ma core that has an asymmetry concordant with SE-side up shear sense observed in sigma porphyroclasts and mesoscopic S-C fabrics of the mylonite (Fig. 20c).

One monazite grain in the Coal Creek pelitic schist, adjacent to the Idaho Springs-Ralston shear zone, has a date of 1418 +/- 30 Ma and appears to be enclosed in a poikiloblastic andalusite porphyroblast (Fig. 27a,b). This association, suggesting that andalusite grew during or after 1.42 Ga deformation, has not been observed elsewhere in the Colorado Mineral Belt shear zone system. However, farther north in the Front Range, andalusite, staurolite, cordierite, and garnet porphyroblasts overprint earlier assemblages, and andalusite grew across Paleoproterozoic fabrics, suggesting that these minerals grew during a relatively low-pressure episode of metamorphism at ~1.4 Ga based on hornblende $^{40}Ar/^{39}Ar$ dates (Selverstone et al., 1997; Shaw et al., 1999).

3.15 THE 1.38-1.4 GA MOVEMENTS

1.38-1.4 Ga movements are recorded in SE-side down mylonites in the Homestake and Idaho Springs-Ralston shear zones (Fig. 18). In the Homestake shear zone, a population of monazites from the >30 meter wide SE-side down

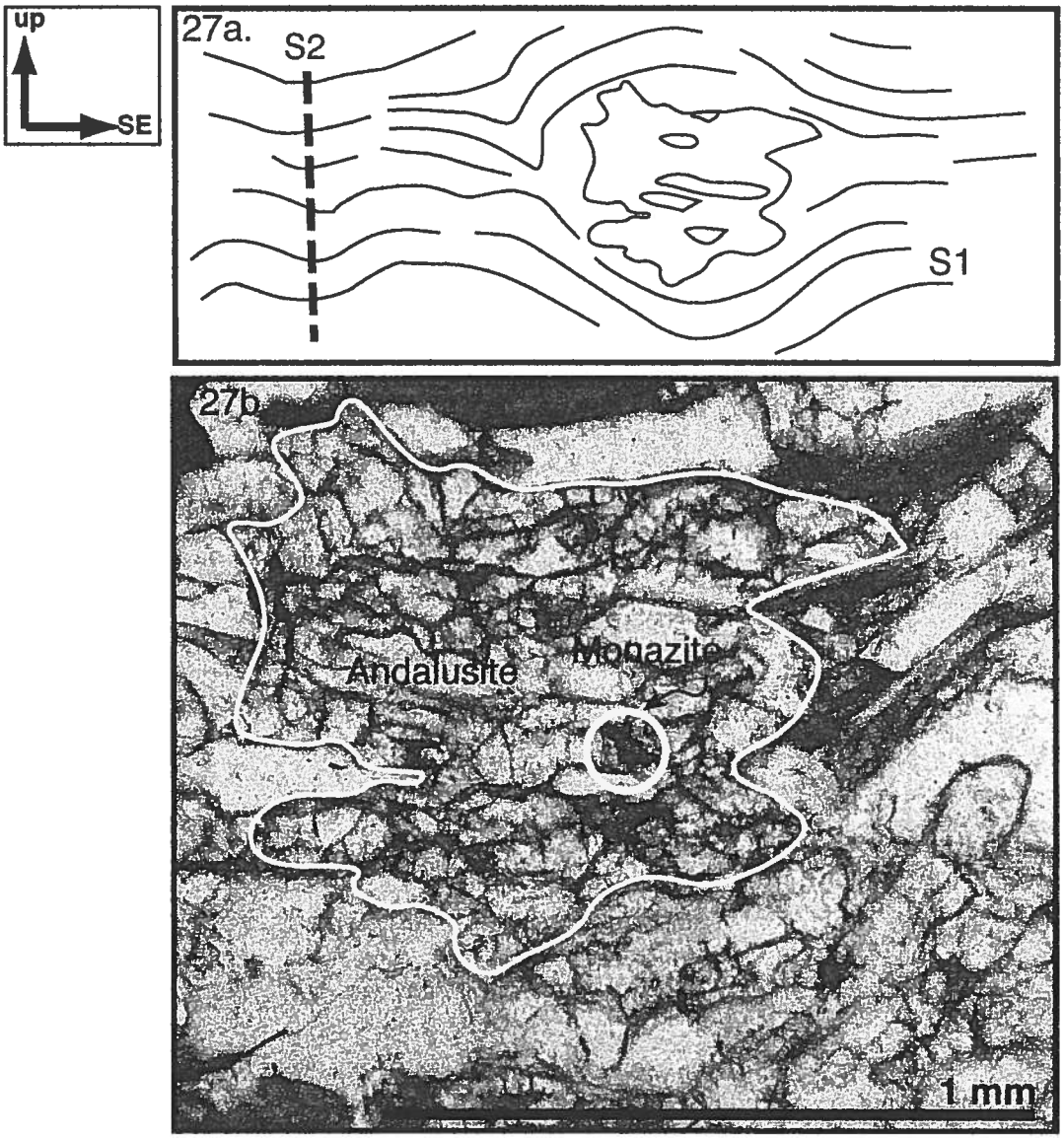

Figure 27: 1.42 Ga monazite in andalusite porphyroblast in hinge of F2 Coal Creek synform along Idaho Springs-Ralston shear zone. Andalusite overgrew S1, but fabric appears to have been deflected during development of F2 crenulation.

and slightly dextral main mylonite strand gives an average date of 1376 +/- 11 Ma (Shaw et al., 2001). Along the southern extent of the Homestake, SE-side down mylonites moved during St. Kevin batholith emplacement at 1396 Ma ([U-Pb], Doe and Pearson, 1969).

The mylonites and ultramylonites of the Gore Range shear zone have not yet provided any datable monazite. The few monazites that have been detected are shattered grains with only small patches of true monazite enclosed in a material with high REE concentrations, but no phosphorus. Fluid flux within the shear zone appears to have leached P out of monazites, leaving behind pockets of immobile REEs. Because the Gore Range shear zone is directly along strike of the Homestake and, like the Homestake, contains strands of SE-side down mylonites and SE-side up ultramylonites (Fig. 26a), we consider the Gore Range shear zone to be the discrete northeastern continuation of the Homestake shear zone.

The Idaho Springs-Ralston shear zone includes a >30 meter wide, SE-side down and slightly dextral mylonite strand that deforms the contact between the Coal Creek quartzite and quartz monzonite of the Boulder Creek batholith. A population of small (~10 micron diameter) monazites, elongate parallel to fabric

and enclosed in recrystallized quartz grains in mylonitized Coal Creek quartzite, has an average date of 1384 +/- 14 Ma. One elongate monazite from the Coal Creek pelitic schist adjacent to the mylonite zone yields a date of 1373 +/- 19 Ma, and is boudinaged due to subsequent deformation. Other elongate monazites from the Coal Creek pelitic schist give an average date of 1396 +/- 18 Ma, possibly representing a separate movement.

3.16 THE POST-1.38 GA MOVEMENTS

Post-1.38 Ga movements are recorded in SE-side up ultramylonites that overprint SE-side down mylonites in the Homestake and Idaho Springs-Ralston shear zones, and in SE-side down ultramylonites that overprint SE-side up mylonites in the St. Louis Lake shear zone (Fig. 18). In the Homestake shear zone, monazites within a >30 meter wide SE-side up ultramylonite strand, which partly overprints a >30 meter wide SE-side down mylonite strand, do not give a clear date of ultramylonitization. Many monazite grains present in this ultramylonite bear dates that are similar to those in the overprinted mylonite, and it is possible that no new monazite grew during ultramylonitization. However, the Homestake ultramylonite contains a 1375 +/- 14 Ma monazite grain that is offset

along an antithetic bookshelf fault consistent with the SE-side up shear sense of the ultramylonite strand. This would suggest that ultramylonitization in the Homestake shear zone occurred after 1375 Ma. The youngest monazite dates from the Homestake shear zone come from one grain with an average date of 1.29 Ga, and several other spot analyses that yielded dates of 1.25 Ga (Shaw et al., 2001). These post-1.38 Ga dates are provocative, but more data are needed to define the timing of post-1.38 Ga deformation.

In the St. Louis Lake shear zone, SE-side down ultramylonites with post-1.38 Ga dates overprint the 1.42 Ga SE-side up mylonites. A monazite from a 10 meter wide, SE-side down strand of ultramylonitized Silver Plume granite has a core with a date of 1343 +/- 11 Ma and a rim with a date of 1294 +/- 21 Ma (Fig. 18, Fig. 20a,b). The core of the grain is elongate parallel to the ultramylonite fabric and has been boudinaged, with younger monazite forming in the boudin neck and around the rim. These dates suggest that two shear zone movements occurred after the emplacement of the Silver Plume granite. Another elongate monazite grain from the same ultramylonite sample gives a date of 1297 +/- 22 Ma. This monazite grain is also elongate parallel to the ultramylonite fabric and has a corona of apatite and a narrow outermost corona of non-stoichiometric clay

with high Ce-content. The complicated corona on this and other grains from several locations along the St. Louis Lake shear zone segment suggest that fluids rich in Ca may have been moving through the shear zone during deformation, dissolving monazite and growing apatite, and leaving a residue of incompatible, immobile REEs in an outer corona of non-stoichiometric clay.

In the Idaho Springs-Ralston shear zone, a >10 meter wide, SE-side up and slightly sinistral ultramylonite strand overprints a >30 meter wide, SE-side down and slightly dextral mylonite strand, and contains monazites with dates ranging from 1.25 Ga to 1.36 Ga (Fig. 18). In this ultramylonite strand, one monazite that is elongate parallel to the ultramylonite fabric has a date of 1355 +/- 15 Ma, while another grain that is rimmed by apatite has a date of 1304 +/- 12 Ma. A third grain bears an elongate core with a date of 1306 +/- 4 Ma and an elongate rim with a date of 1253 +/- 18 Ma. In the Coal Creek pelitic schist, at the margin of the Idaho Springs-Ralston shear zone segment, one monazite with a 1.4 Ga core has an elongate rim with a date of ~1337 based on several spot analyses. These post-1.38 Ga monazite dates, recorded all along the Colorado Mineral Belt shear zone system, suggest multiple movements and/or fluid flux

events at 1.25 Ga, 1.3 Ga, and 1.35 Ga, or a near continuum of fluid flux between 1.25 and 1.35 Ga.

4.0 DISCUSSION

4.1 TECTONIC FINGERPRINT FOR DEFORMATION ALONG THE COLORADO MINERAL BELT SHEAR ZONE SYSTEM

The record of Mesoproterozoic movements documented in mylonites and ultramylonites of the Colorado Mineral Belt shear zone system, and Paleoproterozoic deformation documented in the higher temperature S1 and S2 domains along the shear zone system, provides a 'tectonic fingerprint' for the deformational history of the Colorado Mineral Belt shear zone system. This tectonic fingerprint is summarized in Figure 18 and includes a >100 Ma long Mesoproterozoic period of orogenesis that includes deformational pulses at 1297 +/- 20 Ma, 1351 +/- 13 Ma, 1378 +/- 17 Ma, 1396 +/- 12 Ma, and 1419 +/- 18 Ma, and a >70 Ma long Paleoproterozoic period of orogenesis that includes deformational pulses at 1620 +/- 20 Ma, 1652 +/- 11 Ma, 1674 +/- 13 Ma, and 1692 +/- 13 Ma.

These 'deformational pulse' ages are determined based on statistically distinct age populations within monazite grains of each shear zone. An alternative interpretation is that the monazite data document near continuums of

deformation and monazite growth from 1.3-1.45 Ga and 1.62-1.7 Ga. The in situ electron microprobe monazite dating technique used here is still in the early stages of development. The technique is dependent on the fundamental assumptions that monazite incorporates negligible common lead during growth and that elemental concentrations have not been significantly modified by subsequent mass transfer (Montel et al., 1996). However, it appears that monazite may dissolve and reprecipitate during low temperature fluid flux events in some mylonite and ultramylonite zones of this study. New background measurement techniques are being developed, which will help eliminate spurious background measurements at the peak position and reduce the standard deviations associated with each spot analysis (Williams, M.L., written communication). Despite the problematic aspects of the technique, analyses of the same grains at two different labs produced statistically similar values, and Williams et al. (1999) show that the electron microprobe monazite dates compare closely with mass spectrometric U-Th-Pb dates. A number of monazite dates determined in the present study are supported by Rb-Sr and U-Th-Pb ages for adjacent syn-deformational plutons, such as a 1418 +/- 8 Ma grain at the margin of the 1422 Ma Silver Plume pluton (1422 +/- 3 Ma [U-Pb]; Hedge, 1969) and a

1674 +/- 13 Ma grain at the margin of the 1675 Ma Cross Creek pluton (Tweto and Lovering, 1977). Therefore, we discuss the details of the monazite age determinations as if they were accurate representations of the timing of deformation. Still, I am cautious about very young dates, which could have been influenced by low temperature fluid flux events, and I am cautious about dates that do not fit within a broad tectonic time framework defined by previous workers for the southwestern U.S., and avoid making conclusions that rely solely on these questionable dates.

The period between >1.73 Ga and <1.66 Ga is marked by development of low-angle S1 foliation and isoclinal folds, based on monazite/fabric relationships along the Homestake and Gore Range shear zones, and relationships between the Coal Creek quartzite and Boulder Creek batholith along the Idaho Springs-Ralston shear zone (Fig. 28a). D1 coincided with early metamorphic temperatures of >600°C that exceeded the second sillimanite isograd during syn-plutonic deformation along the Gore Range shear zone, as well as along the Idaho Springs-Ralston shear zone near Chicago Creek (Moench, 1994). If Coal Creek quartzite was deposited on Boulder Creek granite and incorporated 1.66 Ga detrital zircons, then deformation along S1 continued after 1.66 Ga.

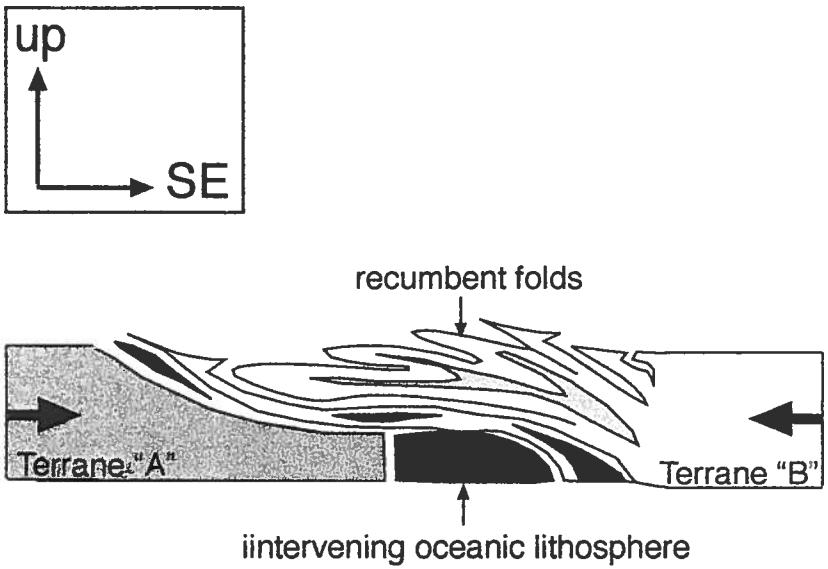

Figure 28a: D1 continental assembly and early intracontinental deformation creates low-angle fabrics. Fragments of oceanic lithosphere are transported along thrust structures and imbricated in accretionary prism.

1.73-1.66 Ga

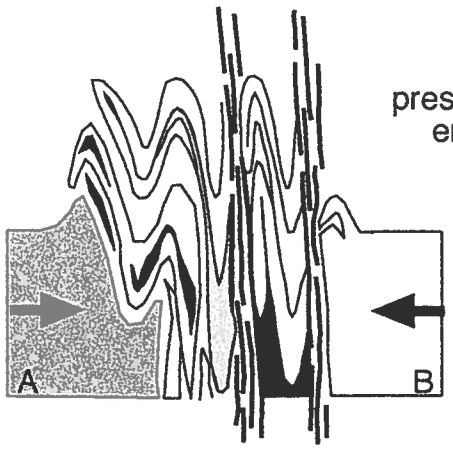

Figure 28b: D2 folding and shearing along broad, steeply-dipping intracontinental tectonic zones facilitates shortening of the lithosphere subsequent to assembly.

1.65-1.63 Ga

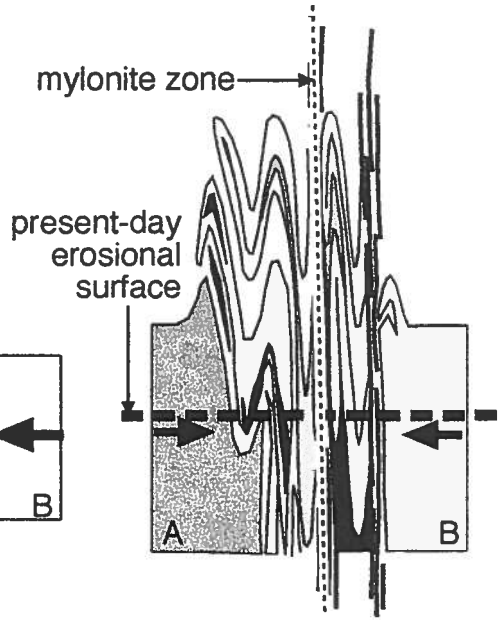

Figure 28c: D3 shearing along discrete, steeply-dipping mylonites and ultramylonites that reactivate D2 tectonic zones facillitates further shortening of the lithosphere in response to far-field stresses transmitted from a distant convergent margin.

1.42-1.3 Ga

Between 1.65 and 1.62 Ga, D2 deformation coincided with the steepening of D1 sheet-like structures along subvertical NE-trending structures (Fig. 28b). Metamorphic minerals that grew post-D1 along the Idaho Springs-Ralston shear zone document peak metamorphic temperatures of about 550°C. In the Gore Range shear zone, migmatites folded by tight F2 folds show retrogression of garnet to andalusite + biotite, which may have occurred during D2.

Mesoproterozoic mylonitization reactivated S2 domains between 1.45 and 1.3 Ga (Fig. 28c, Fig. 29) and was accompanied by retrogression of aluminosilicates and amphibolite grade assemblages to greenschist grade assemblages containing chlorite and muscovite (although 1.42 Ga mylonitization may have resulted in growth of andalusite in the Idaho Springs-Ralston shear zone).

4.2 A REGIONAL CONTEXT FOR TIMING OF DEFORMATION ALONG THE COLORADO MINERAL BELT SHEAR ZONE SYSTEM

The multiple periods of Proterozoic deformation along the Colorado Mineral Belt shear zone system correspond to magmatic and orogenic events

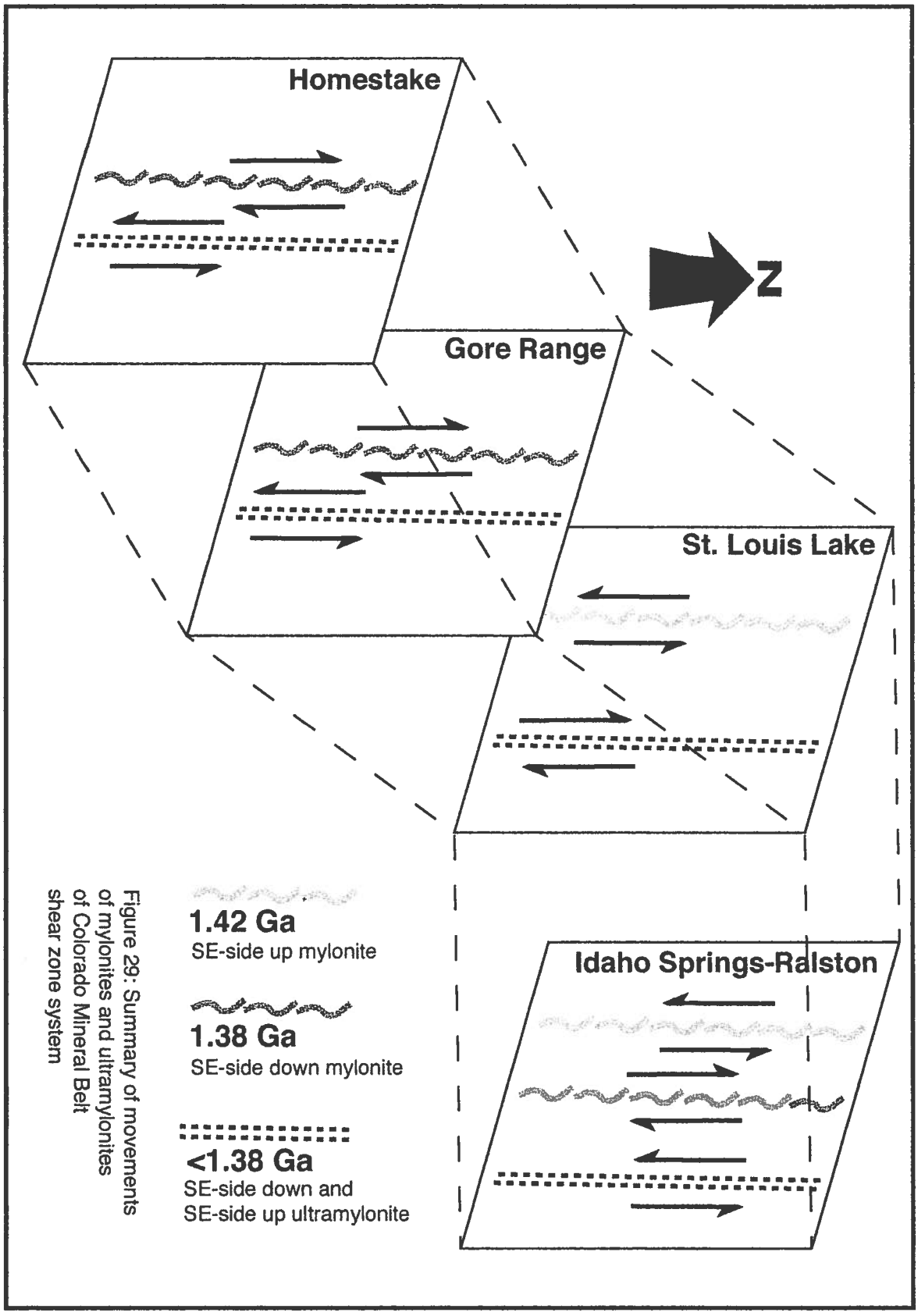

Figure 29: Summary of movements of mylonites and ultramylonites of Colorado Mineral Belt shear zone system

documented throughout Colorado and the southwestern U.S., suggesting that movement along the shear zones reflects responses to large-scale thermal and tectonic events instead of local events, such as the emplacement of individual plutons.

The few 1.73-1.72 Ga dates obtained in the Gore Range and Idaho Springs-Ralston shear zones may correspond with emplacement of the Boulder Creek and Rawah batholiths at 1721 +/- 15 Ma ([U-Pb SHRIMP], Premo and Fanning, 2000) and 1720 +/- 8 Ma ([U-Pb], Premo and Van Schmus, 1989), respectively. In Big Thompson Canyon, northern Front Range, a 1726 +/- 15 Ma trondhjemite pluton was emplaced shortly before an important stage of regional metamorphism ([U-Pb], Barovich, 1986). 1.73 Ga dates come from the arc-like volcanic supracrustal rocks in the Salida-Gunnison block south of the Colorado Mineral Belt shear zone system (Bickford and Boardman, 1984). Deformation between 1.73 and 1.72 Ga in central Colorado appears to have coincided with the completion of suturing between the Green Mountain arc and the Cheyenne Belt to the north, and the initiation of the Salida-Gunnison arc to the south (Reed et al., 1987).

1.7 Ga deformation dates in S1 domains of the Colorado Mineral Belt shear zone system are similar to deformation dates of 1.72-1.7 Ga associated with initially shallowly dipping foliations and subrecumbent folds in central Arizona (Karlstrom and Bowring, 1991). The Yavapai orogeny in central Arizona appears to have involved partitioned crustal shortening during amalgamation of lithospheric fragments to North America between 1.7 and 1.69 Ga (Karlstrom and Bowring, 1991).

Monazite growth at ~1.67 Ga in the Gore Range shear zone may have been a more local event coinciding with intrusion of the adjacent Cross Creek batholith, because 1.67 Ga deformation dates are not as abundant in the Homestake and Idaho Springs-Ralston shear zones.

1.65 to 1.62 Ga deformation dates coincide with the Mazatzal orogeny in southeastern Arizona (Karlstrom and Bowring, 1991), during which subvertical NE-trending fabrics developed. The Mazatzal orogeny is interpreted to have coincided with the development of a continental margin batholith above a northwest- or north-dipping subduction system located in southeastern Arizona (Selverstone et al., 1999) and traced across southern Colorado (Shaw and Karlstrom, 1999). In New Mexico, Bauer and Williams (1994) defined an

important deformation event between 1664 and 1654 Ma, based on intrusion of 1654 +/- 1 Ma Magdalena granite into 1664 +/- 3 Ma supracrustal rocks and the lack of foliation in the Magdalena granite. Bauer and Williams (1994) attributed this deformation to N-directed crustal shortening contemporaneous with the Mazatzal orogeny in southeastern Arizona.

1.62 Ga deformation dates correspond to dates of >1618 +/- 22 Ma for the Big Creek gneiss of the northern Front Range, 1627 +/- 4 Ma age for a quartz monzonite pluton in the Sierra Madre of northern Colorado, and emplacement ages for plutons in the Mount Tyndall area of the Wet Mountains, southern Colorado ([U-Pb], Premo and Van Schmus, 1989; [U-Pb], Bickford et al., 1989).

Mesoproterozoic movements in the Colorado Mineral Belt shear zone system correspond in time with intrusions emplaced between 1.3 and 1.5 Ga along a belt that spans Laurentia-Baltica (Nyman et al., 1994). Although the plutons have been described as anorogenic, recent studies have shown evidence for ~1.4 Ga deformation and metamorphism in the vicinity of many plutons (Nyman et al., 1994). In Colorado and New Mexico, ~1.4 Ga shear zones are moderately- to steeply-dipping and show evidence for synmagmatic deformation (Kirby and Karlstrom, 1993; Nyman et al., 1994). In the northern

Front Range of Colorado, the NE-trending, steeply-dipping Moose Mountain shear zone shows evidence for reverse-sense reactivation synchronous with intrusion of the ~1.4 Ga St. Vrain pluton (Selverstone et al., 2000). This shear zone is located 50 kilometers north of, and is roughly parallel to, the Idaho Springs-Ralston shear zone. The relationship of the Moose Mountain shear zone, and several other shear zones of northern Colorado suspected to have been active at ~1.4 Ga, to the Colorado Mineral Belt shear zone system is not fully understood. However, the northern Front Range shear zones do not appear to extend southwest across Colorado, as the Colorado Mineral Belt shear zone system does. Movement along the Colorado Mineral Belt shear zone system probably coincided with movement along northern Front Range shear zones at some time in the Mesoproterozoic.

4.3 TECTONIC SIGNIFICANCE OF THE COLORADO MINERAL BELT SHEAR ZONE SYSTEM

The Mesoproterozoic mylonites of the Colorado Mineral Belt shear zone system, and the Paleoproterozoic S2 high-strain domains that they overprint, record primarily dip-slip movements on subvertical fault planes (Fig. 7a,b). The

zones appear to have become subvertical during D2, with discrete mylonites reactivating broad S2 domains at middle crustal levels. Given these geometries, the shear zones appear to have caused large scale 'jostling' of blocks through 'non-Andersonian' kinematics. These types of movements could occur along a flower structure or as part of a transpressive system, but we do not find extensive evidence for either horizontal stretching lineations or horizontal shear sense indicators of strike-slip movement. So the question arises: What is the origin of this type of subvertical, dip-slip zone?

Major geologic discontinuities have not been identified across mylonite zones, S2 high-strain domains, or S1. The melange of oceanic-type rocks along the St. Louis Lake shear zone may represent a boundary that juxtaposed far-travelled packages of rocks during Paleoproterozoic accretion, similar to that proposed for the Moose Mountain shear zone in the northern Front Range (Selverstone et al., 2000). However, the St. Louis Lake shear zone does not appear to separate packages of rocks with different structural and metamorphic histories, as does the Moose Mountain shear zone (Selverstone et al., 2000). More likely, the St. Louis Lake shear zone juxtaposed rocks from different

structural levels during D2 intracontinental steepening of the initially low-angle, continental assembly-related S1 fabrics.

The mapping presented in this thesis shows the melange along the St. Louis Lake shear zone as an isolated fragment of oceanic-type rocks that was tectonically juxtaposed with granites and biotite schists along the shear zone during D2. This is in contrast to the oceanic melange observed along the Buckhorn Creek shear zone in the northern Front Range, which is interpreted to represent intact oceanic lithosphere into which arc plutons intruded during Paleoproterozoic continental accretion (Cavosie, 2001).

The Paleoproterozoic structures, with inferred deformation dates spanning 1.7-1.62 Ga, developed during a time of regional tectonism that was likely associated with the 'welding' together of arcs, and the welding of packages of arcs to the Archean Wyoming craton. This period of crustal shortening followed initial collisions between different arcs and the accretion of crustal material. Syn-tectonic plutons and batholiths of this period, such as the Cross Creek and Boulder Creek batholiths, do not appear to represent parts of the initial magmatic arcs, since they do not have isotopic signatures characteristic of arc plutons, and

there is no evidence andesites or adjacent suture zones (Shaw and Karlstrom, 1999; Aleinikoff, 1993; Reed, 1987).

In contrast to the D1 and D2 crustal assembly-related deformation that affected broad regions of Colorado, the Mesoproterozoic Colorado Mineral Belt shear zone system formed as a relatively narrow zone at a time when plate convergence was probably occurring some 1,000 kilometers to the south, based on the proposed boundary between the Mazatzal Province and the Grenville Province near the present-day New Mexico/Texas border (Karlstrom et al., 1999). Such a great distance from this margin, the mylonite system seems to have reactivated a zone of weakness related to Paleoproterozoic assembly. However, Mesoproterozoic mylonitization led to the development of a more focused belt of weakness and defined the trend that has influenced Phanerozoic deformation and magmatism along the Colorado Mineral Belt.

Comparison of the Colorado Mineral shear zone system with younger analogues can shed light on the importance of intracontinental zones of deformation, and the similarities among these zones, and can link the surface and shallow crustal level expression of such zones to their middle crustal analogues.

One relatively recent analogue is the Tien Shan of central Asia, where reactivation has taken place primarily along moderately- to steeply-dipping reverse structures (Avouac et al., 1993; Brookfield, 2000). Like the Colorado Mineral Belt shear zone system, the Tien Shan records a complex tectonic history of continental assembly that occurred within a broad, diffuse zone containing slices of many different rock packages (Allen and Vincent, 1997). In both areas, broad zones of assembly-related structural grain were reactivated as narrower, more discrete zones of intracontinental deformation thousands of kilometers from the plate margin. Structures within the Tien Shan and the Colorado Mineral Belt shear zone system are adjacent to plutons, and there is evidence for early syn-plutonic deformation (Brookfield, 2000). Although the magnitude of Precambrian offset across the Colorado Mineral Belt shear zone segments is difficult to determine, the Tien Shan faults have experienced several kilometers of offset during Cenozoic intracontinental reactivation (Yin et al., 1998). Most earthquakes on the Tien Shan faults have thrust solutions, indicating that this intracontinental zone of deformation is facilitating crustal shortening (Yin et al., 1998).

The North Tien Shan fault is interpreted to have originated as a steeply-dipping 'back-stop' to a zone of lithospheric fragments assembled in the late Paleozoic (Allen and Vincent, 1997). The fault was reactivated in the Cenozoic as a steeply-dipping north-directed thrust following the Paleozoic structural grain, but there is some evidence for dextral strike-slip movement (Allen and Vincent, 1997). A comparison of maps and cross-sections across the Colorado Mineral Belt shear zone system and the North Tien Shan fault illustrates some of the similarities and differences between these structures (Fig. 30a,b,c,d).

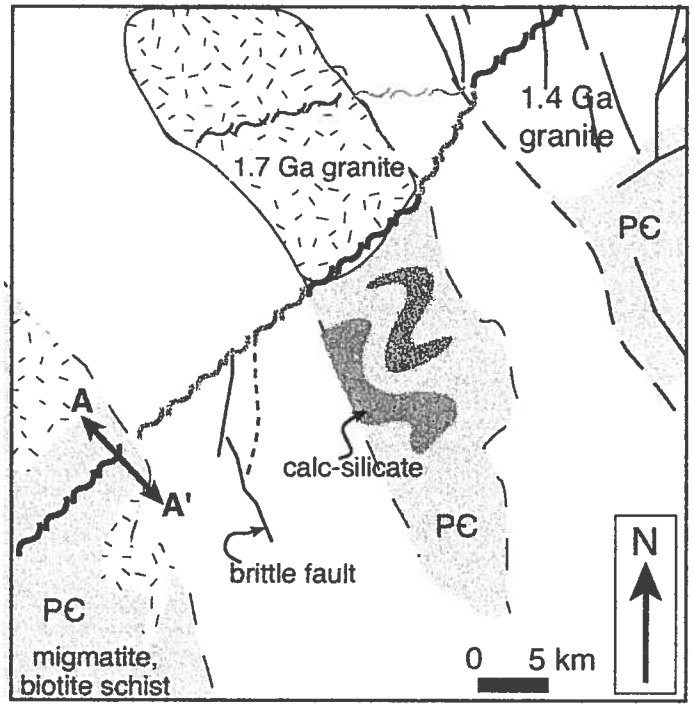

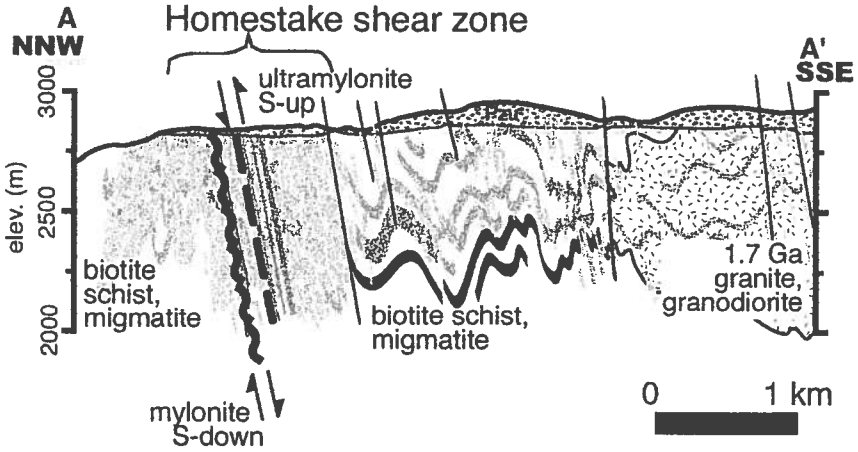

Figure 30: Comparison of maps and cross-sections of two intracontinental zones of deformation: the Homestake shear zone of the Colorado Mineral Belt shear zone system (after Shaw et al., 2001), and the North Tien Shan fault of the Tien Shan (after Allen and Vincent, 1997).

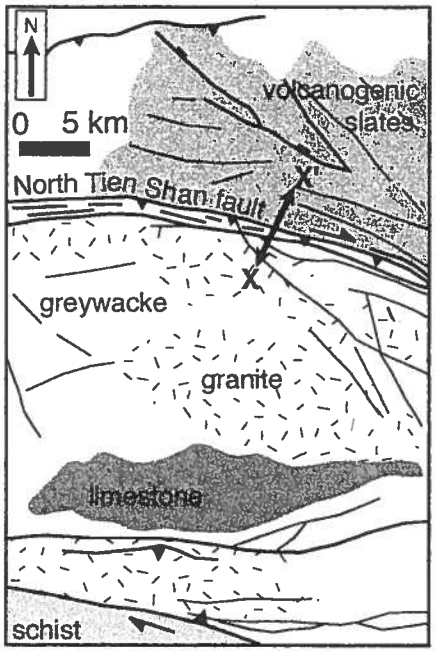

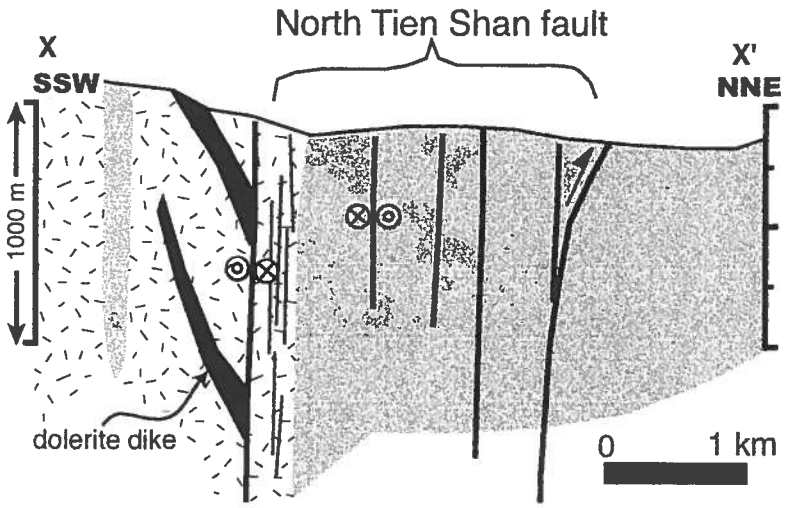

5.0 CONCLUSIONS

The Colorado Mineral Belt shear zone system is here defined as a Mesoproterozoic system of mylonites and ultramylonites, segments of which have moved contemporaneously during a protracted period of orogenesis between 1.3 and 1.45 Ga. Though the shear zone system is Mesoproterozoic, the system overprints a broader higher temperature high-strain domain that records a >70 Ma Paleoproterozoic orogenic episode. In this way, the Colorado Mineral Belt shear zone system may have reactivated a more diffuse zone of weakness associated with continental assembly, and in doing so, defined the trend that controlled Phanerozoic deformation and localization of magmatic systems along the Colorado Mineral Belt.

The long history of deformation along the Colorado Mineral Belt shear zone system indicates that lithospheric zones of weakness, first established as diffuse zones of weakness during continental assembly and later reactivated as narrow intracontinental zones, may remain as loci of geologic processes for hundreds of millions of years. This study of the Colorado Mineral Belt shear zone system documents many characteristics of intracontinental tectonic zones including 1. Origination of such zones in broad, subvertical domains of high strain

and foliation intensification that have steepened what are inferred to be initially low-angle sheet-like structures (Fig. 28a,b), 2. Reactivation of such zones as progressively narrower, discrete domains of increasingly lower-T/higher strain rate grain size reduction at progressively shallower depths (Fig. 28c), 3. Emplacement of plutons and mineralization multiple times along the zone (Fig. 1; Fig 4), and 4. Development of lithospheric-scale inhomogeneities such as negative gravity anomalies and slow mantle anomalies associated with the zone (Fig. 1; Fig 2; Fig. 3).

The Colorado Mineral Belt shear zone system is dominated by steeply-dipping structures with steeply-plunging mineral stretching lineations, indicating primarily dip slip movements along subvertical zones. A kinematic model that accounts for these movements involves the 'jostling' of blocks, up and then down along the same zone of weakness, possibly facilitating pluton emplacement or an interplay between crustal shortening and crustal collapse. What we do know about these movements is that they are observed in other intracontinental zones of deformation, such as the Tien Shan of central Asia, the Atlas Mountains of northern Africa, and the Laramide Rocky Mountains. Therefore, dip-slip movement along subvertical zones may be an important characteristic of

intracontinental zones of deformation that have remained as weak zones in the lithosphere, experiencing multiple episodes of reactivation over hundreds of millions of years.

6.0 APPENDICES

6.1 APPENDIX 1: MONAZITE ANALYTICAL TECHNIQUES

Spot analyses were accomplished using 15 kV accelerating voltage, 200 nA beam current, and a counting time of 600 seconds per element, resulting in a spot diameter of 3 to 5 microns. Several major element spot analyses were conducted for each population of monazite grains (for each sample, or subgroups of grains with distinct morphologies and chemical signatures within one sample). Major element results were hand-entered and used in trace element analyses.

Weight percent Y was measured to correct for the interference of the $Y_{L\gamma}$ peak with $Pb_{M\alpha}$. The Y correction was determined by Montel et al. (1996) by measuring the intensity of $Y_{L\gamma}$ on synthetic YPO_4. Extrapolation down to the Y content of monazite (<2 wt%) shows that this creates a maximum overestimate of the Pb content of about 30 ppm. In this study, 275 spot analyses gave an average 1.43 +/- 0.55 wt% Y. I corrected the total Pb by subtracting (wt%Y*0.0018) from measured the Pb, correcting the Pb value by an average of 25.8 ppm.

Using the corrected Pb, U, and Th measurements, and assuming negligible amounts of common Pb (Parrish, 1990), I applied the age equation of

Montel et al. (1996) to calculate the time of monazite growth. Although the closure temperature for monazite during crystallization is estimated at 800 C (M.L. Williams, personal communication), the mineral may be dissolved and reprecipitated at much lower temperatures (above ~300 C). Therefore, monazite dates can represent the timing of primary or metamorphic growth, or low-T deformation synchronous with fluid flux. Because monazite grains are analyzed in situ, I use crystal morphology, compositional zoning patterns, and textural context to better understand the events that triggered monazite growth at different times in the Proterozoic.

As a means of comparison, four grains were analyzed at both the University of Massachusetts electron microprobe lab and the New Mexico Institute of Technology lab. Dates obtained from each lab for the age domains within each grain were statistically similar within a 95% confidence interval when compared using a pooled t-test. The monazite analysis technique used in this study is identical to that used by Shaw, et al. (2001) in their study of the Homestake shear zone.

Monazite dates from within and around the Colorado Mineral Belt shear zone system are summarized in Figure 15. Date populations from these shear

zones were grouped together using the condition that they were statistically similar within a 95% confidence interval in pooled t-tests. Weighted means and standard deviations were calculated for the grouped date populations to summarize the deformational pulses recorded in the CMBSZ. Frequency curves for monazite grains from the Gore Range, St. Louis Lake, and Idaho Springs-Ralston shear zone segments were compared to curves for Homestake shear zone grains published in Shaw et al. (2001) to emphasize the similarities in date populations in each shear zone.

6.2 APPENDIX 2: RESTORING STRUCTURAL DATA

Because Phanerozoic strata are not exposed in the vicinity of Gore Range, St. Louis Lake, and Idaho Springs-Ralston shear zones, it is difficult to assess the effects of Phanerozoic tectonism on original orientations of structures andfabrics along these zones. At Homestake shear zone, bedding in overlying Upper Sawatch quartzite has an average orientation 320, 10E. This information was used to restore the field measurements in Table 1 and 2 to the Proterozoic orientations in Table 3.

Paleomagnetism studies, which provided information on regional tilting within tens of kilometers of the other shear zones, were used to restore Proterozoic measurements in those zones. Table 1 and 2 shows the average field measurements for fabric orientations in and along the shear zones and Table 3 shows the restored values. Field evidence and paleomagnetic data from late Cretaceous to mid-Tertiary intrusives in the northern Mosquito Range, about 25 km southeast of Gore Range shear zone, indicate that approximately 20 degrees of eastward tilt along a horizontal N-S axis occurred prior to sill emplacement around 65 Ma (Oppenheimer and Geissman, 1988).

Field observations and paleomagnetic studies conducted at Red Mountain, about 20 km southeast of St. Louis Lake shear zone, indicate between 15 and 25 degrees of tilting to the southeast, about a nearly horizontal axis with an azimuth of 015 (Geissman et al., 1992) in late Oligocene and younger time. Similar tilting has been documented for the easternmost, east-tilted flank of the Front Range (Kellogg, 1973; Hoblitt and Larson, 1975).

Paleomagnetic studies and mapping of the Paleozoic rocks near Table Mountain, 13 km southeast of Idaho Springs-Ralston shear zone, show evidence for eastward tilting of Paleozoic strata by 60° along a horizontal axis with azimuth

of 325° after intrusion of the 62 Ma Table Mountain intrusives (Hoblitt and Larson, 1975). Tilting of the intrusives and host beds resulted from uplift of the Precambrian block to the west, which may have included Idaho Springs-Ralston shear zone. However, Phanerozoic deformation in the Front Range is especially complex and many faults lie between Idaho Springs-Ralston shear zone and Table Mountain.

Table 3: Restored S2 and S3 tectonites, mineral stretching lineations, and F2 fold axial planes and fold axes presented in Table 1 of the text.

	Restored orientations	10° to W about horiz axis 320° az.	20° to W about horiz axis 0° az.	20° to W about horiz axis 015° az.	60° to W about horiz axis 325° az.
	Shear zone	HS	GR	SLL	ISR
S3a SE-side up mylonite/ phyllonite	strike and dip			083, 57S	233, 55N
	trend and plunge			48 to 132	27 to 242
S3b SE-side down mylonite	strike and dip	046, 79S	096, 72S/ 228, 88N		243, 79N
	trend and plunge	76 to 104	54 to 124/ 40 to 045		56 to 046
S3c SE-side up ultramylonite	strike and dip	030, 77E	035, 79E		035, 79E
	trend and plunge	66 to 060	78 to 107		62 to 058
S3d SE-side down mylonite	strike and dip			068, 71S	
	trend and plunge			65 to 123	
S2 hi-T tectonite	strike and dip	036, 83E	044, 67E	083, 60S	062, 86 S
	trend and plunge	78 to 074	63 to 094	53 to 131	42 to 068
F2	Axial plane strike and dip	036, 83E	205, 54W/ 116, 38S	073, 64S	227, 71 N
	Fold axis trend and plunge	41 to 042	24 to 007/ 36 to 222	61 to 142	35 to 243

Sample	Wt % Y	Wt % U	Wt % Th	Wt % Pb	Age (Ma)	Excluded da	Domain
A00TM1m1.1	1.7289	0.501	3.2501	0.379	1609		rim
A00TM1m1.2	0.9871	0.7339	3.0355	0.4346	1644		core
A00TM1m1.3	1.6861	0.4814	3.405	0.3961	1651	off edge of grain	
A00TM1m1.4	0.9026	0.8289	2.5235	0.4218	1645		core
A00TM1m1.5	0.8497	0.8158	2.6308	0.4385	1685		core
A00TM1m1.6	0.8443	0.8381	2.6395	0.439	1664		core
A00TM1m1.7	0.8373	0.8424	2.5541	0.4394	1684		core
A00TM1m1.8	0.9453	0.8473	2.776	0.4592	1687		core
A00TM1m1.9	0.5736	0.1637	3.8853	0.3353	1616	on inclusion	
A00TM1m1.10	1.0506	0.7405	2.6336	0.4135	1672		core
A00TM1m1.11	0.8539	0.799	2.8166	0.4445	1674		core
A00TM1m1.12	1.0121	0.1904	4.4992	0.399	1655	on domain bndary	
A00TM1m1.13	0.9298	0.7414	2.6307	0.4162	1682		core
A00TM1m1.14	0.8751	0.649	3.0477	0.4131	1649		core
A00TM1m103.1	2.6577	0.2588	4.4966	0.4156	1636		rim
A00TM1m103.2	2.4021	0.2239	5.3589	0.4659	1620		rim
A00TM1m103.3	2.2203	0.1798	5.3067	0.4476	1612		rim
A00TM1m103.4	1.8166	0.1875	6.1614	0.5033	1585		rim
A00TM1m103.5	1.2687	0.1868	5.5805	0.4786	1646		rim
A00TM1m103.6	1.2343	0.1913	5.5793	0.4631	1592		rim
A00TM1m103.7	0.9568	0.212	5.7323	0.4785	1590		rim
A00TM1m103.8	1.4686	0.1789	5.3617	0.4559	1632		rim
A00TM1m103.9	2.2585	0.2143	5.5169	0.4739	1617		rim
A00TM1m103.10	2.6397	0.2394	4.7106	0.4322	1657		rim
A00TM1m103.11	2.5856	0.23	4.3036	0.3981	1656		rim
A00TM1m103.12	1.9977	0.1898	5.2517	0.4521	1634		rim
A00TM1m103.13	1.341	0.192	5.5	0.4581	1594		rim
A00TM1m103.14	0.8472	0.1819	5.0573	0.4225	1595		rim
A00TM1m103.15	0.8067	0.1733	5.144	0.4217	1579	on a fracture	
A00TM1m103.16	1.3277	0.2034	5.8262	0.477	1569		rim
A00TM1m103.17	1.8928	0.1906	6.0291	0.5032	1611		rim
A00TM1m103.18	2.5237	0.2347	4.8131	0.4307	1628		rim
A00TM1m103.19	1.3098	0.7123	3.2467	0.4718	1732		core

Statistics

A00TM1m1	
	core
mean	1669
stdev	17
sterr	5
count	10
	rim
mean	1609
stdev	
sterr	
count	1

A00TM1m103	
	core
mean	1732
stdev	
sterr	
count	1
	rim
mean	1669
stdev	17
sterr	5
count	10

Sample	Wt % Y	Wt % U	Wt % Th	Wt % Pb	Age (Ma)	Excluded da	Domain
A00TM1m183.1	1.3242	0.391	3.5389	0.3858	1671		core
A00TM1m183.2	2.1118	0.4727	4.6366	0.4969	1677		core
A00TM1m183.3	1.0502	0.2114	5.2251	0.4353	1569	off edge of grain	
A00TM1m183.4	1.2923	0.3201	4.6611	0.4441	1642		rim
A00TM1m183.5	1.2569	0.3495	4.7097	0.4511	1626		rim
A00TM1m183.6	1.1414	0.311	4.6444	0.4454	1660		rim
A00TM1m191.1	1.8409	0.5375	4.4934	0.4916	1641		rim
A00TM1m191.2	1.8496	0.5356	4.4504	0.4916	1654		rim
A00TM1m191.3	1.6835	0.4491	4.5359	0.4728	1649		rim
A00TM1m191.4	2.0863	0.3952	3.6479	0.389	1641	on domain bndary	
A00TM1m191.5	2.1608	0.461	3.8718	0.4339	1676		core
A00TM1m191.6	1.977	0.5514	4.0655	0.4736	1674		core
A00TM1m191.7	1.9851	0.5413	4.4357	0.4947	1659		core
A00TM1m191.8	1.9197	0.4592	4.1608	0.4535	1669		core
A00TM1m191.9	1.3151	0.3666	3.2263	0.3527	1662		core
A00TM1m191.10	1.3026	0.3301	2.8011	0.3116	1671		core
A00TM1m191.11	1.6431	1.1297	3.4175	0.5841	1671		core
A00TM1m191.12	1.1573	0.2749	3.0676	0.3181	1680		core
A00TM1m191.13	1.192	0.2856	2.4932	0.2744	1668		core
A00TM1m191.14	1.1678	0.3287	2.7539	0.3143	1706		core
A00SL1m12.1	0.4596	0.0935	5.7246	0.4035	1445		one domain
A00SL1m12.2	0.4742	0.0874	5.5391	0.4099	1517		one domain
A00SL1m12.3	0.4231	0.0766	5.6743	0.4266	1552		one domain
A00SL1m12.4	0.4755	0.0906	5.554	0.4137	1524		one domain
A00SL1m12.5	0.4933	0.0923	5.9757	0.456	1564		one domain
A00SL1m12.6	0.3987	0.0757	4.7475	0.3384	1462		one domain
A00SL1m12.7	0.3965	0.0695	4.9691	0.3633	1508		one domain
A00SL1m12.8	0.4119	0.0959	5.3829	0.3967	1501		one domain
A00SL1m12.9	0.4234	0.1027	5.9489	0.4556	1560		one domain
A00SL1m12.10	0.4713	0.1057	6.3055	0.4771	1545		one domain

Statistics

A00TM1m183	
	core
mean	1674
stdev	4
sterr	3
count	2
	rim
mean	1643
stdev	17
sterr	10
count	3

A00TM1m191	
	core
mean	1674
stdev	13
sterr	4
count	10
	rim
mean	1648
stdev	7
sterr	4
count	3

A00SL1m12	
mean	1518
stdev	40
sterr	13
count	10

Sample	Wt % Y	Wt % U	Wt % Th	Wt % Pb	Age (Ma)	Excluded da	Domain
A00SL1m32.1	0.5275	0.0994	5.4194	0.4042	1515		one domain
A00SL1m32.2	0.5191	0.0922	5.5554	0.4161	1530		one domain
A00SL1m32.3	0.4786	0.1024	6.2012	0.4607	1519		one domain
A00SL1m32.4	0.4235	0.0819	5.0312	0.3854	1565		one domain
A00SL1m32.5	0.5029	0.0961	5.5537	0.413	1516		one domain
A00SL1m32.6	0.3589	0.1078	7.4773	0.5526	1523		one domain
A00SL1m32.7	0.3316	0.0987	6.7364	0.508	1551		one domain
A00SL1m32.8	0.3326	0.1076	6.969	0.5314	1564		one domain
A00SL1m32.9	0.3622	0.1205	8.2078	0.6267	1570		one domain
A00SL1m32.10	0.3406	0.0933	6.8501	0.4835	1461		one domain
A00BP1m51.1	0.9199	0.098	6.2516	0.3918	1291		rim
A00BP1m51.2	1.6266	0.4436	7.8976	0.5857	1343		core
A00BP1m51.3	2.0186	0.7514	8.5421	0.6971	1351		core
A00BP1m51.4	1.8562	0.6746	8.2958	0.6617	1345		core
A00BP1m51.5	1.6017	0.3621	7.9441	0.5628	1325		core
A00BP1m51.6	0.9831	0.1158	7.3688	0.4656	1302		rim
A00BP1m51.7	1.0592	0.1645	7.625	0.4838	1282.5		rim
A00BP1m51.8	1.5467	0.2632	7.9125	0.5348	1313.5		rim
A00BP1m51.9	1.8886	0.6826	8.1493	0.6605	1357		core
A00BP1m51.10	0.9873	0.0808	6.0432	0.3901	1338		core
A00BP1m51.11	1.6971	0.4709	9.0003	0.6325	1290		rim
A00BP1m51.12	1.6366	0.4462	9.1534	0.6488	1314		rim
A00BP1m51.13	1.8039	0.1506	5.6006	0.3701	1306		rim
A00BP1m51.14	1.1941	0.1368	7.9761	0.4857	1249.5		rim
A00BP1m108.1	2.005	0.4918	8.845	0.6448	1323		one domain
A00BP1m108.2	1.9225	0.4838	8.6912	0.6208	1297		one domain
A00BP1m108.3	2.0049	0.3684	8.5334	0.5977	1319		one domain
A00BP1m108.4	2.2005	0.3071	6.7207	0.4501	1251		one domain
A00BP1m108.5	0.9112	0.1605	8.1602	0.519	1294		one domain
A00BP1m108.6	0.9379	0.155	8.5981	0.5427	1292		one domain
A00BP1m108.7	0.9583	0.1589	8.5797	0.5375	1280		one domain
A00BP1m108.8	2.5076	0.4866	7.5857	0.5681	1323		one domain
A00BP1m108.9	2.4016	0.535	7.9178	0.5882	1301		one domain
A00BP1m108.10	2.0012	0.4543	8.4895	0.5986	1288		one domain

Statistics

A00SL1m32	
mean	1531
stdev	33
sterr	10
count	10

A00BP1m51	
	core
mean	1343
stdev	11
sterr	5
count	6
	rim
mean	1294
stdev	21
sterr	7
count	8

A00BP1m108	
mean	1297
stdev	22
sterr	7
count	10

Sample	Wt % Y	Wt % U	Wt % Th	Wt % Pb	Age (Ma)	Excluded da	Domain
K00IS1m5.1	1.3253	0.3512	2.6667	0.2948	1610		core
K00IS1m5.2	2.5245	0.8453	3.0666	0.4671	1635		core
K00IS1m5.3	2.0916	0.9539	2.8271	0.4074	1416		rim
K00IS1m5.4	0.9708	0.4229	1.9649	0.1252	808	off edge of grain	
K00IS1m5.5	1.9142	0.8027	3.0912	0.4521	1622		core
K00IS1m5.6	1.9236	0.7958	2.8647	0.38	1440		rim
K00IS1m5.b1	1.9013	0.8888	2.8468	0.3989	1434		rim
K00IS1m5.b2	2.0044	0.8164	3.033	0.3826	1394		rim
K00IS1m5.b3	1.6547	0.4611	2.9889	0.3362	1556	on domain bndary	
K00IS1m5.b4	1.3161	0.5908	3.0296	0.3684	1542	on domain bndary	
K00IS1m5.b5	2.1017	0.8184	2.9162	0.4134	1521	on domain bndary	
K00IS1m5.b6	2.5477	0.4882	3.0352	0.3676	1636		core
K00IS1m5.b7	1.2788	0.3465	2.7266	0.2966	1603		core
K00IS1m5.b8	1.4577	0.4105	3.2276	0.346	1581	on domain bndary	
K00IS1m5.b9	1.6202	0.4851	4.3056	0.4207	1502	on domain bndary	
K00IS1m5.b10	1.3672	0.3339	3.0743	0.3093	1557	on domain bndary	
K00IS1m5.b11	2.6547	0.5248	2.992	0.3747	1636		core
K00IS1m5.b12	2.442	0.9563	2.8939	0.4802	1622		core
K00IS1m5.b13	2.493	0.8723	3.2035	0.4729	1598	on domain bndary	
K00IS1m5.b14	2.4264	1.0542	3.2579	0.5166	1575	on domain bndary	
K00IS1m5.b15	1.2789	0.8832	2.6419	0.4151	1542	on domain bndary	
K00IS1m5.b16	1.1853	0.6779	1.8953	0.3269	1618		core

Statistics

K00IS1m5	
	core
mean	1623
stdev	12
sterr	4
count	8
	rim
mean	1421
stdev	21
sterr	10
count	4

Sample	Wt % Y	Wt % U	Wt % Th	Wt % Pb	Age (Ma)	Excluded da	Domain
K00IS1m14.1	2.0686	1.0656	3.0682	0.4506	1422		core
K00IS1m14.2	1.6421	1.0711	3.078	0.4387	1384		rim
K00IS1m14.3	1.5543	0.9701	2.8781	0.3964	1363		rim
K00IS1m14.4	0.5001	0.5215	1.5203	0.0553	379	off edge of grain	
K00IS1m14.b1	1.9176	0.931	3.1424	0.424	1421		core
K00IS1m14.b2	1.932	0.9213	3.2755	0.4275	1412		core
K00IS1m14.b3	2.0236	1.0977	3.2446	0.4699	1422		core
K00IS1m14.b4	2.0818	1.2799	3.1805	0.5103	1428		core
K00IS1m14.b5	2.0401	0.9656	3.2368	0.4386	1420		core
K00IS1m14.b6	2.0909	0.8942	3.3278	0.4304	1428		core
K00IS1m14.b7	2.0566	0.8442	3.4536	0.4199	1407		core
K00IS1m14.b8	2.2296	0.842	3.3956	0.4197	1418		core
K00IS1m14.b9	0.3373	0.7232	1.064	0.1148	729	off edge of grain	
K00IS1m14.b10	0.8667	0.6341	2.0294	0.2102	1088	off edge of grain	
K00IS1m14.b11	1.9497	0.7601	3.3014	0.3897	1404		core
K00IS9m1.1	0.6652	0.0567	4.0125	0.2417	1249		one domain
K00IS9m2.1	1.3482	0.126	6.6777	0.4324	1318		one domain
K00IS9m2.2	1.1447	0.0736	4.8179	0.3109	1327		one domain
K00IS9m2.3	1.0546	0.0836	4.6951	0.3006	1307		one domain
K00IS9m3.1	1.083	0.1766	7.2016	0.4725	1313		one domain
K00IS9m3.2	1.0344	0.0831	4.7549	0.2952	1270		one domain
K00IS9m3.3	0.7292	0.0294	3.5928	0.2123	1248		one domain
K00IS9m5.1	1.4726	0.3783	12.4913	0.8516	1340		one domain
K00IS9m5.2	1.364	0.1557	6.1506	0.4107	1330		one domain

Statistics

K00IS1m14	
	core
mean	1418
stdev	8
sterr	3
count	10
	rim
mean	1374
stdev	15
sterr	11
count	2

K00IS9m2	
mean	1317
stdev	10
sterr	6
count	3

K00IS9m3	
mean	1277
stdev	33
sterr	19
count	3

Sample	Wt % Y	Wt % U	Wt % Th	Wt % Pb	Age (Ma)	Excluded da	Domain
A00GG5m103.1	0.9548	0.1746	1.2319	0.1196	1389		one domain
A00GG5m103.2	1.2211	0.2175	3.6048	0.2847	1406		one domain
A00GG5m103.3	1.1308	0.1684	2.0708	0.1786	1439		one domain
A00GG5m105.1	1.3423	0.6391	4.0563	0.3976	1365		one domain
A00GG5m105.2	1.3398	0.6777	4.3858	0.436	1392		one domain
A00GG5m105.3	1.3066	0.6962	4.1078	0.4171	1376		one domain
A00GG5m105.4	1.5128	0.3589	3.5225	0.3004	1356		one domain
A00GG5m105.5	1.1805	0.4687	4.1823	0.3657	1356		one domain
A00GG5m105.6	1.3154	0.3895	3.6083	0.3172	1376		one domain
A00GG5m105.7	1.5496	0.4093	4.8114	0.3895	1348		one domain
A00GG5m105.8	1.1849	0.2493	4.8759	0.3747	1408		one domain
A00GG5m105.9	1.3189	0.4105	3.8659	0.3437	1398		one domain
A00GG5m105.10	1.2844	0.5303	4.1036	0.3809	1380		one domain
A00GG5m105.11	1.1372	0.2173	2.0089	0.1779	1380		one domain
A00GG5m105.12	1.1848	0.2166	4.0074	0.296	1343		one domain
A00GG5m105.13	1.1851	0.1815	4.5204	0.3175	1333	on an inclusion	
A00GG5m105.14	1.3291	0.4556	4.2306	0.368	1365		one domain
A00GG5m105.15	1.2931	0.546	4.7924	0.4265	1375		one domain
A00GG5m160.1	1.3939	0.4812	7.8857	0.6063	1373		one domain
A00GG5m160.2	1.0649	0.1415	2.3119	0.1879	1437		one domain
A00GG5m160.3	1.1251	0.2403	3.3497	0.2692	1386		one domain
A00GG5m160.4	1.257	0.3689	4.8716	0.3942	1382		one domain
A00GG5m160.5	1.2447	0.3136	4.0712	0.3358	1402		one domain
A00GG5m224.1	1.1511	0.2467	3.2385	0.2635	1386		one domain
A00GG5m224.2	1.398	0.4027	4.9948	0.4133	1394		one domain
A00GG5m224.3	1.2522	0.2928	2.9165	0.2705	1472		one domain
A00GG5m224.4	1.1372	0.2116	2.6846	0.2292	1438		one domain
A00GG5m224.5	1.1979	0.3082	5.2241	0.387	1331	on an inclusion	
A00GG5m224.6	1.2816	0.355	5.0806	0.4157	1419		one domain
A00GG5m224.7	1.3981	0.3006	5.2649	0.3945	1351	on an inclusion	
A00GG5m224.8	1.3987	0.3415	5.6135	0.5034	1585	off edge of grain	
A00GG5m224.9	1.1384	0.1813	2.6453	0.2127	1395		one domain
A00GG5m224.10	1.0915	0.1404	2.0778	0.1701	1421		one domain

Statistics

A00GG5m103	
mean	1411
stdev	25
sterr	15
count	3

A00GG5m105	
mean	1373
stdev	19
sterr	5
count	14

A00GG5m160	
mean	1396
stdev	25
sterr	11
count	5

A00GG5m224	
mean	1418
stdev	30
sterr	11
count	7

Sample	Wt % Y	Wt % U	Wt % Th	Wt % Pb	Age (Ma)	Excluded da	Domain
A00GG5m305.1	1.2915	0.4639	3.5153	0.3351	1405		core
A00GG5m305.2	1.1349	0.1779	4.2074	0.3217	1437	off edge of grain	
A00GG5m305.3	1.2116	0.2058	5.8799	0.4061	1334		rim
A00GG5m305.4	1.2668	0.3213	7.1773	0.5128	1340		rim
A00GG5m305.5	1.3118	0.3611	5.6903	0.4678	1451	on domain bndary	
A00GG5m305.6	1.2927	0.3079	3.2876	0.2808	1386		core
A00GG5m305.7	1.1784	0.2973	3.1867	0.2766	1409		core
A00GG5m305.8	1.2175	0.3079	2.9084	0.2586	1397		core
A00GG5m305.9	1.2127	0.3402	3.1076	0.2812	1409		core
A00GG5m305.10	1.266	0.4166	3.4234	0.3104	1372		core
A00GG5m305.11	1.2719	0.4364	3.3645	0.3258	1432	on domain bndary	
A00GG11m1.1	1.5621	0.4199	12.2284	0.8025	1275		rim
A00GG11m1.2	1.5905	0.4423	13.7582	0.8828	1256		rim
A00GG11m1.3	1.6199	0.4743	13.3198	0.8586	1248		rim
A00GG11m1.4	1.6204	0.4298	15.4273	0.9566	1232		rim
A00GG11m1.5	1.0695	0.1471	7.7579	0.4962	1303		core
A00GG11m1.6	1.5867	0.4354	15.4075	0.947	1220	overlap with .4	
A00GG11m1.7	1.2309	0.2779	11.4629	0.6946	1218	off edge of grain	
A00GG11m1.8	1.1374	0.1176	6.5613	0.4204	1309		core
A00GG11m2.1	1.1738	0.1166	6.9588	0.4525	1332		one domain
A00GG11m2.2	1.1385	0.1195	6.4947	0.4259	1336		one domain
A00GG11m2.3	1.1776	0.1203	5.5861	0.3808	1372		one domain
A00GG11m2.4	1.1128	0.1022	5.5271	0.3655	1346		one domain
A00GG11m2.5	1.171	0.1481	7.316	0.4901	1356		one domain
A00GG11m2.6	1.1141	0.1366	6.4781	0.4386	1366		one domain
A00GG11m2.7	1.1809	0.1588	6.8172	0.4665	1367		one domain
A00GG11m2.8	1.0841	0.1328	6.7279	0.4452	1343		one domain
A00GG11m2.9	1.1302	0.1372	7.3284	0.4962	1377		one domain
A00GG11m2.10	1.162	0.1205	6.1366	0.4097	1355		one domain

Statistics

A00GG5m305	
	core
mean	1396
stdev	15
sterr	6
count	6
	rim
mean	1337
stdev	4
sterr	3
count	2

A00GG11m1	
	core
mean	1306
stdev	4
sterr	3
count	2
	rim
mean	1253
stdev	18
sterr	9
count	4

A00GG11m2	
mean	1355
stdev	15
sterr	5
count	10

Sample	Wt % Y	Wt % U	Wt % Th	Wt % Pb	Age (Ma)	Excluded da	Domain
A00GG11m52.1	1.5703	0.4346	10.5725	0.7323	1315		one domain
A00GG11m52.2	1.6129	0.426	9.9557	0.692	1313		one domain
A00GG11m52.3	1.6231	0.4057	11.6057	0.7765	1296		one domain
A00GG11m52.4	1.6497	0.4373	10.2347	0.7131	1316		one domain
A00GG11m52.5	1.5817	0.4359	10.8321	0.7327	1289		one domain
A00GG11m52.6	1.0197	0.1848	9.5215	0.6046	1294		one domain
A00GG11m52.7	1.3276	0.3089	10.1133	0.6472	1259	on inclusion	
K00IS1m1.1	1.3649	0.3555	2.0618	0.2692	1715		
K00IS1m2.1	1.3904	0.4116	2.3033	0.3093	1739		
K00IS1m2.2	1.3337	0.3649	2.099	0.2784	1735		
K00IS1m4.1	1.5697	1.5716	3.5654	0.7354	1703		core
K00IS1m4.2	1.7469	1.2092	3.3439	0.6034	1677		rim
K00IS1m4.3	1.4536	0.5534	1.9361	0.2123	1191	on fracture	
K00IS1m4.4	2.0947	0.8298	2.4242	0.3895	1549	on fracture	
K00IS1m4.5	2.4217	0.7222	3.3435	0.4656	1672		rim
K00IS1m4.b1	1.3631	1.3014	3.1962	0.5841	1597	on domain bndary	
K00IS1m4.b2	1.3116	0.3475	2.4126	0.2876	1677		rim
K00IS1m4.b3	1.2825	0.3901	2.8869	0.3401	1694		core
K00IS1m4.b4	1.7746	1.1965	3.5093	0.6155	1684		core
K00IS1m4.b5	2.1183	0.5676	3.0088	0.3973	1677		rim
K00IS1m4.b6	2.109	0.5849	2.9893	0.4067	1700		core
K00IS1m4.b7	1.4307	0.7844	3.1276	0.4697	1688		core
K00IS1m4.b8	2.1827	0.5369	2.8324	0.3686	1650		rim
K00IS1m4.b9	1.7682	0.2745	3.1521	0.2542	1330	off edge of grain	
K00IS1m4.b10	2.4254	0.6002	3.2145	0.4254	1686		rim
K00IS1m4.b11	2.1303	0.6401	2.8726	0.3842	1597	off edge of grain	

Statistics

A00GG11m52	
mean	1304
stdev	12
sterr	5
count	6

K00IS1m4	
	core
mean	1694
stdev	8
sterr	4
count	5
	rim
mean	1673
stdev	12
sterr	5
count	6

Sample	Wt % Y	Wt % U	Wt % Th	Wt % Pb	Age (Ma)	Excluded da	Domain
K00IS1m8.1	1.2809	0.3703	2.004	0.2653	1695		core
K00IS1m8.2	1.4345	0.3883	2.6495	0.3226	1701		core
K00IS1m8.3	1.3116	0.356	1.9963	0.2617	1701		core
K00IS1m8.4	1.4699	0.4363	3.1391	0.3736	1696		core
K00IS1m8.5	1.9706	0.8145	3.1057	0.4821	1702		core
K00IS1m8.6	2.206	0.6062	3.1439	0.4203	1683		core
K00IS1m8.7	2.0608	0.7388	3.0649	0.3752	1423		rim
K00IS1m8.8	1.9284	0.7549	2.9248	0.3709	1428		rim
K00IS1m8.9	2.0489	0.492	3.0377	0.3868	1712		core
K00IS1m8.10	1.8255	1.8064	2.7832	0.6988	1618	on domain boundary	
K00IS1m8.11	2.6312	0.7379	2.92	0.4497	1713		core
K00IS1m8.12	2.232	0.7535	2.8764	0.386	1492	on domain boundary	
K00IS1m8.b1	2.2337	0.5571	3.1624	0.4135	1703		core
K00IS1m8.b2	1.9706	0.7789	3.1238	0.4639	1672		core
K00IS1m8.b3	2.095	0.8891	3.419	0.5173	1670		core
K00IS1m8.b4	1.9752	0.7987	3.1843	0.4796	1689		core
K00IS1m8.b5	2.0554	0.5058	3.119	0.3894	1681		core
K00IS1m8.b6	1.8009	1.985	2.8649	0.7691	1647		intermed
K00IS1m8.b7	1.7894	1.9094	2.859	0.7534	1658		intermed
K00IS1m8.b8	2.7075	0.6888	2.8948	0.4201	1664		intermed
K00IS1m8.b9	1.3914	0.3669	2.7248	0.317	1675		core
K00IS1m8.b10	1.2888	0.3816	2.4876	0.3024	1674		core
K00IS1m8.b11	1.6931	1.5294	2.6199	0.6491	1703		core
K00IS1m8.b12	2.4559	0.6621	2.9905	0.4178	1658		intermed
K00IS1m8.b13	1.4917	0.8588	2.7623	0.4553	1664		intermed
K00IS1m8.b14	2.2924	0.5497	3.0799	0.3856	1629		intermed
K00IS1m8.b15	2.1012	0.7966	3.1534	0.4146	1489	on domain boundary	
K00IS1m8.b16	2.0883	0.7592	3.1687	0.3784	1394		rim
K00IS1m8.b17	0.2561	0.3801	0.939	0.1396	1335	off edge of grain	
K00IS1m9.1	1.9818	0.8965	3.455	0.5132	1645		

Statistics

K00IS1m8	
	core
mean	1692
stdev	14
sterr	4
count	16
	intermediate
mean	1653
stdev	13
sterr	5
count	6
	rim
mean	1415
stdev	18
sterr	11
count	3

Sample	Wt % Y	Wt % U	Wt % Th	Wt % Pb	Age (Ma)	Excluded da	Domain
K00IS10m2.1	1.3004	2.3907	7.1765	1.003	1395		one domain
K00IS10m2.2	1.2844	1.0072	5.9405	0.6108	1395		one domain
K00IS10m2.3	0.5174	1.2698	3.9424	0.538	1389		one domain
K00IS10m3.1	1.0432	0.8863	1.6471	0.3107	1406		one domain
K00IS10m3.2	0.9793	0.8206	1.6826	0.287	1360		one domain
K00IS10m3.3	1.0818	1.0379	1.8329	0.3508	1383		one domain
K00IS10m4.1	1.2678	1.9054	10.1618	1.0666	1374		one domain
K00IS10m4.2	1.1729	3.3013	11.9345	1.4918	1376		one domain
K00IS10m5.1	1.1422	3.6657	6.5762	1.2411	1383		one domain
K00IS10m5.2	1.1715	2.0145	5.5184	0.8208	1409		one domain
K00IS10m5.3	0.9604	0.7533	4.5431	0.4526	1365		one domain
K00IS10m7.1	1.0586	3.0707	8.8856	1.2608	1390		one domain
K00IS10m7.2	0.9274	1.1485	12.7217	1.0604	1376		one domain
K00IS10m7.3	0.7577	1.1548	10.5305	0.9245	1377		one domain

Statistics

K00IS10multi	
mean	1384
stdev	14
sterr	4
count	14

Homestake Shear Zone

S1a/S1b fol		L1 MSL		Location	Rock type	S1a/S1b fol		L1 MSL		Location	Rock type
strike	dip	trend	plunge			strike	dip	trend	plunge		
50	77 S			Hrnsilver	Xmigmatite	230	73 W			Tennessee Ps	Xmigmatite
22	55 E			Hrnsilver	Xmigmatite	221	73 W			Tennessee Ps	Xmigmatite
20	65 E			Hrnsilver	Xmigmatite	205	80 W	25	45	Tennessee Ps	Xmigmatite
55	74 S			Hrnsilver	Xmigmatite	218	72 W			Tennessee Ps	Xmigmatite
40	64 E			Hrnsilver	Xmigmatite	46	88 S			Tennessee Ps	Xmigmatite
260	77 N			Hrnsilver	Xmigmatite	35	85 E	355	50	Tennessee Ps	Xmigmatite
250	80 N	38	34	Hrnsilver	Xmigmatite	210	70 W			Tennessee Ps	Xmigmatite
210	80 W	346	76	Hrnsilver	Xmigmatite	360	79 E			Tennessee Ps	Xmigmatite
50	85 S			Hrnsilver	Xmigmatite	185	78 W			Tennessee Ps	Xmigmatite
318	54 N			Hrnsilver	Xmigmatite	360	85 E			Tennessee Ps	Xmigmatite
340	38 E			Hrnsilver	Xmigmatite	10	90 V			Tennessee Ps	Xmigmatite
322	40 E			Hrnsilver	Xmigmatite	25	90 V			Tennessee Ps	Xmigmatite
310	55 N			Hrnsilver	Xmigmatite	30	90 V			Tennessee Ps	Xmigmatite
282	31 N			Hrnsilver	Xmigmatite	55	90 V			Hmestke Ck/Eagle Rv	Xgranodiorite
320	39 N			Hrnsilver	Xmigmatite	15	11 E	145	11	Hmestke Ck/Eagle Rv	Xgranodiorite
326	22 N			Hrnsilver	Xmigmatite	250	8 N	352	7	Hmestke Ck/Eagle Rv	Xgranodiorite
195	66 W			W of Hmestke Ck	Xmigmatite	246	28 N			Hmestke Ck/Eagle Rv	Xgranodiorite
350	90 V			W of Hmestke Ck	Xmigmatite	285	11 N	348	22	Hmestke Ck/Eagle Rv	Xgranodiorite
235	81 W			W of Hmestke Ck	Xmigmatite	5	65 E			Hmestke Ck/Eagle Rv	Xgranodiorite
99	88 S			W of Hmestke Ck	Xmigmatite	23	40 E			Hmestke Ck/Eagle Rv	Xgranodiorite
30	74 E			W of Hmestke Ck	Xmigmatite	15	39 E			Hmestke Ck/Eagle Rv	Xgranodiorite
270	71 N			W of Hmestke Ck	Xmigmatite	350	62 E			Hmestke Ck/Eagle Rv	Xgranodiorite
259	60 N			W of Hmestke Ck	Xmigmatite	42	46 S			Hmestke Ck/Eagle Rv	Xgranodiorite
296	58 N			W of Hmestke Ck	Xmigmatite	170	90 V			Hmestke Ck/Eagle Rv	Xgranodiorite
55	65 S			W of Hmestke Ck	Xmigmatite	340	70 E	199	37	Hmestke Ck/Eagle Rv	Xgranodiorite
15	60 E			W of Hmestke Ck	Xmigmatite	178	72 W			Hmestke Ck/Eagle Rv	Xgranodiorite
202	70 W			W of Hmestke Ck	Xmigmatite	210	52 W	355	40	Hmestke Ck/Eagle Rv	Xgranodiorite
274	54 N			Tennessee Ps	Xmigmatite	175	85 W			Hmestke Ck/Eagle Rv	Xgranodiorite
328	68 N			Tennessee Ps	Xmigmatite	360	85 E			Hmestke Ck/Eagle Rv	Xgranodiorite
208	72 W			Tennessee Ps	Xmigmatite	185	75 W	rake 55 frm N		Hmestke Ck/Eagle Rv	Xgranodiorite
20	90 V			Tennessee Ps	Xmigmatite	208	80 W			Hmestke Ck/Eagle Rv	Xgranodiorite

Homestake Shear Zone cont.

S1a/S1b fol			L1 MSL		Location	Rock type
strike	dip		trend	plunge		
25	74	E			Hmestke Ck/Eagle Rv	Xgranodiorite
46	54	S			Hmestke Ck/Eagle Rv	Xgranodiorite
40	60	E			Hmestke Ck/Eagle Rv	Xgranodiorite
7	64	E			Hmestke Ck/Eagle Rv	Xgranodiorite
25	62	E			Hmestke Ck/Eagle Rv	Xgranodiorite
3	40	E			Hmestke Ck/Eagle Rv	Xgranodiorite
10	25	E			Hmestke Ck/Eagle Rv	Xgranodiorite
351	40	E			Hmestke Ck/Eagle Rv	Xgranodiorite
340	90	V			Hmestke Ck/Eagle Rv	Xgranodiorite
340	65	E			Hmestke Ck/Eagle Rv	Xgranodiorite
300	31	N			Hmestke Ck/Eagle Rv	Xgranodiorite
330	20	N			Hmestke Ck/Eagle Rv	Xgranodiorite
255	53	N			Hmestke Ck/Eagle Rv	Xgranodiorite
210	34	W			Hmestke Ck/Eagle Rv	Xgranodiorite
285	15	N			Hmestke Ck/Eagle Rv	Xgranodiorite
263	25	N			Hmestke Ck/Eagle Rv	Xgranodiorite
288	32	N			Hmestke Ck/Eagle Rv	Xgranodiorite
25	78	E			Hmestke Ck/Eagle Rv	Xgranodiorite
202	32	W			Eagle Rv	Xmigmatite
345	47	E	10	40	Eagle Rv	Xmigmatite
315	69	N			Eagle Rv	Xmigmatite
208	68	W			Eagle Rv	Xmigmatite
345	52	E			Eagle Rv	Xmigmatite
288	45	N			Eagle Rv	Xmigmatite

S3 mylonite and ultramylonite data

S3 mylonitic fol			L3 MSL on S3		Shear snse	Location	Rock type
strike	dip		trend	plunge			
45	79	E	160	70	SE-side down	Hrnslvr	Xmigmatite
47	78	S	146	64	SE-side down	Hrnslvr	Xmigmatite
40	65	E	108	71	SE-side down	Hrnslvr	Xmigmatite
51	66	S	170	66	SE-side down	Hrnslvr	Xmigmatite
35	73	E	138	73	SE-side down	Hrnslvr	Xmigmatite
45	85	S	130	85	SE-side down	Hrnslvr	Xmigmatite

S3 ultramyl fol			L3 MSL on S3		Shear snse	Location	Rock type
strike	dip		trend	plunge			
30	82	E	75	78	SE-side up	Hrnslvr	Xmigmatite
25	85	E	60	65	SE-side up	Hrnslvr	Xmigmatite
25	88	E	40	87	SE-side up	Hrnslvr	Xmigmatite
35	75	E	127	71	SE-side up	Hrnslvr	Xmigmatite
24	70	E	47	67	SE-side up	Hrnslvr	Xmigmatite
32	74	E	61	72	SE-side up	Hrnslvr	Xmigmatite
42	43	E	132	43	SE-side up	Hrnslvr	Xmigmatite

Homestake Shear Zone cont.

F1c fold data							
S1a/S1b folded		S1c axial plane		F1c fold axis		Location	Rock type
strike	dip	strike	dip	trend	plunge		
50	87 S	350	86 E	350	6	S of Hrnslver	Xmigmatite
350	73 E	320	70 E	355	55	S of Hrnslver	Xmigmatite
280	65 N	210	73 W	351	65	S of Hrnslver	Xmigmatite
10	80 E	160	74 W	179	49	S of Hrnslver	Xmigmatite
11	80 E	165	68 W	335	78	S of Hrnslver	Xmigmatite
		346	85 E	97	83	S of Hrnslver	Xmigmatite
23	85 E	334	72 E	24	64	S of Hrnslver	Xmigmatite
25	80 E	355	78 E	14	55	S of Hrnslver	Xmigmatite
208	80 W			15	23	S of Hrnslver	Xmigmatite
230	65 W	341	66 E	10	64	S of Hrnslver	Xmigmatite
75	40 S	218	57 W	5	39	S of Hrnslver	Xmigmatite
350	90	320	80 E	352	70	S of Hrnslver	Xmigmatite
235	81 W	268	85 N	296	80	S of Hrnslver	Xmigmatite
355	86 E	282	38 N	355	25	S of Hrnslver	Xmigmatite
42	85 S	245	83 N	360	70	S of Hrnslver	Xmigmatite
209	50 W	233	81 W	239	30	S of Hrnslver	Xmigmatite
167	19 W	102	60 S	270	20	S of Hrnslver	Xmigmatite
315	50 N	245	81 N			S of Hrnslver	Xmigmatite
55	65 S	162	19 W	224	5	S of Hrnslver	Xmigmatite

Gore Range Shear Zone

S1a/S1b fol			L1 MSL		Location	Rock type	Sample	S1a/S1b fol			L1 MSL		Location	Rock type	Sample
strike	dip		trend	plunge				strike	dip		trend	plunge			
189	89	W			N Tenmile Ck	Xmigmatite		351	64	E	143	57	Officer's Gulch	Xcalc-silicate	
189	83	W	206	45	N Tenmile Ck	Xmigmatite		346	77	E			Officer's Gulch	Xcalc-silicate	
212	67	W			N Tenmile Ck	Xmigmatite		354	69	E	151	68	Officer's Gulch	Xcalc-silicate	
185	44	W			N Tenmile Ck	Xmigmatite		304	66	N	98	32	Officer's Gulch	Xcalc-silicate	
338	46	E			N Tenmile Ck	Xgranodiorite		327	65	E	92	64	Officer's Gulch	Xcalc-silicate	
356	68	E			N Tenmile Ck	Xgranodiorite		255	40	N			Eccles Pass	XCross Ck gr	
340	74	E			N Tenmile Ck	Xgranodiorite		161	24	W			Eccles Pass	Xcalc-silicate	
5	80	E			N Tenmile Ck	Xmigmatite		176	43	W	210	28	Eccles Pass	Xcalc-silicate	
334	80	E			N Tenmile Ck	Xgranodiorite		120	40	S	210	39	Eccles Pass	Xcalc-silicate	
32	67	E			N Tenmile Ck	Xgranodiorite		200	54	W			Eccles Pass	Xcalc-silicate	
139	74	W	139	6	N Tenmile Ck	Xgranodiorite		130	50	S	252	37	Eccles Pass	Xcalc-silicate	
259	83	N			N Tenmile Ck	Xgranodiorite		108	48	S	180	46	Eccles Pass	Xcalc-silicate	
255	70	N			N Tenmile Ck	Xgranodiorite		335	49	E			Eccles Pass	Xmigmatite	
255	80	N			N Tenmile Ck	Xgranodiorite		135	48	S			Eccles Pass	Xmigmatite	
5	62	E			N Tenmile Ck	Xmigmatite		24	17	E			Eccles Pass	Xmigmatite	
340	79	E			N Tenmile Ck	Xgranodiorite		50	60	S			Eccles Pass	Xmigmatite	
340	75	E			N Tenmile Ck	Xgranodiorite		18	45	E			Eccles Pass	Xmigmatite	
250	67	N			N Tenmile Ck	Xgranodiorite		32	54	E			Eccles Pass	Xmigmatite	
185	61	W			N Tenmile Ck	Xgranodiorite		168	48	W	177	15	Eccles Pass	Xmigmatite	
198	82	W			N Tenmile Ck	Xgranodiorite		95	56	S			Eccles Pass	Xmigmatite	
169	40	W	208	38	N Tenmile Ck	Xmigmatite		325	65	E			Eccles Pass	Xmigmatite	
198	40	W	259	64	N Tenmile Ck	Xmigmatite		80	21	S			Eccles Pass	Xmigmatite	
195	57	W	220		N Tenmile Ck	Xmigmatite		173	82	W			Eccles Pass	Xcalc-silicate	
201	61	W			N Tenmile Ck	Xmigmatite		153	42	W			Eccles Pass	Xcalc-silicate	
174	51	W			N Tenmile Ck	Xgranodiorite		165	80	W			Eccles Pass	Xcalc-silicate	
147	32	W			N Tenmile Ck	Xgranodiorite		327	81	E			Eccles Pass	Xmigmatite	
199	75	W			N Tenmile Ck	Xgranodiorite		30	80	E			Eccles Pass	Xcalc-silicate	
335	42	W			N Tenmile Ck	Xbiotite gnss	KTM99-11	340	20	E	70	20	Eccles Pass	Xquartzite	
337	61	E	350	26	Officer's Gulch	Xcalc-silicate		345	48	E			Eccles Pass	Xquartzite	
207	76	W			Officer's Gulch	Xcalc-silicate		332	80	E			Eccles Pass	Xquartzite	
336	68	E			Officer's Gulch	Xcalc-silicate		213	45	W			Eccles Pass	Xmigmatite	

Gore Range Shear Zone cont.

S1a/S1b fol			L1 MSL		Location	Rock type	Sample
strike	dip		trend	plunge			
340	20	E	70	20	Eccles Pass	Xquartzite	A00TM6
345	48	E			Eccles Pass	Xquartzite	A00TM7
332	80	E			Eccles Pass		A00TM8
108	48	S	180	46	Eccles Pass	Xmigmatite	A99TM3
247	74	N	327	74	Meadow Ck	XCross Ck gr	
244	83	N	331	81	Meadow Ck	XCross Ck gr	
105	24	S	126	27	Meadow Ck	Xmigmatite	
324	84	E	328	39	Meadow Ck	Xmigmatite	
320	76	E	343	36	Meadow Ck	Xmigmatite	
326	71	E			Meadow Ck	Xmigmatite	
9	85	E			Meadow Ck	Xmigmatite	
358	64	E			Meadow Ck	Xmigmatite	
345	90	V			Meadow Ck	Xmigmatite	
146	85	W			Meadow Ck	Xmigmatite	
12	80	E			Meadow Ck	Xmigmatite	
174	75	W			Meadow Ck	Xmigmatite	
10	50	E			Meadow Ck	Xmigmatite	
163	68	W			Meadow Ck	Xmigmatite	
190	82	W			Meadow Ck	Xmigmatite	
185	71	W			Meadow Ck	Xmigmatite	
188	73	W			Meadow Ck	Xmigmatite	
206	54	W			Meadow Ck	Xmigmatite	
14	84	E			Meadow Ck	Xmigmatite	
300	56	S			Meadow Ck	XCross Ck gr	KTM99-2
320	76	E			Meadow Ck	Xgranodiorite	KTM99-3
335	70	W			Meadow Ck	Xmigmatite	KTM99-5
225	45	E			Meadow Ck	Xmigmatite	KTM99-6
262	44	N			Corral Ck	Xmigmatite	

S1a/S1b fol			L1 MSL		Location	Rock type	Sample
strike	dip		trend	plunge			
195	17	W			Corral Ck	Xmigmatite	
220	30	W			Corral Ck	Xmigmatite	
254	71	N			Corral Ck	Xmigmatite	
251	39	N			Corral Ck	Xmigmatite	
253	50	W			Corral Ck	Xmigmatite	
344	65	E			Corral Ck	Xmigmatite	
192	51	W			Corral Ck	Xmigmatite	
220	48	W			Corral Ck	Xmigmatite	
156	64	W	246	64	Corral Ck	Xmigmatite	
190	36	W			Corral Ck	Xmigmatite	
130	74	W	134	12	Corral Ck	Xmigmatite	
305	54	N			Corral Ck	Xmigmatite	
217	45	W			Corral Ck	Xmigmatite	
288	22	N			Corral Ck	Xmigmatite	
253	44	N			Corral Ck	Xmigmatite	
245	32	N			Corral Ck	Xmigmatite	
160	59	W			Uneva Ridge	Xmigmatite	
120	42	S			Uneva Ridge	Xmigmatite	
15	70	E			Uneva Ridge	Xmigmatite	
220	50	W			Uneva Ridge	Xmigmatite	
30	87	E			Uneva Ridge	Xmigmatite	
255	67	N			Uneva Ridge	Xcalc-silicate	
223	66	W			Uneva Ridge	Xcalc-silicate	
246	58	N			Uneva Ridge	Xcalc-silicate	
355	37	E	90	35	Uneva Ridge	Xmigmatite	
170	72	W	189	24	Uneva Ridge	Xmigmatite	
40	76	S	43	0	Uneva Ridge	Xmigmatite	
40	76	S	220	28	Uneva Ridge	Xmigmatite	
64	72	S	82	49	Uneva Ridge	Xmigmatite	
355	37	E	90	35	Uneva Ridge	Xmigmatite	A00TM1
170	72	W	189	24	Uneva Ridge	Xmigmatite	A00TM2

Gore Range Shear Zone cont.

F1c fold data									
S1a/S1b folded			S1c axial plane			F1c fold axis		Location	Rock type
strike	dip		strike	dip		trend	plunge		
130	50	S	154	40W	W	212	36	Eccles Pass	Xcalc-silicate
130	50	S	110	26S	S	176	24	Eccles Pass	Xcalc-silicate
32	54	E	168	50W	W	340	27	Eccles Pass	Xcalc-silicate
						210	36	Eccles Pass	Xcalc-silicate
			293	10N	N	145	0	Eccles Pass	Xquartzite

S2 hi-T hi-strain zo			L2 MSL		Location	Rock type	Shear snse	Sample
strike	dip		trend	plunge				
41	83	E	212	49	N Tenmile Ck	Xmigmatite	SE-side up	
39	81	E	54	69	N Tenmile Ck	Xmigmatite	SE-side up	
50	88	S	95	86	N Tenmile Ck	Xmigmatite	SE-side up	
39	84	E	90	83	N Tenmile Ck	Xmigmatite	SE-side up	
195	56	W	256	52	N Tenmile Ck	Xmigmatite	SE-side up	
22	76	E	193	34	N Tenmile Ck	Xmigmatite	SE-side up	
204	54	W	232	20	N Tenmile Ck	Xmigmatite	SE-side down	
178	62	W	279	60	Corral Ck	Xmigmatite		
35	63	E	209	6	Uneva Ridge	Xmigmatite	SE-side up	
40	76	S	220	28	Uneva Ridge	Xmigmatite		A00TM9
41	86	E			Meadow Ck	XCross Ck gr	SE-side up	KTM99-4
39	81	E	54	69	Meadow Ck	Xmigmatite	SE-side up	A99TM1
39	84	E	90	83	Meadow Ck	Xmigmatite	SE-side up	A99TM2

Gore Range Shear Zone cont.

F2 fold data					
S1a/S1b folded	S2 axial plane	F2 fold axis		Location	Rock type
strike dip	strike dip	trend plunge			
8 86 E	200 33 W	330	28	N Tenmile Ck	Xmigmatite
8 86 E	195 39 W	20	13	N Tenmile Ck	Xmigmatite
8 86 E	218 32 W	0	29	N Tenmile Ck	Xmigmatite
8 86 E	237 58 W	300	55	N Tenmile Ck	Xmigmatite
24 54 W	16 70 E	21	67	N Tenmile Ck	Xmigmatite
195 57 W	220 41 W			N Tenmile Ck	Xmigmatite
336 68 E	225 44 W	12	18	Officer's Gulch	Xcalc-silicate
327 65 E	213 41 W	344	26	Officer's Gulch	Xcalc-silicate
161 24 W	112 59 S	279	33	Eccles Pass	Xcalc-silicate
200 54 W	88 36 S	229	18	Eccles Pass	Xcalc-silicate
200 54 W	89 32 S	235	17	Eccles Pass	Xcalc-silicate
130 50 S	42 57 E	205	28	Eccles Pass	Xcalc-silicate
173 82 W	345 60 E	150	29	Eccles Pass	Xmigmatite
130 50 S	72 68 S	234	46	Eccles Pass	Xmigmatite
285 24 S	16 84 E	170	51	Meadow Ck	Xmigmatite
130 74 W	115 57 S	106	19	Corral Ck	Xmigmatite

S3 mylonite						
S3 mylonite fol	L3 MSL on S3		Shear snse	Location	Rock type	Sample
strike dip	trend plunge					
243 78 N	333	76	SE-side down	N Tenmile Ck	Xmigmatite	KTM99-9b
236 86 N	326	86	SE-side down	N Tenmile Ck	XCross Ck gr	KTM99-17
210 76 W	314	71	SE-side down	S Willow Ck	XCross Ck gr	

Gore Range Shear Zone cont.

S3 mylonite							
S3 mylonite fol		L3 MSL on S3		Shear snse	Location	Rock type	Sample
strike	dip	trend	plunge				
227	65 W	38	52	SE-side down	Meadow Ck	Xmigmatite	A99TM12
38	80 W	35	55	SE-side down	Meadow Ck	Xmigmatite	KTM99-1
231	76 W	38	52	SE-side down	Meadow Ck	Xmigmatite	A99TM13
228	75 W	40	30	SE-side down	Meadow Ck	Xmigmatite	A99TM4
230	73 W	38	20	SE-side down	Meadow Ck	Xmigmatite	A99TM5
356	81 E				Meadow Ck	Xmigmatite	
211	81 W	252	79	SE-side up	Meadow Ck	Xmigmatite	
84	65 S	168	67	SE-side down	Uneva Ridge	Xmigmatite	A00TM3
98	61 S	143	55	SE-side down	Uneva Ridge	Xmigmatite	
95	76 S	155	70	SE-side down	Uneva Ridge	Xmigmatite	
88	82 S	125	65	SE-side down	Uneva Ridge	Xmigmatite	
100	62 S	139	60	SE-side down	Uneva Ridge	Xmigmatite	A00TM10
79	70 S	153	68	SE-side down	Uneva Ridge	XCross Ck gr	
85	76 S	175	73	SE-side down	Uneva Ridge	XCross Ck gr	
90	55 S	164	54	SE-side down	Uneva Ridge	XCross Ck gr	
96	61 S	160	59	SE-side down	Uneva Ridge	XCross Ck gr	A00TM11
93	68 S	138	65		Uneva Ridge	Xmigmatite	
93	85 S	97	67	SE-side down	Uneva Ridge	Xmigmatite	A00TM12
93	71 S	159	68	SE-side down	Uneva Ridge	Xmigmatite	A00TM13
210	76 W	314	71	SE-side down	South Willow C	Xmigmatite	
231	49 W	331	near dd	SE-side down	N Tenmile Ck	Xmigmatite	
203	80 W	293	near dd	SE-side down	N Tenmile Ck	Xmigmatite	
255	75 N	345	near dd	SE-side down	N Tenmile Ck	Xmigmatite	
258	78 S	130	65	SE-side down	N Tenmile Ck	Xmigmatite	KTM99-8
243	78 N	333	76	SE-side down	N Tenmile Ck	Xmigmatite	KTM99-9a

Gore Range Shear Zone cont.

S3 ultramylonite							
S3 ultramyl fol		L3 MSL on S3		Shear snse	Location	Rock type	Sample
strike	dip	trend	plunge				
214	85 W	244	82	SE-side up	Meadow Ck	Xmigmatite	A99TM15
49	81 E	139	81	SE-side up	Meadow Ck	Xmigmatite	A99TM16
218	75 W			SE-side up	Meadow Ck	XCross Ck gr	GB99TM4
69	90 V			SE-side up	Meadow Ck	XCross Ck gr	GB99TM5
101	67 S	165	56	SE-side up	Booth Lake	XCross Ck gr	A00BL1
73	86 S	80	46	SE-side up	Booth Lake	XCross Ck gr	A00BL2
	80 S	140	72	SE-side up	Booth Lake	XCross Ck gr	A00BL3
196	75 W	325	56	SE-side up	Eccles Pass	Xmigmatite	A00TM4
205	60 W	295	near dd	SE-side up	Eccles Pass	Xmigmatite	
200	65 W	290	near dd	SE-side up	Eccles Pass	Xmigmatite	
226	85 W	230	37	SE-side up	Eccles Pass	Xmigmatite	A00TM5
212	90 V	219	27	SE-side up	Eccles Pass	Xmigmatite	
231	57 W	240	15	SE-side up	Eccles Pass	Xmigmatite	
40	77 E	194	42	SE-side up	Eccles Pass	Xmigmatite	

S3 phyllonite							
S3 phyllon fol		L3 MSL on S3		Shear snse	Location	Rock type	Sample
strike	dip	trend	plunge				
240	65 W	13	25	SE-side down	Meadow Ck	Xmigmatite	
254	64 N	344	down-dp	SE-side down	Meadow Ck	Xmigmatite	
232	81 W	322	down-dp	SE-side down	Meadow Ck	Xmigmatite	
160	51 W	330	30		Officer's Glch	Xmigmatite	
90	90 V		down-dp	SE-side up?	Meadow Ck	Xmigmatite	KTM99-12
284	60 N	350	39	SE-side down	Meadow Ck	Xmigmatite	KTM99-13

Drag folds folding mylonites at Uneva Ridge				
axial plane		fold axis		Sample
strike	dip	trend	plunge	
251	83 N	256	5	Xmigmatite/Cross Ck gr

Gore Range Shear Zone cont.

Pegmatite/granite dike orientations				
strike	dip	Location	Rock type	Sample
201	48 W	N Tenmile Ck	Xwhitepeg	KTM99-7
3	80 E	N Tenmile Ck	Xwhitepeg	
250	67 N	N Tenmile Ck	XCross Ck gr	
194	48 W	N Tenmile Ck	XCross Ck gr	
200	53 W	N Tenmile Ck	XCross Ck gr	
216	57 W	N Tenmile Ck	XCross Ck gr	
185	61 W	N Tenmile Ck	XCross Ck gr	
347	76 E	N Tenmile Ck	XCross Ck gr	
10	85 E	N Tenmile Ck	XCross Ck gr	
108	86 S	N Tenmile Ck	Xwhitepeg	
74	75 S	N Tenmile Ck	Xwhitepeg	
111	48 S	Officer's Gulch	Xwhitepeg	
86	34 S	Officer's Gulch	Xwhitepeg	
159	71 W	Officer's Gulch	Xwhitepeg	
142	35 W	Officer's Gulch	Xwhitepeg	
174	76 W	N Tenmile Ck	Xamphibolite	
41	86 E	Meadow Ck	XCross Ck gr	
211	77 W	Eccles Pass	XCross Ck gr	
56	72 S	Uneva Ridge	XCross Ck gr	
317	76 E	N Tenmile Ck	XCross Ck gr	
10	85 W	N Tenmile Ck	XCross Ck gr	

St. Louis Lake Shear Zone

S1a/S1b fol			L1 MSL			Location	Rock type	Sample
strike	dip		trend	plunge				
353	19	E				St. Louis Lk	Xamphibolite	
247	18	N				St. Louis Lk	Xamphibolite	
313	36	N				St. Louis Lk	Xamphibolite	
275	29	N				St. Louis Lk	Xamphibolite	
342	25	W				St. Louis Lk	Xamphibolite	
90	57	S				St. Louis Lk	Xbiotite gneiss	
92	65	S				St. Louis Lk	Xamphibolite	
320	83	E	33		83	St. Louis Lk	Xcalc-silicate	
270	74	N				St. Louis Lk	Xamphibolite	
12	85	E	192		43	St. Louis Lk	Xamphibolite	
85	75	S	196		69	St. Louis Lk	Xamphibolite	
315	88	N	48		81	St. Louis Lk	Xamphibolite	
26	54	E	74		46	St. Louis Lk	Xamphibolite	
16	82	E				St. Louis Lk	XBoulder Ck gr	
54	74	S				St. Louis Lk	Xamphibolite	
20	90	V	191		40	St. Louis Lk	Xcalc-silicate	
343	88	E				St. Louis Lk	Xcalc-silicate	
90	64	S				St. Louis Lk	Xbiotite gneiss	
90	84	S				St. Louis Lk	Xcalc-silicate	K00SL1
50	90	V				St. Louis Lk	XBoulder Ck gr	K00SL2
155	54	W				St. Louis Lk	Xgrabbro	A00SL26
24	77	E				St. Louis Lk	Xcalc-silicate	
50	66	S				St. Louis Lk	Xcalc-silicate	
76	90	V				Winter Park	Xamphibolite	
75	69	S	115		49	Vasquez Ck	Xgranodiorite	
180	66	W				Fool Ck	Xamphibolite	

S1a/S1b fol			L1 MSL			Location	Rock type	Sample
strike	dip		trend	plunge				
271	49	N				Fool Ck	Xamphibolite	
76	35	S	140		30	Fool Ck	Xamphibolite	
326	15	E				Fool Ck	Xamphibolite	
45	67	E	80		57	Fool Ck	Xamphibolite	
37	84	E				Fool Ck	Xamphibolite	
285	64	N				Fool Ck	Xamphibolite	
35	26	E				Fool Ck	Xamphibolite	
20	45	E				Fool Ck	Xamphibolite	
34	30	E				Mizpah Camp	Xbiotite gneiss	
253	77	N				Mizpah Camp	Xbiotite gneiss	
40	54	E				Mizpah Camp	Xbiotite gneiss	
52	55	S				Mizpah Camp	Xbiotite gneiss	
90	62	S	230		22	Mizpah Camp	Xbiotite gneiss	
62	73	S	152		61	Mizpah Camp	XBoulder Ck gr	
25	23	E	164		20	Mizpah Camp	Xamphibolite	
58	70	S				Mizpah Camp	XBoulder Ck gr	
30	65	E				Mizpah Camp	Xbiotite gneiss	

St. Louis Lake Shear Zone cont.

S2 hi-T hi-strain zone fol		L2 MSL		Location	Rock type	Shear snse
strike	dip	trend	plunge			
70	58 S	125	60	St. Louis Lk	Xamphibolite	
62	76 S	155	68	St. Louis Lk	XBoulder Ck gr	SE-side up
65	74 S	118	61	St. Louis Lk	Xcalc-silicate	
53	82 S			St. Louis Lk	Xamphibolite	SE-side up?
65	76 S			St. Louis Lk	Xcalc-silicate	
57	64 S			Winter Park	Xamphibolite	
55	52 S			Mizpah Camp	Xbiotite gneiss	
55	59 S	90	50	Mizpah Camp	Xbiotite gneiss	
65	56 S	190	53	Mizpah Camp	Xbiotite gneiss	

F2 fold data							
S1a/S1b folded		S2 axial plane		F2 fold axis		Location	Rock type
strike	dip	strike	dip	trend	plunge		
54	74 S	90	76 S	114	69	St. Louis Lk	Xcalc-silicate
343	88 E	83	72 S	210	74	St. Louis Lk	Xcalc-silicate
		35	78 E			St. Louis Lk	Xcalc-silicate
		42	68 E	152	67	St. Louis Lk	Xcalc-silicate
		42	68 E	150	64	St. Louis Lk	Xcalc-silicate
24	77 E	25	81 E	178	72	St. Louis Lk	Xcalc-silicate
		55	65 S			St. Louis Lk	Xcalc-silicate
180	66 W	209	75 W	205	39	Fool Ck	Xbiotite gneiss
37	84 E	24	53 E			Fool Ck	Xbiotite gneiss
285	64 N	84	36 S	290	47	Fool Ck	Xbiotite gneiss
35	26 E	84	74 S	228	53	Fool Ck	Xbiotite gneiss
55	59 S	73	67 S	130	73	Mizpah Camp	Xbiotite gneiss
40	54 E	73	52 S			Mizpah Camp	Xbiotite gneiss
52	55 S	31	38 E			Mizpah Camp	Xbiotite gneiss
		250	70 N	95	30	E. Portal, Moff	Xcalc-silicate

St. Louis Lake Shear Zone cont.

S3 mylonite							
S3 myl fol		L3 MSL on S3		Shear snse	Location	Rock type	Sample
strike	dip	trend	plunge				
71	65 S	140	63	SE-side up	Vasquez Ck	Xgranodiorite	A00SL7, A00SL8
70	74 S	160	74	SE-side up	Vasquez Ck	Xgranodiorite	
65	80 S	155	80	SE-side up	Vasquez Ck	Xgranodiorite	
67	76 S	125	66	SE-side up	Vasquez Ck	Xgranodiorite	A00SL9, A00SL10
88	75 S	178	75	SE-side up	Vasquez Ck	Xgranodiorite	A00SL11
95	74 S	164	64	SE-side up	Vasquez Ck	Xgranodiorite	A00SL12
75	63 S	165	55	SE-side up	St. Louis Lk	XBoulder Ck gr	A00SL6
80	74 S	152	72	SE-side up	St. Louis Lk	XBoulder Ck gr	A00SL20
66	65 S	150	65	SE-side up	St. Louis Lk	XBoulder Ck gr	A00SL21
286	90 V	70	66	SE-side up	St. Louis Lk	Xgabbro	A00SL25
75	74 S	95	36	SE-side up	St. Louis Lk	Xgabbro	A00SL26
90	83 S	165	82	SE-side up	St. Louis Lk	Ysilver Plume gr	A00SL27
75	85 S	85	64	SE-side up	St. Louis Lk	Ysilver Plume gr	A00SL28
73	63 S	115	52	SE-side up	St. Louis Lk	Ysilver Plume gr	A00SL29
58	71 S	120	52	SE-side up	St. Louis Lk	XBoulder Ck gr	

St. Louis Lake Shear Zone cont.

S3 ultramylonite							
S3 ultramylonite fol		L3 MSL on S3		Shear snse	Location	Rock type	Sample
strike	dip	trend	plunge				
65	80 S	139	77	SE-side down	St. Louis Lk	XBoulder Ck gr	
250	88 N	75	81	SE-side down shear ban	St. Louis Lk	Xamphibolite	
70	78 S	160	78	SE-side down	St. Louis Lk	XBoulder Ck gr	
90	90 V	236	80	SE-side down	St. Louis Lk	XBoulder Ck gr	
72	81 S	162	81	SE-side down	St. Louis Lk	XBoulder Ck gr	
60	78 S	150	78	SE-side down	St. Louis Lk	XBoulder Ck gr	
260	61 N	5	49	SE-side down	St. Louis Lk	XBoulder Ck gr	
60	80 S	194	80	SE-side down	St. Louis Lk	XBoulder Ck gr	
240	76 N	330	76	SE-side down	St. Louis Lk	Xcalc-silicate	
236	77 N	326	77	SE-side down	St. Louis Lk	XBoulder Ck gr	
66	84 S	230	81	SE-side down	St. Louis Lk	XBoulder Ck gr	
263	76 N	353	76	SE-side down	St. Louis Lk	XBoulder Ck gr	
80	73 S	135	55	SE-side down	St. Louis Lk	XBoulder Ck gr	
50	79 S	195	69	SE-side down	St. Louis Lk	XBoulder Ck gr	
239	83 N	260	75	SE-side down	St. Louis Lk	Xbiotite gneiss	
48	90 V	224	70	SE-side down	St. Louis Lk	XBoulder Ck gr	A00SL1
86	79 S	176	79	SE-side down	St. Louis Lk	XBoulder Ck gr	
352	89 E	190	63	SE-side down	St. Louis Lk	XBoulder Ck gr	
65	78 S	155	90	SE-side down	St. Louis Lk	XBoulder Ck gr	A00SL22
192	90 V	282	90	SE-side down	Berthoud Ps	Ysilver Plume gr	A00BP1
17	72 E	97	66	SE-side down	Berthoud Ps	Ysilver Plume gr	
51	90 V	56	24	protomylonite	Jones Ps	Ysilver Plume gr	

Idaho Springs-Ralston Shear Zone

S1a/S1b fol			L1 MSL		Location	Rock type	Sample	S1a/S1b fol			L1 MSL		Location	Rock type	Sample
strike	dip		trend	plunge				strike	dip		trend	plunge			
244	84	N	285	69	Deer Ck	Xpelitic schist	A00GG2	52	61	S	50	26	Deer Ck	Xpelitic schist	
170	40	W			Deer Ck	Xpelitic schist	A00GG3	353	42	E	83	42	Deer Ck	Xpelitic schist	
250	64	N	290	64	Deer Ck	Xpelitic schist	A00GG4	44	39	E	80	38	Deer Ck	Xpelitic schist	
35	25	E	178	17	Deer Ck	Xpelitic schist	A00GG5	332	31	E			Deer Ck	Xpelitic schist	
45	65	S	85	24	Deer Ck	Xpelitic schist	A00GG8	260	84	N			Deer Ck	Xpelitic schist	
45	24	S	67	5	Deer Ck	Xpelitic schist	A00GG6	24	60	E			Deer Ck	XBoulder Ck gr	
258	75	N			Deer Ck	XBoulder Ck gr		270	56	N			Deer Ck	XBoulder Ck gr	
314	35	N			Deer Ck	XBoulder Ck gr		58	76	S			Deer Ck	Xquartzite	
235	54	N	295	48	Deer Ck	Xquartzite		265	46	N			Deer Ck	Xquartzite	
230	80	N			Deer Ck	Xquartzite		320	20	E			Deer Ck	XBoulder Ck gr	
60	71	S	208	49	Deer Ck	XBoulder Ck gr		270	45	N			Deer Ck	Xquartzite	
242	83	N			Deer Ck	XBoulder Ck gr		28	50	E	88	43	Deer Ck	Xpelitic schist	
41	67	S	190	51	Deer Ck	Xpelitic schist		28	50	E	190	30	Deer Ck	Xpelitic schist	
52	60	S			Deer Ck	Xpelitic schist		45	59	S	33	21	Deer Ck	Xquartzite	
45	68	S			Deer Ck	Xpelitic schist		85	62	S			Deer Ck	Xquartzite	
30	42	E	190	10	Deer Ck	Xpelitic schist		175	12	W	265	12	Deer Ck	Xpelitic schist	
50	85	S			Deer Ck	Xpelitic schist		255	79	N	258	73	Deer Ck	Xpelitic schist	A00GG1
358	45	E			Deer Ck	Xpelitic schist		244	84	N	285	69	Deer Ck	Xpelitic schist	A00GG2
34	37	S			Deer Ck	Xpelitic schist		170	40	W			Deer Ck	Xpelitic schist	A00GG3
54	56	S			Deer Ck	Xquartzite		250	64	N	290	64	Deer Ck	Xpelitic schist	A00GG4
345	27	E	24	16	Deer Ck	Xquartzite		35	25	E	178	17	Deer Ck	Xpelitic schist	A00GG5
345	27	E	65	26	Deer Ck	Xquartzite		45	24	S	67	0	Deer Ck	Xpelitic schist	A00GG6
275	36	N	342	34	Deer Ck	Xquartzite		45	65	S	85	24	Deer Ck	Xpelitic schist	A00GG8
53	90	V			Deer Ck	Xquartzite		65	78	S			Deer Ck	XBoulder Ck gr	
45	72	S	194	57	Deer Ck	Xpelitic schist		206	85	N			Deer Ck	XBoulder Ck gr	
45	72	S	215	8	Deer Ck	Xpelitic schist		62	54	S	193	40	Burro Tr	XBoulder Ck gr	
62	86	S	235	66	Deer Ck	Xpelitic schist		68	90	V	235	60	Burro Tr	XBoulder Ck gr	
59	58	S			Deer Ck	Xpelitic schist		260	64	N			Burro Tr	Xquartzite	
272	46	N	60	24	Deer Ck	Xpelitic schist		276	46	N			Burro Tr	Xquartzite	
46	57	S			Deer Ck	Xquartzite		256	40	N			Burro Tr	Xquartzite	
52	61	S	188	47	Deer Ck	Xpelitic schist		277	50	N			Burro Tr	Xquartzite	

Idaho Springs-Ralston Shear Zone cont.

S1a/S1b fol			L1 MSL		Location	Rock type	Sample
strike	dip		trend	plunge			
285	35	N			Burro Tr	Xquartzite	
267	18	N			Burro Tr	Xquartzite	
335	25	N			Burro Tr	Xpelitic schist	
250	68	N			Burro Tr	Xmigmatite	
45	45	S			Burro Tr	XBoulder Ck gr	
46	27	S			Burro Tr	Xpelitic schist	
265	82	N			Burro Tr	Xpelitic schist	
305	16	N			Burro Tr	Xquartzite	
23	30	E			Burro Tr	Xquartzite	
67	73	S			Burro Tr	Xquartzite	A01GG26
30	79	E	45	40	Burro Tr	Xquartzite	A01GG27
57	83	S	240	74	Burro Tr	Xquartzite	A01GG28
283	49	N			Burro Tr	Xquartzite	
0	40	E			Burro Tr	Xquartzite	
38	87	S	218	53	Knott Ck	Xquartzite	A01GG20
52	68	S			Knott Ck	Xquartzite	A01GG21
45	79	S			Knott Ck	Xquartzite	A01GG22
56	86	S	225	76	Knott Ck	Xquartzite	A01GG23
240	79	S	65	11	Knott Ck	Xconglomerate	K01CC51
234	86	N	240	58	Knott Ck	XBoulder Ck gr	A01GG30
52	85	S	223	63	Knott Ck	Xconglomerate	K01CC53/W01CC02
65	78	S			Knott Ck	XBoulder Ck gr	
230	83	N			Knott Ck	Xquartzite	
239	63	N	239	57	Knott Ck	Xquartzite	
257	56	N	282	41	Knott Ck	XBoulder Ck gr	
138	17	S			Knott Ck	XBoulder Ck gr	
230	78	N			Knott Ck	XBoulder Ck gr	
54	87	S			Knott Ck	Xquartzite	
58	67	S			Knott Ck	Xquartzite	
128	67	S			Schoolhse Rd	Xpelitic schist	
115	78	S			Schoolhse Rd	Xpelitic schist	

S1a/S1b fol			L1 MSL		Location	Rock type	Sample
strike	dip		trend	plunge			
300	90	V			Schoolhse	Xbiotite schist	KIS0017
246	68	N			Quarry	Xquartzite	
272	43	N			Quarry	Xquartzite	
284	13	N	298	3	Rollins Pass	Xamphibolite	
262	47	N			Rollins Pass	XBoulder Ck gr	
235	70	N	41	66	Chicago Ck	Xbiotite gneiss	
345	80	E	75	80	Chicago Ck	Xbiotite schist	KIS005
60	76	N			Chicago Ck	Xbiotite schist	K00IS3
345	80	E	75	80	Chicago Ck	Xbiotite schist	K00IS5

F1b fold data

S1b axial plane			F1b fold axis		Location	Rock type	Sample
strike	dip		trend	plunge			
335	28	N	45	20	Burro Tr	Xquartzite	
355	38	E	35	23	Burro Tr	Xpelitic schist	A01GG9
238	83	N	55	56	Deer Ck	Xquartzite	
58	80	S	50	10	Deer Ck	Xquartzite	
65	75	S	65	32	Deer Ck	Xquartzite	A01GG15

Idaho Springs-Ralston Shear Zone cont.

S2 hi-T hi-strain zo			L2 MSL			Location	Rock type	Shear snse	Sample
strike	dip		trend	plunge					
335	45	N	4	24		Rollins Ps	Xbiotite gneiss	SE-side down	
55	84	S	225	55		Knott Ck	XBoulder Ck gr		A01GG1
249	90	V	250	70		Knott Ck	XBoulder Ck gr		
55	82	S	198	74		Knott Ck	XBoulder Ck gr		
254	55	N	285	44		Burro Tr	XBoulder Ck gr		

F2 fold data											
S1a/S1b folded			S2 axial plane				F2 fold axis		Location	Rock type	Sample
strike	dip		strike	dip			trend	plunge			
35	25	E	70	86	S		95	27	Deer Ck	Xpelitic schist	
255	79	N	238	83	N		55	56	Deer Ck	Xpelitic schist	
170	40	W	23	65	E		202	16	Deer Ck	Xpelitic schist	
35	25	E	70	86	S		95	27	Deer Ck	Xpelitic schist	
230	83	N	91	80	S		45	21	Deer Ck	Xquartzite	
170	40	W	23	65	E		202	16	Deer Ck	Xpelitic schist	
258	75	N	68	76	S				Deer Ck	XBoulder Ck gr	
68	90	V	235	58	N		62	14	Deer Ck	Xpelitic schist	A01GG13
80	74	S					95	36	Deer Ck	Xpelitic schist	A01GG12
34	46	E	52	90	V		50	35	Deer Ck	Xpelitic schist	A01GG14
256	40	N	76	76	S		56	14	Burro Tr	Xpelitic schist	
			27	67	E		48	12	Burro Tr	Xpelitic schist	
			250	68	N		60	17	Burro Tr	Xpelitic schist	
46	27	S	240	64	N		75	0	Burro Tr	Xpelitic schist	
115	78	S	237	59	N		300	47	Schoolhse Rd	Xpelitic schist	
230	83	N	91	80	S		45	21	Knott Ck	Xquartzite	

S3 phyllonite data								
S3 phyllon fol			L3 MSL on S3			Shear snse	Location	Rock type	Sample
strike	dip		trend	plunge					
265	72	N	62	32		SE-side up	Chicago Ck	Xbiotite schist	KIS001
240	90	V	60	50		SE-side up	Chicago Ck	Xbiotite schist	KIS002

Idaho Springs-Ralston Shear Zone cont.

S3 mylonite data							
S3 mylonite fol		L3 MSL on S3		Shear snse	Location	Rock type	Sample
strike	dip	trend	plunge				
255	79 N	258	73	SE-side down	Deer Ck	Xpelitic schist	A00GG1
72	86 S	252	49	SE-side down	Deer Ck	Xquartzite	A00GG9
260	82 N	265	65	SE-side down	Deer Ck	XBoulder Ck gr	
260	87 N	267	68	SE-side down	Deer Ck	XBoulder Ck gr	KIS009
77	86 S	210	70	SE-side down	Deer Ck	Xquartzite	KIS0010
70	90 V	160	90	SE-side down	Deer Ck	Xpelitic schist	KIS0012
77	88 S	236	65	SE-side down	Deer Ck	Xquartzite	KIS0011
50	90 V	140	90	SE-side down	Deer Ck	Xpelitic schist	KIS0013
80	80 S	255	62	SE-side down	Deer Ck	Xamphibolite	
68	90 V	250	60	SE-side down	Deer Ck	XBoulder Ck gr	KIS0015
68	90 V	245	80	SE-side down	Deer Ck	XBoulder Ck gr	
65	90 V	240	43	SE-side down	Deer Ck	XBoulder Ck gr	KIS0016
239	72 N	40	15	SE-side down	Ralston Ck	XBoulder Ck gr	KIS006
260	48 N	45	25	SE-side down	Ralston Ck	XBoulder Ck gr	KIS007
50	80 S	140	80	SE-side down	Coal Ck Can	XBoulder Ck gr	
252	85 N	45	65	SE-side down	Chicago Ck	YMt Evans granit	KIS004

S3 ultramylonite data							
S3 ultramylonite fol		L3 MSL on S3		Shear snse	Location	Rock type	Sample
strike	dip	trend	plunge				
80	80 N	255	62	SE-side up	Deer Ck	XBoulder Ck gr	KIS0014
80	84 S	257	61		Deer Ck	XBoulder Ck gr	A01GG16
74	87 S	244	46		Deer Ck	XBoulder Ck gr	A01GG17
54	78 S	212	47	SE-side up	Burro Tr	XBoulder Ck gr	A01GG2
218	85 N	224	50	SE-side up	Burro Tr	XBoulder Ck gr	A01GG8
234	90 V	263	72	SE-side up	Burro Tr	XBoulder Ck gr	
234	90 V	225	60	SE-side up	Burro Tr	XBoulder Ck gr	A01GG10
75	65 S	202	60	SE-side up	Knott Ck	XBoulder Ck gr	K01CC50
60	90 V	250	65	SE-side up	Knott Ck	XBoulder Ck gr	
235	77 N	250	65	SE-side up	Knott Ck	Xconglomerate	A00GG10
72	78 S	240	45	SE-side up	Knott Ck	XBoulder Ck gr	
56	77 S	140	85	SE-side up	Knott Ck	XBoulder Ck gr	A00GG11

6.5 APPENDIX 5

Homestake shear zone

poles to S1 foliation

L1 mineral stretching lineation on S1

poles to S2 high-T high strain domain

F2 fold axis

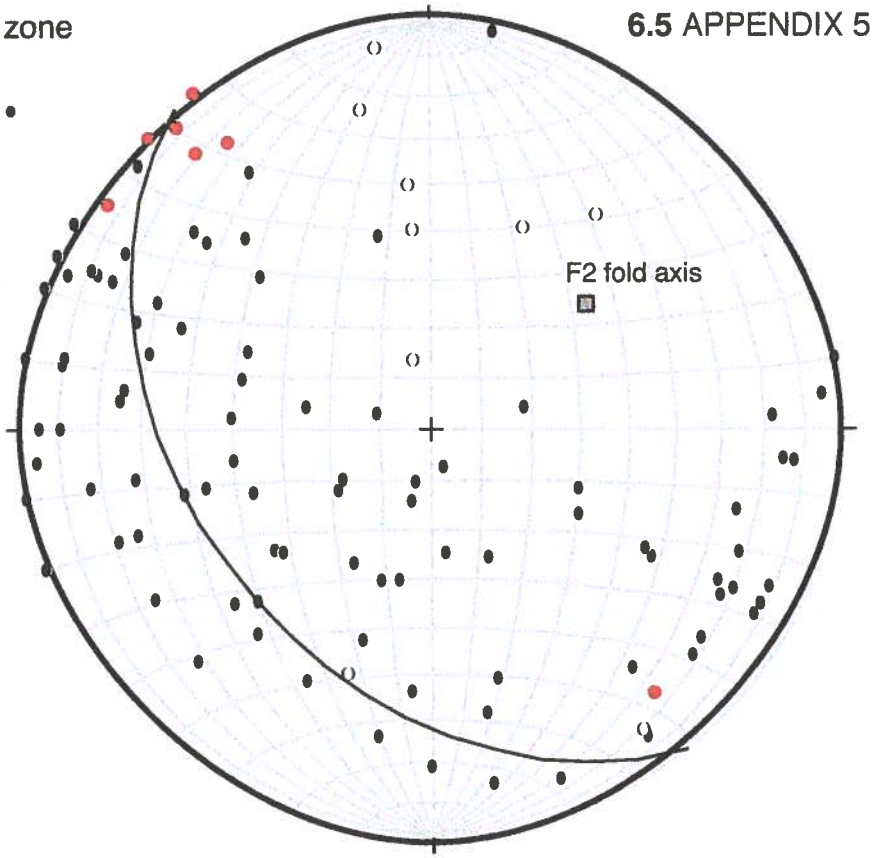

Homestake shear zone

poles to SE-side down mylonite fabric

Mineral stretching lineation on SE-side down mylonite

poles to SE-side up ultramylonite fabric

Mineral stretching lineation on SE-side up ultramylonite

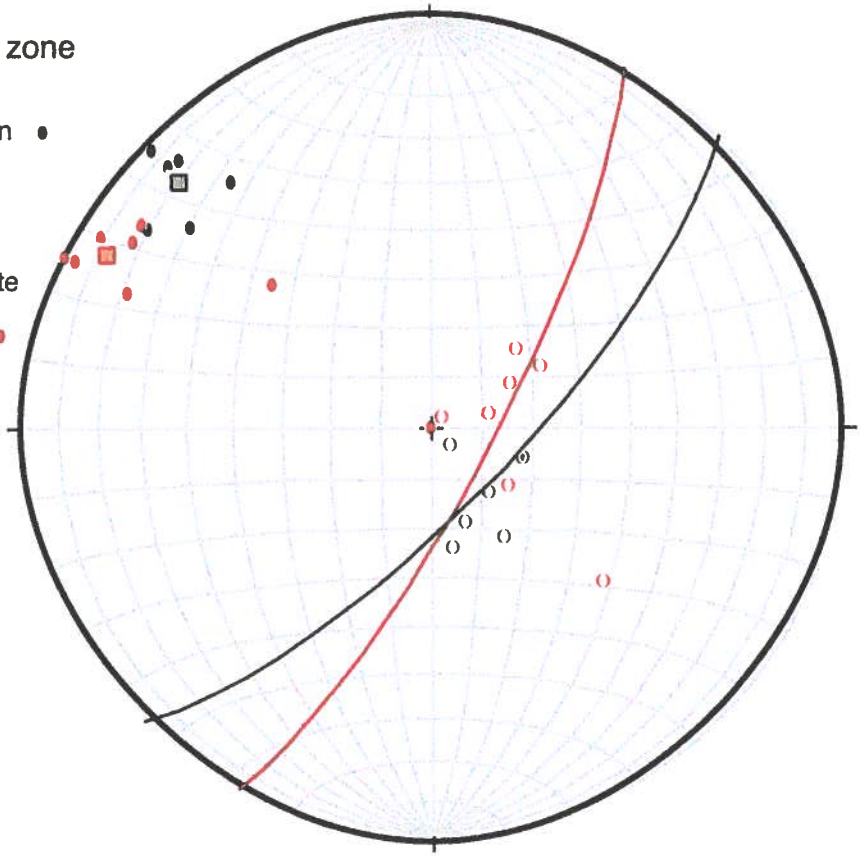

Gore Range shear zone

poles to S1 foliation •

L1 *mineral stretching* o
lineation on S1

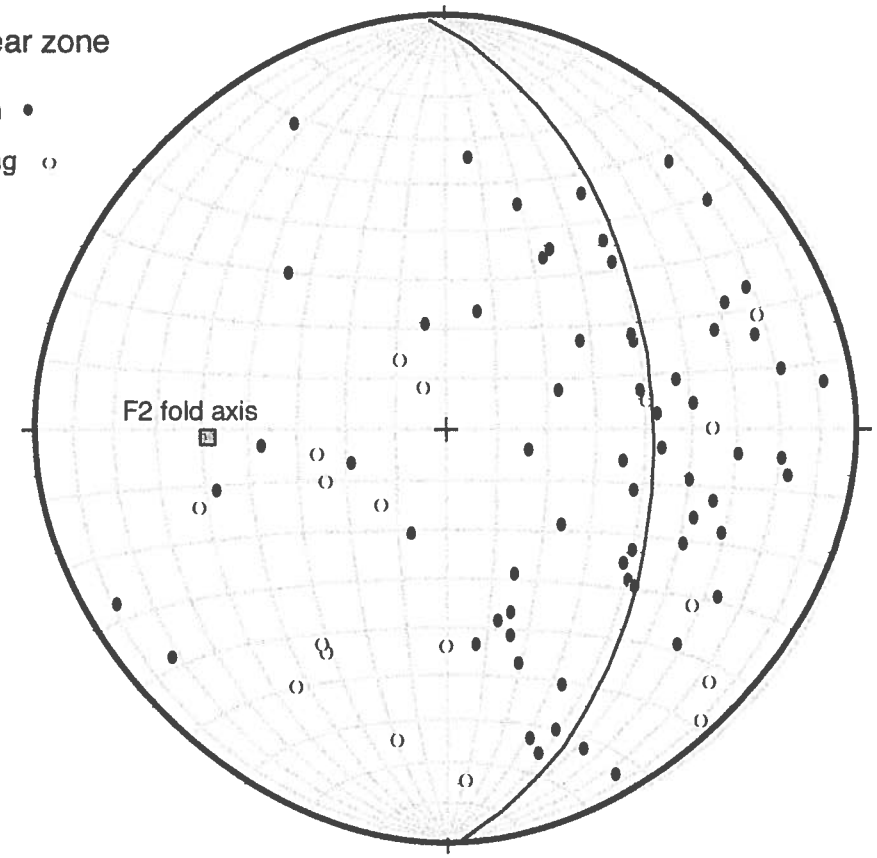

Gore Range shear zone

poles to S2 high-T •
high strain domains

L2 mineral stretching o
lineation on S2

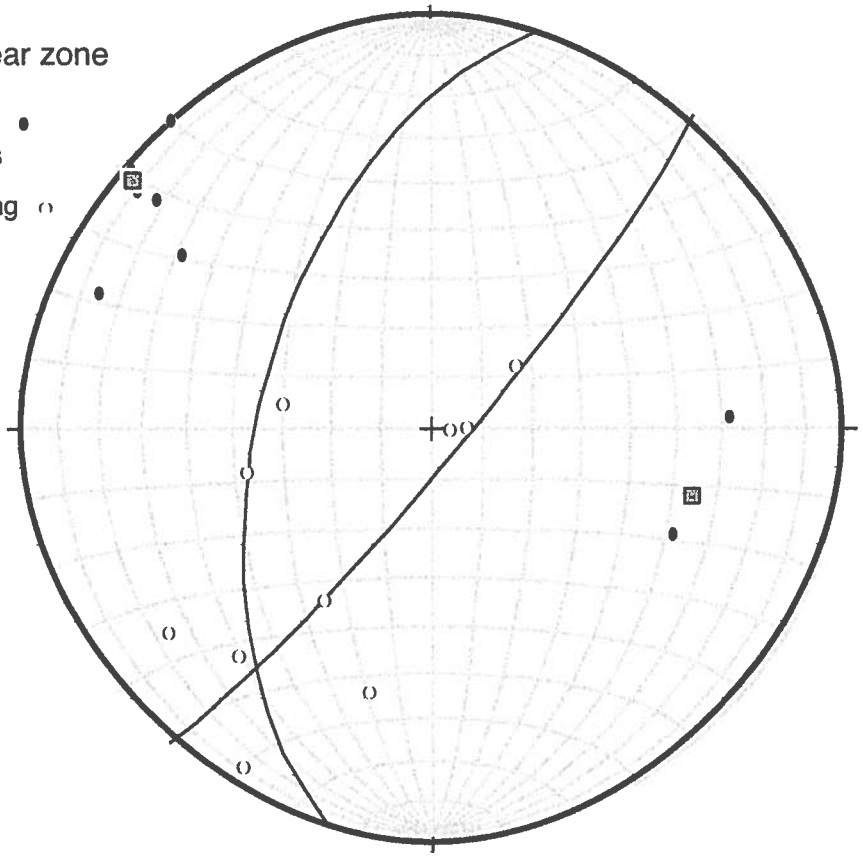

Gore Range shear zone

poles to F2 axial plane

F2 fold axis

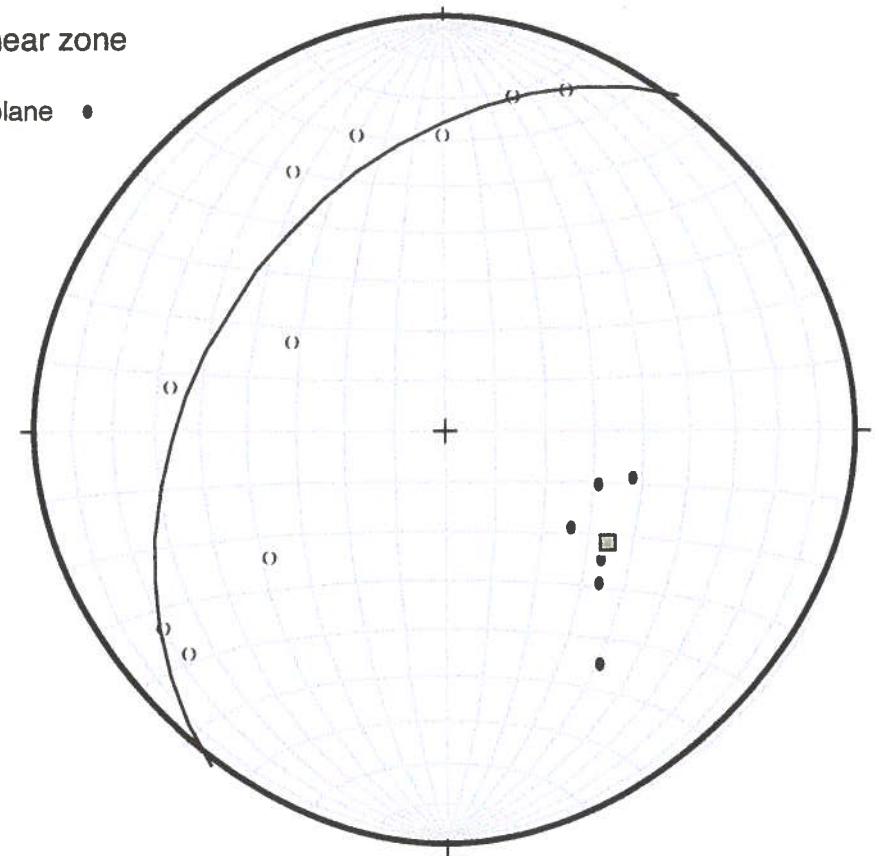

Gore Range shear zone

poles to SE-side down mylonite fabric

mineral stretching lineation on SE-side down mylonite

poles to SE-side up ultramylonite fabric

mineral stretching lineation on SE-side up ultramylonite

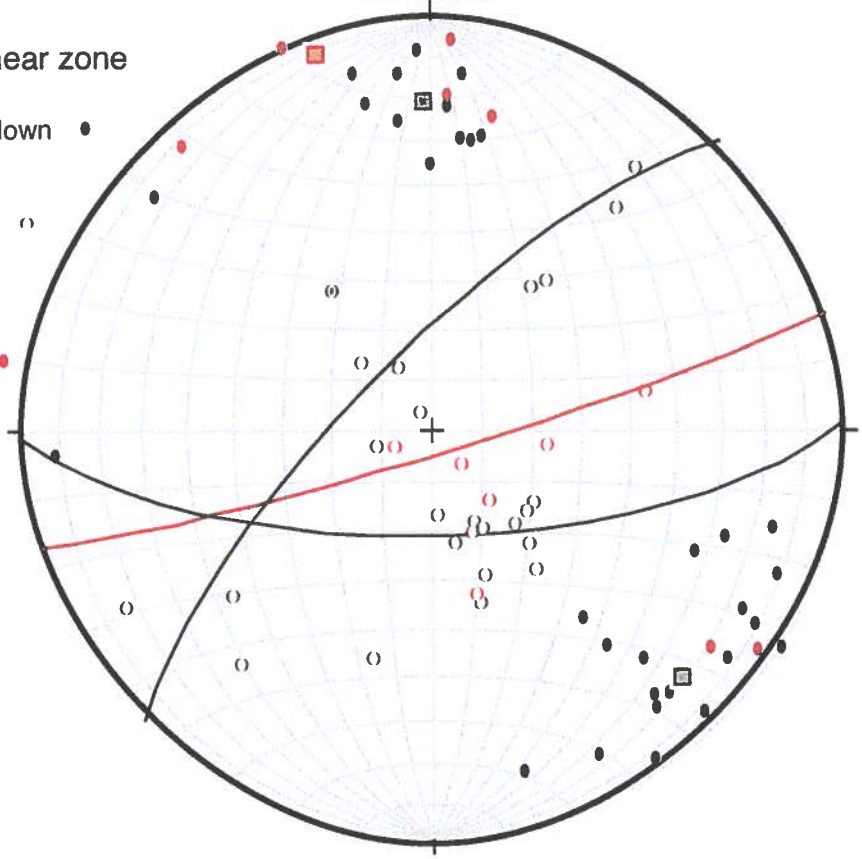

St. Louis Lake shear zone

poles to S1 foliation •

L1 mineral stretching lineation on S1 o

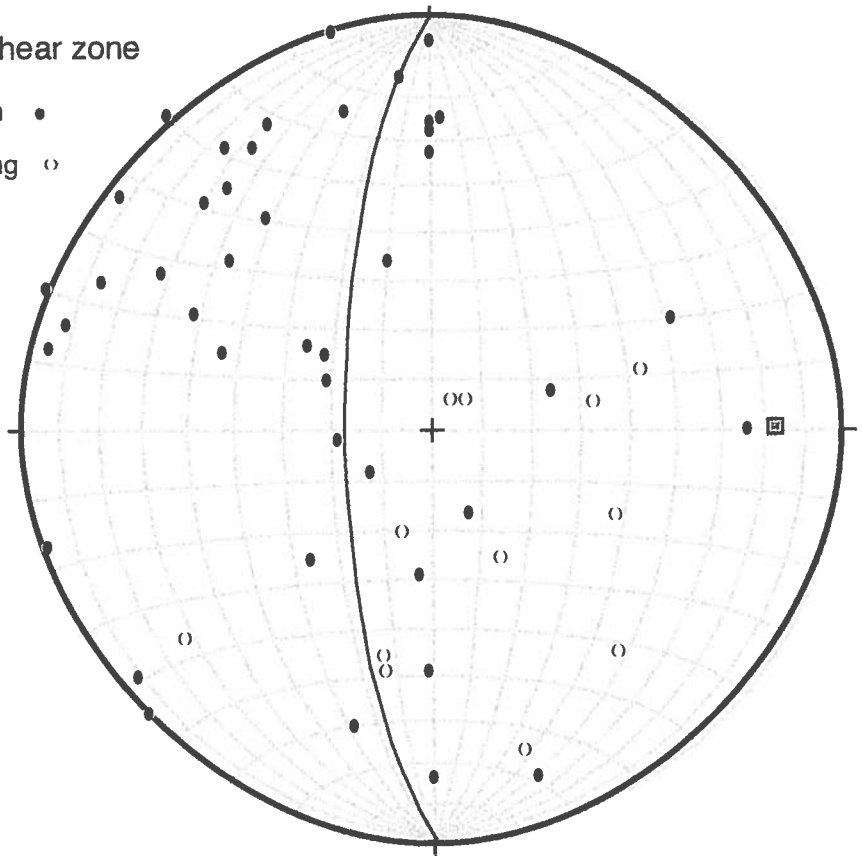

St. Louis Lake shear zone

poles to S2 high-T high strain domains •

L2 mineral stretching lineation on S2 o

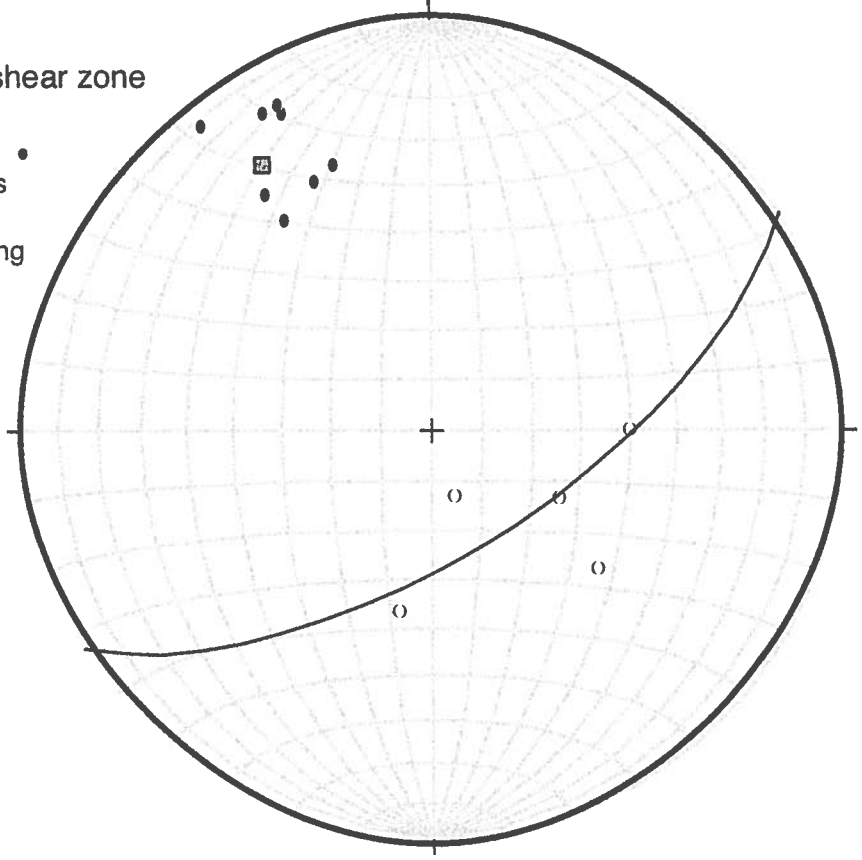

St. Louis Lake shear zone

poles to F2 axial plane

F2 fold axis

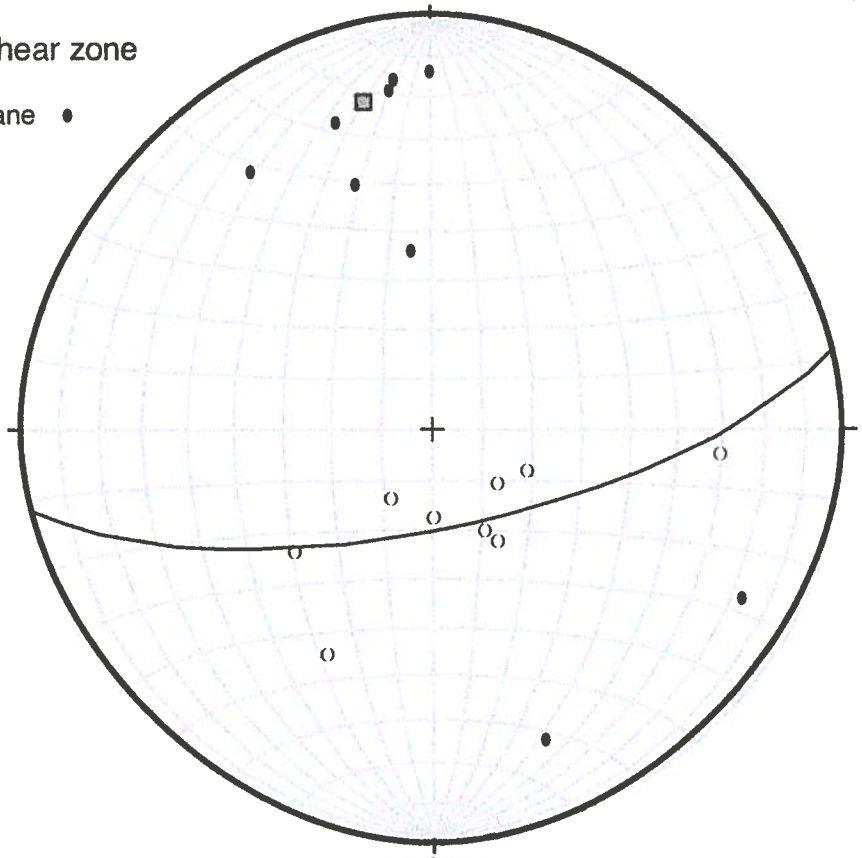

St. Louis Lake shear zone

poles to SE-side up mylonite fabric

mineral stretching lineation on SE-side up mylonite

poles to SE-side down ultramylonite fabric

mineral stretching lineation on SE-side down ultramylonite

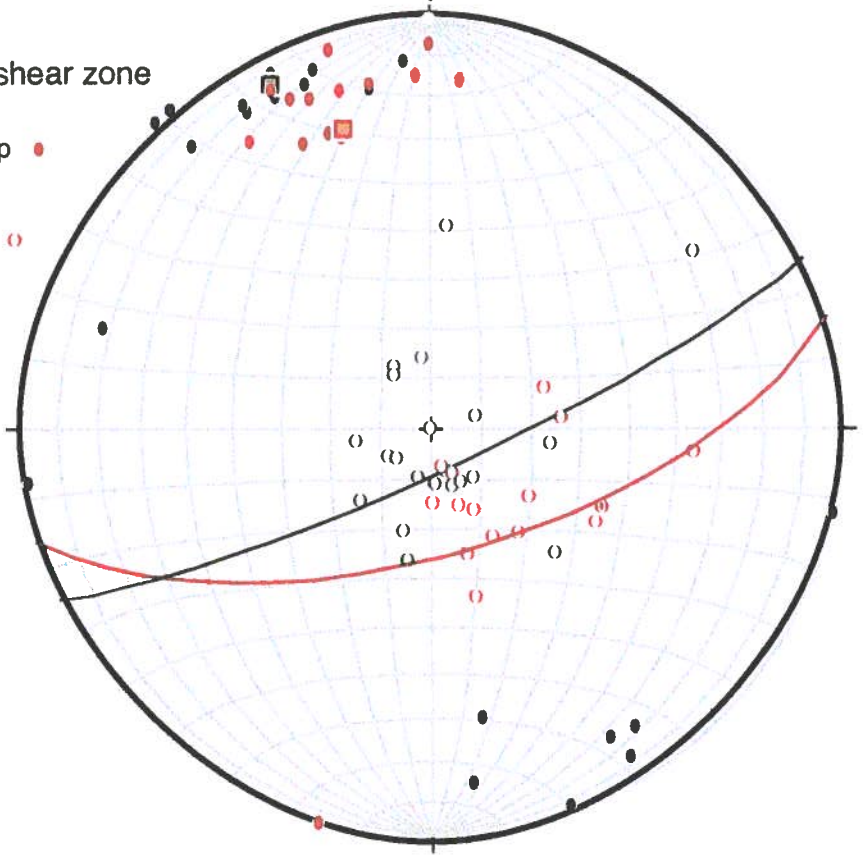

Idaho Springs-Ralston shear zone

poles to S1 foliation

poles to S2 high-T high strain domains

L1 mineral stretching lineation on S1

L2 mineral stretching lineation on S2

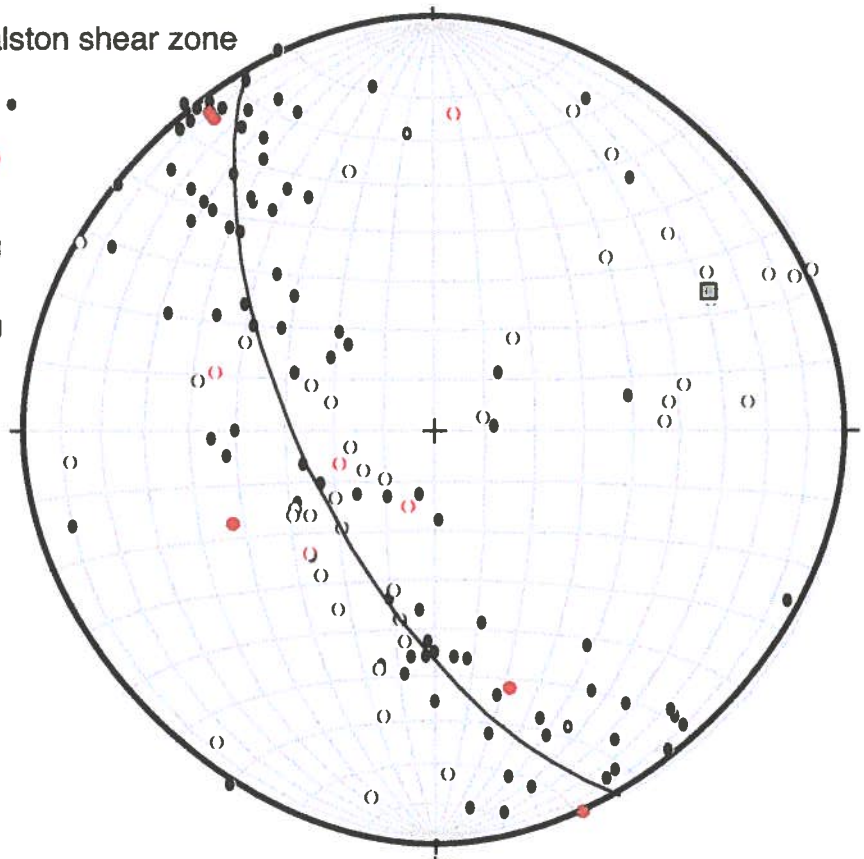

Idaho Springs-Ralston shear zone

poles to F1b axial plane

F1b fold axis

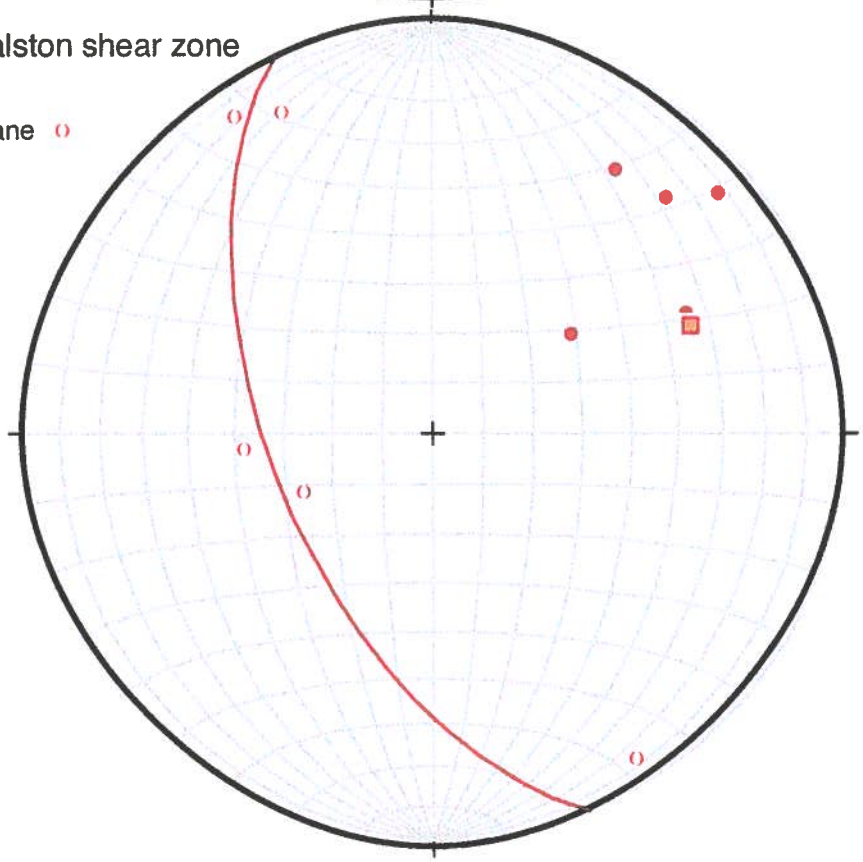

Idaho Springs-Ralston shear zone

poles to F2 axial plane

F2 fold axis

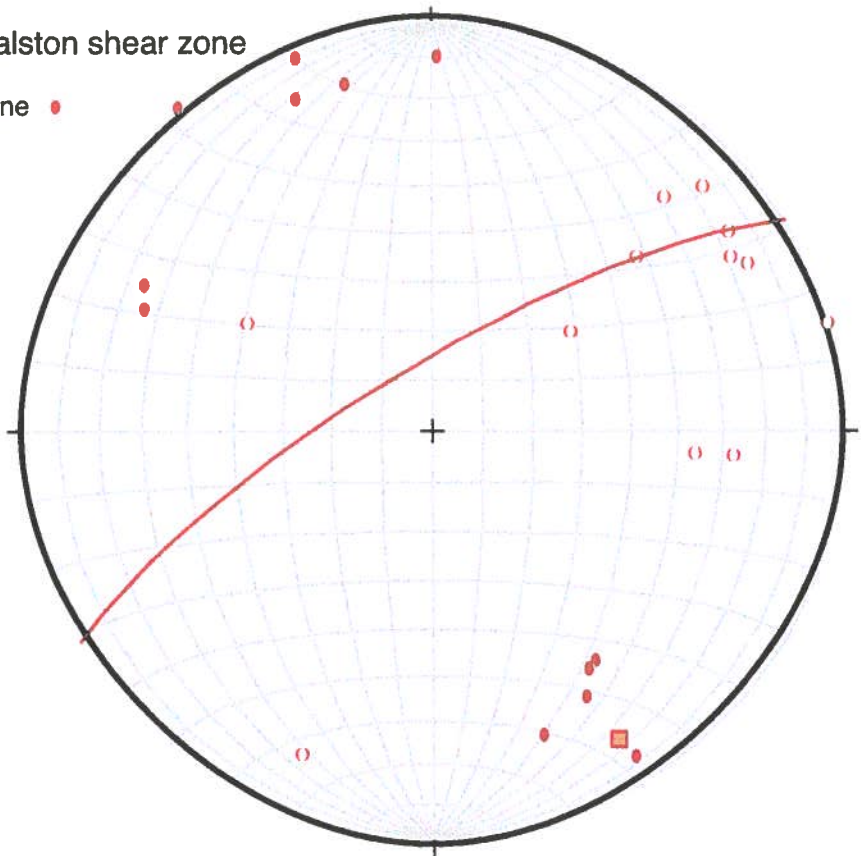

Idaho Springs-Ralston shear zone

poles to SE-side up mylonite fabric

poles to SE-side down mylonite fabric

poles to SE-side up ultramylonite fabric

mineral stretching lineation on SE-up mylonite

mineral stretching lineation on SE-side down mylonite

mineral stretching lineation on SE-up ultramylonite

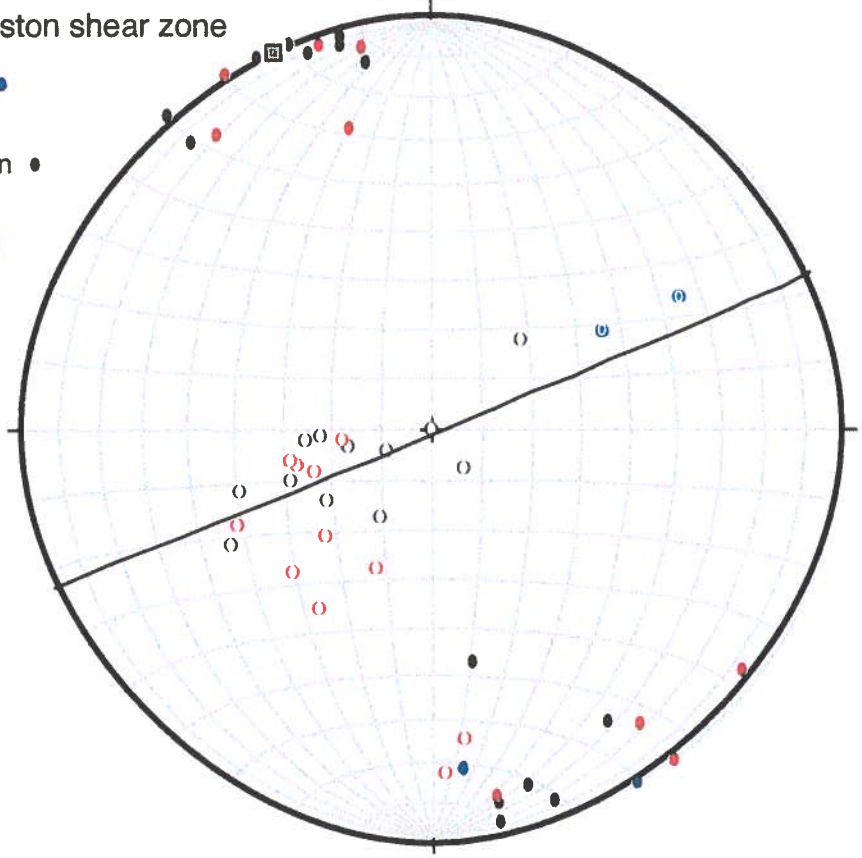

6.6 APPENDIX 6: PRELIMINARY MAJOR AND TRACE ELEMENT DATA FOR COAL CREEK QUARTZITE PROBABLE REGOLITH

	Coal Creek samples				Blue Ridge samples			
	potential regolith (1 meter from contact with granite)	potential regolith (1 meter from contact with granite)	arkosic qtzite (15 meters from contact with granite)	qtzite conglom (100 meters from contact)	metacom glom w/ schist matrix and granite clasts	metacom glom w/ schist matrix and granite clasts	metacomgl om w/ schist matrix and granite clasts	*low total weight, problem with SiO2 measureme nt?
XRF Major Element Analyses								
wt %	K01CC52	A01GG30	A01GG5	K01CC53	K00BR1	K00BR3	K00BR14*	
SiO2	72.08	71.7	91.37	92.361	77.43	72.34	65.73	
Al2O3	14.36	14.31	5.63	1.408	13.33	15.51	16.11	
Fe2O3	2.075	2.04	1.47	3.155	1.43	3.24	3.64	
FeO								
Fe Total	2.075	2.04	1.47	3.155	1.43	3.24	3.64	
MgO	0.78	0.74	0.22	0.235	0.53	0.67	1.26	
CaO	1.23	1.04	0.5	0.895	0.35	0.28	0.92	
Na2O	3.07	3.22	0.095	0.107	0.23	0.2	0.21	
K2O	4.4	4.72	0.314	0.118	5.74	5.04	6.12	
TiO2	0.25	0.274	0.347	0.279	0.056	0.427	0.613	
P2O5	0.125	0.1	0.01	0.016	0.07	0.08	0.11	
MnO	0.07	0.087	0.001	0	0.015	0.014	0.047	
XRF Trace Element Analyses								
Ba	1071	1098	264	160	490	293	1005	
Co	23	17	35	1	36	14	56	
Cr	51	50	52	57	76	83	90	
Cu	11	19	9	9	9	8	10	
Nb	22	31	17	14	17	21	14	
Ni	38	32	26	24	26	25	32	
Sr	216	188	53	306	87	26	51	
Y	21	22	16	16	24	32	59	
Zr	151	145	285	239	36	155	196	
Rb	256	227	37	31	288	245	264	
Zn	110	127	10	5	47	68	142	

Idaho Springs-Ralston shear zone samples

S1a/S1b fol			L1 MSL		Location	Rock type	Sample	Thin
strike	dip		trend	plunge				section?
255	79	N	258	73	Deer Ck	Xpelitic schist	A00GG1	y
244	84	N	285	69	Deer Ck	Xpelitic schist	A00GG2	y
170	40	W			Deer Ck	Xpelitic schist	A00GG3	y
250	64	N	290	64	Deer Ck	Xpelitic schist	A00GG4	y
35	25	E	178	17	Deer Ck	Xpelitic schist	A00GG5	y
45	24	S	67	0	Deer Ck	Xpelitic schist	A00GG6	y
45	65	S	85	24	Deer Ck	Xpelitic schist	A00GG8	y
60	76	N			Chicago Ck	Xbiotite schist	K00IS3	n
345	80	E	75	80	Chicago Ck	Xbiotite schist	K00IS5	n
300	90	V			Schoolhse Rd	Xbiotite schist	KIS0017	y
355	38	E	35	23	Burro Tr	Xpelitic schist	A01GG9	n
65	75	S	65	32	Deer Ck	Xquartzite	A01GG15	n
38	87	S	218	53	Knott Ck	Xquartzite	A01GG20	n
52	68	S			Knott Ck	Xquartzite	A01GG21	n
45	79	S			Knott Ck	Xquartzite	A01GG22	n
56	86	S	225	76	Knott Ck	Xquartzite	A01GG23	n
67	73	S			Burro Tr	Xquartzite	A01GG26	n
30	79	E	45	40	Burro Tr	Xquartzite	A01GG27	n
57	83	S	240	74	Burro Tr	Xquartzite	A01GG28	n
234	86	N	240	58	Knott Ck	XBoulder Ck gr	A01GG30	y
240	79	S	65	11	Knott Ck	Xconglomerate	K01CC52	y
52	85	S	223	63	Knott Ck	Xconglomerat e	K01CC53/W0 1CC02	n

Idaho Springs-Ralston shear zone samples cont.

S2 hi-T hi-strain zone		L2 MSL		Location	Rock type	Shear snse	Sample	Thin section?
strike	dip	trend	plunge					
55	84 S	225	55	Knott Ck	XBoulder Ck gr		A01GG1	n

F2 fold data										
S1a/S1b folded		S2 axial plane		F2 fold axis		Location	Rock type	Sample	Thin section?
strike	dip	strike	dip	trend	plunge				
68	90 V	235	58 N	62	14	Deer Ck	Xpelitic schist	A01GG13	n
80	74 S			95	36	Deer Ck	Xpelitic schist	A01GG12	n
34	46 E	52	90 V	50	35	Deer Ck	Xpelitic schist	A01GG14	n

S3 phyllonite data								
S3 phyllon fol		L3 MSL on S3		Shear snse	Location	Rock type	Sample	Thin section?
strike	dip	trend	plunge					
265	72 N	62	32	SE-side up	Chicago Ck	Xbiotite schist	KIS001	y
240	90 V	60	50	SE-side up	Chicago Ck	Xbiotite schist	KIS002	y

S3 mylonite data								
S3 mylonite fol		L3 MSL on S3		Shear snse	Location	Rock type	Sample	Thin section?
strike	dip	trend	plunge					
255	79 N	258	73	SE-side down	Deer Ck	Xpelitic schist	A00GG1	n
72	86 S	252	49	SE-side down	Deer Ck	Xquartzite	A00GG9	n
252	85 N	45	65	SE-side down	Chicago Ck	YMt Evans gra	KIS004	n
239	72 N	40	15	SE-side down	Ralston Ck	XBoulder Ck gr	KIS006	n
260	48 N	45	25	SE-side down	Ralston Ck	XBoulder Ck gr	KIS007	n
260	87 N	267	68	SE-side down	Deer Ck	XBoulder Ck gr	KIS009	n
77	86 S	210	70	SE-side down	Deer Ck	Xquartzite	KIS0010	y
77	88 S	236	65	SE-side down	Deer Ck	Xquartzite	KIS0011	n
70	90 V	160	90	SE-side down	Deer Ck	Xpelitic schist	KIS0012	y
50	90 V	140	90	SE-side down	Deer Ck	Xpelitic schist	KIS0013	n
68	90 V	250	60	SE-side down	Deer Ck	XBoulder Ck gr	KIS0015	y
65	90 V	240	43	SE-side down	Deer Ck	XBoulder Ck gr	KIS0016	n

Idaho Springs-Ralston shear zone samples cont.

S3 ultramylonite data								
S3 ultramylonite fol		L3 MSL on S3		Shear snse	Location	Rock type	Sample	Thin
strike	dip	trend	plunge					section?
80	80 N	255	62	SE-side up	Deer Ck	XBoulder Ck gr	KIS0014	n
235	77 N	250	65	SE-side up	Knott Ck	Xconglomerate	A00GG10	y
56	77 S	140	85	SE-side up	Knott Ck	XBoulder Ck gr	A00GG11	y
234	90 V	225	60	SE-side up	Burro Tr	XBoulder Ck gr	A01GG10	n
80	84 S	257	61	SE-side up	Deer Ck	XBoulder Ck gr	A01GG16	n
74	87 S	244	46	SE-side up	Deer Ck	XBoulder Ck gr	A01GG17	n
54	78 S	212	47	SE-side up	Burro Tr	XBoulder Ck gr	A01GG2	n
218	85 N	224	50	SE-side up	Burro Tr	XBoulder Ck gr	A01GG8	n
75	65 S	202	60	SE-side up	Knott Ck	XBoulder Ck gr	K01CC50	n
sample of arkosic quartzite from probable regolith					Knott Ck	Xquartzite	A01GG5	

St. Louis Lake shear zone samples

S1a/S1b fol		Location	Rock typ	Sample	Thin
strike	dip				section?
90	84 S	St. Louis L	Xcalc-silic	K00SL1	n
50	90 V	St. Louis L	XBoulder	K00SL2	y
155	54 W	St. Louis L	Xgrabbro	A00SL26	n

S2 high-strain domain						Thin
strike	dip	trend	plunge	Location	Rock type	section?
75	69 S	115	49	Vasquez Ck	Xgranodiorite	y

S3 ultramylonite								
S3 ultramylonite fol		L3 MSL on S3		Shear snse	Location	Rock type	Sample	Thin
strike	dip	trend	plunge					section?
48	90 V	224	70	SE-side down	St. Louis Lk	XBoulder Ck gr	A00SL1	y
65	78 S	155	90	SE-side down	St. Louis Lk	XBoulder Ck gr	A00SL22	y
192	90 V	282	90	SE-side down	Berthoud Ps	Ysilver Plume g	A00BP1	y

St. Louis Lake shear zone samples cont.

S3 mylonite							
S3 myl fol		L3 MSL on S3		Shear snse	Location	Rock type	Sample	Thin
strike	dip	trend	plunge					section?
75	63 S	165	55	SE-side up	St. Louis Lk	XBoulder Ck gr	A00SL6	y
71	65 S	140	63	SE-side up	Vasquez Ck	Xgranodiorite	A00SL7, A0	y
67	76 S	125	66	SE-side up	Vasquez Ck	Xgranodiorite	A00SL9, A0	y
88	75 S	178	75	SE-side up	Vasquez Ck	Xgranodiorite	A00SL11	y
95	74 S	164	64	SE-side up	Vasquez Ck	Xgranodiorite	A00SL12	y
80	74 S	152	72	SE-side up	St. Louis Lk	XBoulder Ck gr	A00SL20	y
66	65 S	150	65	SE-side up	St. Louis Lk	XBoulder Ck gr	A00SL21	y
286	90 V	70	66	SE-side up	St. Louis Lk	Xgabbro	A00SL25	y
75	74 S	95	36	SE-side up	St. Louis Lk	Xgabbro	A00SL26	y
90	83 S	165	82	SE-side up	St. Louis Lk	Ysilver Plume g	A00SL27	n
75	85 S	85	64	SE-side up	St. Louis Lk	Ysilver Plume g	A00SL28	y
73	63 S	115	52	SE-side up	St. Louis Lk	Ysilver Plume g	A00SL29	y

Gore Range shear zone samples

S1a/S1b fol		L1 MSL		Location	Rock type	Sample	Thin
strike	dip	trend	plunge				section?
108	48 S	180	46	Eccles Pass	Xmigmatite	A99TM3	n
335	42 W			N Tenmile Ck	Xbiotite gnss	KTM99-11	y
300	56 S			Meadow Ck	XCross Ck gr	KTM99-2	y
320	76 E			Meadow Ck	Xgranodiorite	KTM99-3	y
335	70 W			Meadow Ck	Xmigmatite	KTM99-5	y
225	45 E			Meadow Ck	Xmigmatite	KTM99-6	y
355	37 E	90	35	Uneva Ridge	Xmigmatite	A00TM1	y
170	72 W	189	24	Uneva Ridge	Xmigmatite	A00TM2	y
340	20 E	70	20	Eccles Pass	Xquartzite	A00TM6	y
345	48 E			Eccles Pass	Xquartzite	A00TM7	y
332	80 E			Eccles Pass		A00TM8	y

Gore Range shear zone samples cont.

S2 hi-T hi-strain zone		L2 MSL		Location	Rock type	Shear snse	Sample	Thin
strike	dip	trend	plunge					section?
41	86 E			Meadow Ck	XCross Ck gr	SE-side up	KTM99-4	y
39	81 E	54	69	Meadow Ck	Xmigmatite	SE-side up	A99TM1	n
39	84 E	90	83	Meadow Ck	Xmigmatite	SE-side up	A99TM2	n
40	76 S	220	28	Uneva Ridge	Xmigmatite		A00TM9	y
64	72 S	82	49	Uneva Ridge	Xmigmatite		A00TM14	y

S3 mylonite

S3 mylonite fol		L3 MSL on S3		Shear snse	Location	Rock type	Sample	Thin
strike	dip	trend	plunge					section?
227	65 W	38	52	SE-side down	Meadow Ck	Xmigmatite	A99TM12	n
231	76 W	38	52	SE-side down	Meadow Ck	Xmigmatite	A99TM13	y
228	75 W	40	30	SE-side down	Meadow Ck	Xmigmatite	A99TM4	n
230	73 W	38	20	SE-side down	Meadow Ck	Xmigmatite	A99TM5	n
38	80 W	35	55	SE-side down	Meadow Ck	Xmigmatite	KTM99-1	y
236	86 N	326	86	SE-side down	N Tenmile Ck	XCross Ck gr	KTM99-17	y
258	78 S	130	65	SE-side down?	N Tenmile Ck	Xmigmatite	KTM99-8	y
243	78 N	333	76	SE-side down?	N Tenmile Ck	Xmigmatite	KTM99-9a	y
243	78 N	333	76	SE-side down	N Tenmile Ck	Xmigmatite	KTM99-9b	y
345	43 W			SE-side down	N Tenmile Ck	Xmigmatite	KTM99-10	y

S3 mylonite fol		L3 MSL on S3		Shear snse	Location	Rock type	Sample	Thin
strike	dip	trend	plunge					section?
100	62 S	139	60	SE-side down	Uneva Ridge	Xmigmatite	A00TM10	y
96	61 S	160	59	SE-side down	Uneva Ridge	XCross Ck gr	A00TM11	y
93	85 S	97	67	SE-side down	Uneva Ridge	Xmigmatite	A00TM12	y
93	71 S	159	68	SE-side down	Uneva Ridge	Xmigmatite	A00TM13	n
84	65 S	168	67	SE-side down	Uneva Ridge	Xmigmatite	A00TM3	y

Gore Range shear zone samples cont.

S3 ultramylonite

S3 ultramyl fol		L3 MSL on S3		Shear snse	Location	Rock type	Sample	Thin section?
strike	dip	trend	plunge					
214	85 W	244	82	SE-side up	Meadow Ck	Xmigmatite	A99TM15	y
49	81 E	139	81	SE-side up	Meadow Ck	Xmigmatite	A99TM16	y
218	75 W			SE-side up	Meadow Ck	XCross Ck gr	GB99TM4	y
69	90 V			SE-side up	Meadow Ck	XCross Ck gr	GB99TM5	y
101	67 S	165	56	SE-side up	Booth Lake	XCross Ck gr	A00BL1	y
73	86 S	80	46	SE-side up	Booth Lake	XCross Ck gr	A00BL2	y
	80 S	140	72	SE-side up	Booth Lake	XCross Ck gr	A00BL3	y
196	75 W	325	56	SE-side up	Eccles Pass	Xmigmatite	A00TM4	y
226	85 W	230	37	SE-side up	Eccles Pass	Xmigmatite	A00TM5	y

S3 phyllonite

S3 phyllon fol		L3 MSL on S3		Shear snse	Location	Rock type	Sample	Thin section?
strike	dip	trend	plunge					
90	90 V		down-dp	SE-side up?	Meadow Ck	Xmigmatite	KTM99-12	n
284	60 N	350	39	SE-side down	Meadow Ck	Xmigmatite	KTM99-13	n

Magmatic fabric				Thin section?
strike	dip	Location	Rock type	
300	56 S	Meadow C	XCross Ck	KTM99-2	n

Pegmatite/granite dike orientations					
strike	dip	Location	Rock type	Sample	
201	48 W	N Tenmile	Xwhitepeg	KTM99-7	y

7.0 REFERENCES

Aleinikoff, John N., Reed, John C. Jr., and DeWitt, Ed, 1993, The Mount Evans batholith in the Colorado Front Range: Revision of its age and reinterpretation of its structure: Geological Society of America Bulletin, v. 105, p. 791-806.

Allen, Joseph L., 1992, Influence of a basement shear zone on stratigraphy of the Cambrian Sawatch Quartzite, northeastern Sawatch Range, Colorado: Geological Society of America Abstracts with Programs, v. 24, n. 6, p. 1.

Allen, Joseph L., 1993, Cambrian-Mississippian reactivation history of the Homestake shear zone, central Colorado: Geological Society of America Abstracts with Programs, v. 25, n. 5, p. 2.

Allen, Joseph L., 1994, Stratigraphic variations, fault rocks, and tectonics associated with brittle reactivation of the Homestake shear zone, central Colorado [Ph.D. thesis]: Lexington, Kentucky, University of Kentucky, 321 p.

Allen, M.B., and Vincent, Stephen J., 1997, Fault reactivation in the Junggar region, northwest China: the role of basement structures during Mesozoic-Cenozoic compression: Journal of the Geological Society, London, v. 154, p. 151-155.

Avouac, J.P., Tapponnier, P., Bai, M., You, H., and Wang, G., 1993, Active thrusting and folding along the Northern Tien Shan and Late Cenozoic rotation of

the Tarim relative to Dzungaria and Kazakhstan: Journal of Geophysical Research, v. 98, n. B4, p. 6755-6804.

Baars, Donald L., 1984, Tectonic significance of Proterozoic faults, San Juan Mountains, southwestern Colorado: Geological Society of America Abstracts with Programs, v. 16, n. 4, p. 214.

Baars, Donald L., Bartleston, B.L., Chapin, C.E., Curtis, B.F., De Voto, R.H., Everett, J.R., Johnson, R.C., Molenaar, C.M., Peterson, Fred, Schenk, C.J., Love, J.D., Merin, I.S., Rose, P.R., Ryder, R.T., Waechter, N.B., Woodward, L.A., 1988, Basins of the Rocky Mountain region: *in* Sloss, L.L., Sedimentary cover: North American Craton, U.S.: Denver, Colorado, Geological Society of America Geology of North America series, p. 109-220.

Barovich, K.M., 1986, Age constraints on Early Proterozoic deformation in the northern Front Range, Colorado [M.S. thesis]: Boulder, Colorado, University of Colorado, 49 p.

Bauer, Paul W., and Williams, Michael L., 1994, The age of Proterozoic orogenesis in New Mexico, U.S.A.: Precambrian Research, v. 67, n. 3-4, p. 349-356.

Bergendahl, M.H., 1969, Geologic map and sections of the southwest quarter of the Dillon Quadrangle, Eagle and Summit Counties, Colorado: U.S. Geological Survey Miscellaneous Geologic Investigations Map I-563, scale 1:24 000.

Bickford, M.E., and Boardman, S.J., 1984, A Proterozoic volcano-plutonic terrane, Gunnison and Sailda areas, Colorado: Journal of Geology, v. 92, p. 657-666.

Bickford, M.E., Cullers, R.L., and Van Schmus, W.R., 1984, U-Pb geochronology of the Proterozoic volcano-plutonic terrane in the Gunnison and Salida areas, Colorado, *in* Grambling J.A., and Tewksbury, B.J., Proterozoic geology of the southern Rocky Mountains: Boulder, Colorado, Geological Society of America Special Paper 235.

Brede, Rainald, Hauptmann, Manfred, and Herbig, Hans-Georg, 1992, Plate tectonics and intracratonic mountain ranges in Morocco – The Mesozoic-Cenozoic development of the Central High Atlas and the Middle Atlas: Geologische Rundschau, v. 81, n. 1, p. 127-141.

Brookfield, M.E., 2000, Geological development and Phanerozoic crustal accretion in the western segment of the southern Tien Shan (Kyrgystan, Uzbekistan, and Tajikistan): Tectonophysics, v. 328, p. 1-14.

Bryant, Bruce, McGrew, L.W., and Wobus, R.A., 1981, Geologic map of the Denver 1 degrees by 2 degrees quadrangle, North-central Colorado: U.S. Geological Survey Miscellaneous Investigations Map I-1163, scale 1:250 000.

Burov, Evgene B., and Molnar, Peter, 1998, Gravity anomalies over the Ferghana Valley (central Asia) and intracontinental deformation: Journal of Geophysical Research, v. 103, n. B8, p. 18137-18152.

Cavosie, Aaron, 2001, Tectonic evolution of an Early Proterozoic ophiolite fragment and a stable isotope study of co-existing aluminum silicates in quartz veins, northern Colorado Front Range [M.S. thesis]: Albuquerque, New Mexico, University of New Mexico.

Doe, B.R., and Pearson, R.C., 1969, U-Th-Pb chronology of zircons from the St. Kevin Granite, northern Sawatch Range, Colorado: Geological Society of America Bulletin, v. 80, p. 2495-2502.

Chang, C.P., Angelier, Jacques, and Huang, Chi-Yue, 2000, Origin and evolution of a melange: the active plate boundary and suture zone of the Longitudinal Valley, Taiwan: Tectonophysics, v. 325, n. 1-2, p. 43-62.

Finiol, Lisa Rae, 1992, Petrology, paleostratigraphy, and paleotectonics of a Proterozoic metasedimentary and metavolcanic sequence in the Colorado Front Range [M.S. thesis]: Golden, Colorado, Colorado School of Mines, 283 p.

Fraser, George D., 1949, Coal Creek quartzite, Jefferson and Boulder Counties, Colorado: Geological Society of America Bulletin, v. 60, n. 12, p. 1960.

Gable, Dolores J., 1980, The Boulder Creek batholith, Front Range, Colorado: U.S. Geological Survey Professional Paper 1101, 88 p.

Gall, Quentin, 1994, The Proterozoic Thelon paleosol, Northwest Territories, Canada: Precambrian Research, v. 68, p. 115-137.

Gay, A.L., and Grandstaff, D.E., 1980, Chemistry and mineralogy of Precambrian paleosols at Elliot Lake, Ontario, Canada: Precambrian Research, v. 12, p. 349-373.

Geissman, John W., Snee, Lawrence W., Graaskamp, Garrett W., Carten, Richard B., and Geraghty, Ennis P., 1992, Deformation and age of the Red Mountain intrusive system (Urad-Henderson molybdenum deposits), Colorado: Evidence from paleomagnetic and $^{40}Ar/^{39}Ar$ data: Geological Society of America Bulletin, v. 104, p. 1031-1047.

Gomez, Francisco, Beauchamp, Weldon, and Barazangi, Muawia, 2000, Role of the Atlas Mountains (northwest Africa) within the African-Eurasian plate-boundary zone: Geology, v. 28, n. 9, p. 775-778.

Grandstaff, D.E., Edelman, M.J., Foster, R.W., Zbinden, E., and Kimberley, M.M., 1986, Chemistry and mineralogy of Precambrian paleosols at the base of the Dominion and Pongola groups (Transvaal, Africa): Precambrian Research, v. 32, p. 97-131.

Graubaud, Cinda M., and Mattinson, J.M., 1990, Syntectonic emplacement of the ~1440 Ma Mt. Evans pluton and history of motion along the Idaho Springs-Ralston Creek shear zone, central Front Range, Colorado: Geological Society of America Abstracts with Programs, v. 22, n. 7, p. A245.

Hedge, C.E., 1969, A petrogenetic and geochronologic study of migmatites and pegmatites in the central Front Range [Ph.D. thesis]: Golden, Colorado, Colorado School of Mines, 158 p.

Hirth, G., and Tullis, J., 1994, The brittle-plastic transition in experimentally deformed quartz aggregates: Journal of Geophysical Research, v. 99, p. 11,731-11,747.

Hoblitt, R., and Larson, E., 1975, Paleomagnetic and geochronologic data bearing on the structural evolution of the northeastern margin of the Front Range, Colorado: Geological Society of America Bulletin, v. 86, p. 237-242.

Holland, H.D., Feakes, C.R., Zbinden, E.A., 1989, The Flin Flon Paleosol and the composition of the atmosphere 1.8 BYBP: American Journal of Science, v. 289, n. 4, p. 362-389.

Jacob, Arthur F., 1983, Mountain front thrust, southeastern Front Range and northeastern Wet Mountains, Colorado, *in* Lowell, James D., and Gries, Robbie, Rocky Mountain foreland basins and uplifts: Denver, Colorado, Rocky Mountain Association of Geologists, p. 229-244.

Karlstrom, K.E., and Bowring, S.A., 1991, Styles and timing of Early Proterozoic deformation in Arizona: Constraints on tectonic models, *in* Karlstrom, K.E., Proterozoic Geology and Ore Deposits of Arizona: Flagstaff, Arizona, Arizona Geological Society Digest 19, p. 1-10.

Karlstrom, Karl E., and Humphreys, Eugene D., 1998, Persistent influence of Proterozoic accretionary boundaries in the tectonic evolution of southwestern North America: interaction of cratonic grain and mantle modification events: Rocky Mountain Geology, v. 33, n. 2, p. 161-179.

Karlstrom, Karl E., Williams, Michael L., McLelland, James, Geissman, John W., Ahall, Karl-Inge, 1999, Refining Rodinia: Geological Evidence for the Australia-Western U.S. connection in the Proterozoic: GSA Today, v. 9, n. 10, p. 1-7.

Kelley, Shari A., Chapin, Charles E., and Raynolds, Robert G., 2001, Influence of the Colorado Mineral Belt on the northwest margin of the Denver Basin, Geological Society of America Abstracts with Programs, v. 33, n. 5, p. A51.

Kirby, Eric, Karlstrom, Karl E., Andronicos, Chris L., and Dallmeyer, R. David, 1995, Tectonic setting of the Sandia Pluton; an orogenic 1.4 Ga granite in New Mexico: Tectonics, v. 14, n. 1, p. 185-201.

Kluth, Charles F., and Coney, Peter J., 1980, Plate tectonics of the Ancestral Rocky Mountains: Geology, v. 9, p. 10-15.

Moench, R.H., 1964, Geology of Precambrian rocks, Idaho Springs district, Colorado: U.S. Geological Survey Bulletin, v. 1182-A, p. A1-A69.

Montel, Jean-Marc, Foret, S., Veschambre, M., Nicollet, C., and Provost, A., 1996, Electron microprobe dating of monazite: Chemical Geology, v. 131, p. 37-53.

Mutschler, Felix E., Larson, Edwin E., Bruce, Robert M., 1987, Laramide and younger magmatism in Colorado: new petrologic and tectonic variations on old themes, *in* Drexler, John W., and Larson, Edwin E., Cenozoic volcanism in the Southern Rocky Mountains, Golden, Colorado, Colorado School of Mines Quarterly, v. 82, n. 4, p. 1-47.

Naeser, C.W., Bryant, Bruce, Kellogg, Karl, and Perry, W.J., 1999, Middle to late Tertiary cooling of the Gore and western Front ranges, central Colorado, from apatite fission-track data: Geological Society of America Abstracts with Programs, v. 31, n. 7, p. 245.

Nyman, M.W., Karlstrom, K.E., Kirby, E., and Graubard, C.M., 1994, Mesoproterozoic contractional orogeny in western North America: Evidence from ca. 1.4 Ga plutons: Geology, v. 22, p. 901-904.

Oppenheimer, William L., and Geissman, John W., 1988, Paleomagnetic data bearing on Laramide and post-Laramide deformation and magmatism in the northern Mosquito Range between Fremont and Hoosier passes, central Colorado: Colorado School of Mines Quarterly, v. 10, p. 33-50.

Parrish, R.R., 1990, U-Pb dating of monazite and its application to geological problems: Canadian Journal of Sciences, v. 27, p. 1435-1450.

Passchier, Cees W., and Trouw, Rudolph A.J., 1996, Microtectonics: New York, NY, Springer, 289 p.

Pattison, D.R.M., Spear, F.S., and Cheney, J.T., 1999, Polymetamorphic origin of muscovite + cordierite + staurolite + biotite assemblages: implications for the metapelitic petrogenetic grid and for P-T paths: Journal of Metamorphic Geology, v. 17, p. 685-703.

Polat, Ali, and Kerrich, Robert, 1999, Formation of an Archean tectonic melange in the Schreiber-Hemlo greenstone belt, Superior Province, Canada: implications for Archean subduction-accretion processes: Tectonics, v. 18, n. 5, p. 733-755.

Premo, W.R., and Fanning, C.M., 2000, SHRIMP U-Pb zircon ages for Big Creek gneiss, Wyoming and Boulder Creek batholith, Colorado: Implications for timing of Paleoproterozoic accretion of the northern Colorado province: Rocky Mountain Geology, v. 35, n. 1, p. 31-50.

Premo, W.R., and Van Schmus, W.R., 1989, Zircon geochronology of Precambrian rocks in northeastern Wyoming and northern Colorado, *in* Grambling, J.A., and Tewksbury, B.J., Geology of the Southern Rocky Mountains: Boulder, Colorado, Geological Society of America Special Paper 235, p. 13-32.

Reed, John C. Jr., Bickford, M.E., Premo, Wayne R., Aleinikoff, John N., and Pallister, John S., 1987, Evolution of the Early Proterozoic Colorado province: Constraints from U-Pb geochronology: Geology, v. 15, p. 861-865.

Selverstone, Jane, Hodgins, Meghan, Shaw, Colin, Aleinikoff, John N., and Fanning, C. Mark, 1997, Proterozoic tectonics of the northern Colorado Front Range: in Bolyard, Dudley and Sonnenberg, Stephen A., Geologic history of the

Colorado Front Range, Denver, CO, Rocky Mountain Association of Geologists, p. 9-18.

Selverstone, Jane, Hodgins, Meghan, Aleinikoff, John N., and Fanning, C. Mark, 2000, Mesoproterozoic reactivation of a Paleoproterozoic transcurrent boundary in the northern Colorado Front Range: Implications for ~1.7- and 1.4 Ga tectonism: Rocky Mountain Geology, v. 35, n. 2, p. 139-162.

Selverstone, Jane, Pun, Aurora, and Condie, Kent C., 1999, Xenolithic evidence for Proterozoic crustal evolution beneath the Colorado Plateau: Geological Society of America Bulletin, v. 111, n. 4, p. 590-606.

Shaw, Colin A., and Karlstrom, Karl E., 1999, The Yavapai-Mazatzal crustal boundary in the Southern Rocky Mountains: Rocky Mountain Geology, v. 34, n. 1, p. 37-52.

Shaw, Colin A., Karlstrom, Karl E., Williams, Michael L., Jercinovic, Michael J., and McCoy, Annie M., 2001, Electron-microprobe monazite dating of ca. 1.71-1.63 Ga and ca. 1.45-1.38 Ga deformation in the Homestake shear zone, Colorado: Origin and early evolution of a persistent itnracontinental tectonic zone: Geology, v. 29, n. 8, p. 739-742.

Shaw, Colin A., Snee, Lawrence W., Selverstone, Jane, Reed, John C., Jr., 1999, $^{40}Ar/^{39}Ar$ thermochronology of Mesoproterozoic metamorphism in the Colorado Front Range: Journal of Geology, v. 107, n. 1, p. 49-67.

Sims, P.K., and Stein, H.J., 1999, Re-Os ages for molybdenite record major Proterozoic crust-forming event in Colorado: Geological Society of America Abstracts with Programs, v. 31, n. 7, p. 260.

Spear, Frank S., 1993, Metamorphic phase equilibria and pressure-temperature-time paths: Washington, D.C., Mineralogical Society of America Monograph, 799 p.

Tullis, J., and Yund, R., 1992, The Brittle-Ductile Transition in Feldspar Aggregates: An Experimental Study: in Evans, Brian and Wong, Teng-fong, Fault mechanics and transport properties of rocks: a festschrift in honor of W.F. Brace, San Diego, CA, Academic Press International geophysics series v. 51, p. 89-117.

Tweto, O.L., and Lovering, T.S., 1977, Geology of the Minturn 15-minute Quadrangle, Eagle and Summit Counties, Colorado: U.S. Geological Survey Professional Paper P-956, 96 p.

Tweto, O.L., and Sims, P.K., 1963, Precambrian ancestry of the Colorado Mineral Belt: Geological Society of America Bulletin, v. 74, p. 991-1014.

Wells, J.D., Sheridan, D. M., and Arden, L.A., 1964, Relationship of Precambrian Quartzite-Schist Sequence Along Coal Creek to Idaho Springs Formation, Front Range, Colorado: U.S. Geological Survey Professional Paper 454-O, 25 p.

Williams, Michael L., and Karlstrom, Karl E., 1996, Looping P-T paths and high-T, low-P middle crustal metamorphism: Proterozoic evolution of the southwestern United States: Geology, v. 24, n. 12, p. 1119-1122.

Williams, M.L., Jercinovic, M.J., and Terry, M.P., 1999, Age mapping and dating of monazite on the electron microprobe: Deconvoluting multistage tectonic histories: Geology, v. 27, p. 1023-1026.

Yin, A., Nie, S., Craig, P., Harrison, T.M., Ryerson, F.J., Qian, Xianglin, and Geng, Yang, 1998, Late Cenozoic tectonic evolution of the southern Tien Shan: Tectonics, v. 17, n. 1, p. 1-27.

VAIL PASS QUADRANGLE
COLORADO
7.5 MINUTE SERIES (TOPOGRAPHIC)

4763 II NE (DILLON)

395 | 396 | 12'30" | 3.3 MI. TO U.S. 6 | 4763 II NW (WILLOW LAKES) | R. 79 W. | 399 | R. 78 W. | 10' | 400 | 401 | 402 | 1 820 000 FEET | 403 | 106°07'30" | 39°37'30"

4386 | 650 000 FEET | 4385 | 4384 | 4383 | 4382 | 35' | 4381 | 4380 | 4379 | 4378 | 4377 | 32'30"

Gore Creek | Buffalo Pass | EAGLE CO | SUMMIT CO | S. Willow Cr | Buffalo Mountain | Salt Lick Gulch | Eccles Pass | Meadow Creek | TRAIL | GORE RANGE | MOUNTAIN | WILDERNESS | BOUNDARY | Prospect | ARAPAHO NATIONAL FOREST | North Tenmile Creek | Tenmile Mountain | RANGE | Uneva Peak | Uneva Pass | Lost Lake | Corral Creek | Black Lake | Rest Area | Officers Gulch Pond | Officers Gulch | Wheeler Lakes | Tenmile Creek | Curtain Ponds | PIPELINE | Wheeler Flats | COLORADO TRAIL | West Tenmile Creek | Smith Gulch | Stafford Gulch | Cutler Gulch | Uneva Lake | Tenmile Pass | Tenmile Creek

Xg Cross Ck granite
Xgd granodiorite and diorite
Xp Pegmatites assoc. with Cross Ck granite
Xcs Calc-silicate rocks and interlayered amphibolite
Xm Migmatite/biotite schist
PPm
Gore Range shear zone

MAP EXPLANATION

50 S1 foliation and L1 mineral stretching lineation
parasitic fold
S2 high temperature hi-strain domain
synform | antiform
A01TM1 sampling location
U D 80 65 mylonite or ultramylonite zone
brittle fault
breccia

395 | 396 12'30" | 397 | (COPPER MOUNTAIN) 4762 I NW | 399 | 10' | R. 79 W. | R. 78 W. | 401 | CLIMAX 11 MI. | 403000m.E. | 39°30' | 106°07'30"

(BRECKENRIDGE) 4762 I NE

SCALE 1:24 000

1 0 1 MILE
1000 0 1000 2000 3000 4000 5000 6000 7000 FEET
1 .5 0 1 KILOMETER

CONTOUR INTERVAL 40 FEET
NATIONAL GEODETIC VERTICAL DATUM OF 1929

GN MN 0°45' 13 MILS 12½° 213 MILS

UTM GRID AND 1987 MAGNETIC NORTH DECLINATION AT CENTER OF SHEET

ROAD CLASSIFICATION

Primary highway, hard surface
Secondary highway, hard surface
Light-duty road, hard or improved surface
Unimproved road
Interstate Route | U. S. Route | State Route

COLORADO
QUADRANGLE LOCATION

THIS MAP COMPLIES WITH NATIONAL MAP ACCURACY STANDARDS
FOR SALE BY U. S. GEOLOGICAL SURVEY
DENVER, COLORADO 80225, OR RESTON, VIRGINIA 22092
A FOLDER DESCRIBING TOPOGRAPHIC MAPS AND SYMBOLS IS AVAILABLE ON REQUEST

Revisions shown in purple and woodland compiled from aerial photographs taken 1983 and other source data. Partial check by U. S. Forest Service. Map edited 1987

VAIL PASS COLO.
39106-E2-TF-024

1970
PHOTOREVISED 1987

INTERIOR-GEOLOGICAL SURVEY, RESTON, VIRGINIA-1988


BLACK HAWK QUADRANGLE
COLORADO
7.5 MINUTE SERIES (TOPOGRAPHIC)
UNITED STATES
DEPARTMENT OF THE INTERIOR
GEOLOGICAL SURVEY
RALSTON BUTTES QUADRANGLE
COLORADO-JEFFERSON CO.
7.5 MINUTE SERIES (TOPOGRAPHIC)
4963 I NW
(LOUISVILLE)
4963 I V NE
(ELDORADO SPRINGS)
PINECLIFFE 13 MI.
BLUE MOUNTAIN
NORTH JEFFCO
MOUNTAIN PARK
GOLDEN GATE CANYON
STATE PARK
Forgotten Creek Valley
Deer Creek
Nott Creek
Ralston Creek
Ralston Buttes
GILPIN CO
JEFFERSON CO
Rocky
Quarry
Picnic Area
Prospects
Mine
Spring
Tailings
Schwartzwalder Mine
Idaho Springs - Ralston
shear zone
MAP EXPLANATION
Xq Coal CK quartzite
Xs Coal CK pelitic schist
Xgd Granodiorite and quartz monzonite of Boulder CK batholith
Xp Pegmatites assoc. with Boulder CK batholith
Xa Amphibolite
Xm Migmatite / biotite schist
Xbs Biotite schist
S1 foliation and L1 mineral stretching lineation
parasitic folds
S2 high temperature hi-strain domain
younging direction in Coal CK quartzite
synform
antiform
A01GG9 sampling location
mylonite or ultramylonite zone
brittle fault

T

BYERS PEAK QUADRANGLE
COLORADO
7.5 MINUTE SERIES (TOPOGRAPHIC)
SW/4 FRASER 15' QUADRANGLE

4863 IV NE (FRASER)

000 FEET (CENTRAL) | 57'30" | 419 | 4863 IV NW (BOTTLE PASS) | 421 | 55' | 422 | FRASER 7.3 MI. | 1 890 000 FEET (NORTH) | 105°52'30" | 39°52'30" | 4414

St. Louis Lake shear zone

MAP EXPLANATION

- Ysp Silver Plume granite
- Xgd Granodiorite of Boulder Ck batholith
- Xme Tectonic melange including amphibolite, gabbro, calc-silicate rocks, marble
- Xc Fragments of metachert in tectonic melange
- Xm Migmatite/biotite schist
- 50 S1 foliation and L1 mineral stretching lineation
- parasitic folds
- S2 high temperature hi-strain domain
- synform / antiform
- A00SL20 sampling location
- U / D 80 / 65 mylonite or ultramylonite zone
- brittle fault

Byers Peak
VABM 12804
Bills Peak
Kreiger Creek
Byers Peak Trail
Iron Creek
St Louis Aqueduct
Launch Creek
Gordon Creek
Mine
St Louis Lake
St Louis Peak
St Louis Pass
Mt Nystrom
Vasquez Lake
Vasquez Creek
Mt Nystrom Trail
W Fork Clear C...
GRAND CO
CLEAR CREEK CO

A00SL1, 2, A00SL26, A00SL22
A00SL6, A00SL20, A00SL21
A00SL25, 26, A00SL27, A00SL28, 29

A R A P
N A T I O N A L
F O R E S T

50'
4409
4408
4406
4405
(BERTHOUD PASS) 4863 IV SE